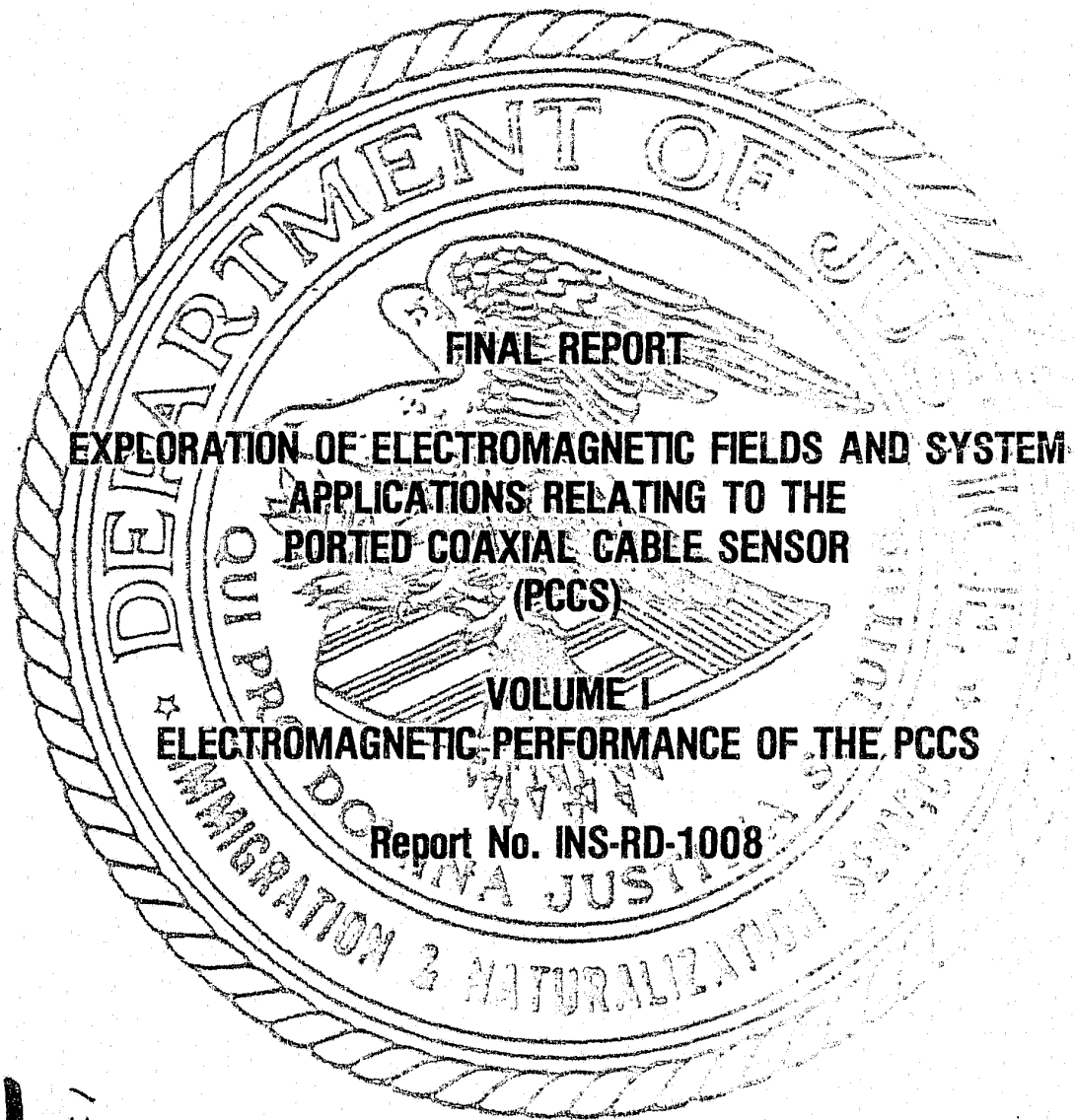

FINAL REPORT

EXPLORATION OF ELECTROMAGNETIC FIELDS AND SYSTEM APPLICATIONS RELATING TO THE PORTED COAXIAL CABLE SENSOR (PCCS)

VOLUME I
ELECTROMAGNETIC PERFORMANCE OF THE PCCS

Report No. INS-RD-1008

FUNDED BY
RESEARCH AND DEVELOPMENT
IMMIGRATION AND NATURALIZATION SERVICE

JULY 1987

By

Cliff H. Halevi and Robert N. Carlile
Department of Electrical and Computer Engineering
University of Arizona
Tucson, Arizona 85721

FINAL REPORT

EXPLORATION OF ELECTROMAGNETIC FIELDS AND SYSTEM APPLICATIONS RELATING TO THE PORTED COAXIAL CABLE SENSOR (PCCS)

VOLUME I
ELECTROMAGNETIC PERFORMANCE OF THE PCCS

by

Cliff H. Halevi and Robert N. Carlile
Department of Electrical and Computer Engineering
University of Arizona
Tucson, Arizona 85721

Report No. INS-RD-1008

July, 1987

FUNDED BY
RESEARCH AND DEVELOPMENT
IMMIGRATION AND NATURALIZATION SERVICE

National Institute of Justice Grant No. 85-IJ-CX-0018
Department of Justice
Immigration and Naturalization Service
Research and Development
425 I Street NW
Washinton, DC 20536

ELECTROMAGNETIC PERFORMANCE OF A PORTED COAXIAL CABLE SENSOR (PCCS) SYSTEM

Cliff Hunter Halevi, M.S.

The University of Arizona, 1987

Director: R. N. Carlile

An experimental analysis of the factors which affect the sensitivity of the Ported Coaxial Cable Sensor (PCCS) system is presented. The measured response profile of the test system is compared against variations of cable separation distance, soil conductivity and permittivity, and magnetic field intensity above the transmitter cable.

These experiments show that higher conductivity and permittivity of the burial medium results in a decrease in the strength of the magnetic field above the transmitter cable, and that this results in a decrease in response number. The results of these experiments are compared with the results obtained from a theoretical analysis of a simplified model.

An experimentally derived relationship between cable separation distance and response number, which is valid for all soil types, can be applied to predictably minimize variations in sensitivity, resulting in a response ratio for each cell which will not exceed 3:1.

ACKNOWLEDGMENTS

I wish to express my great appreciation to my advisor, Dr. R. N. Carlile, for his support and guidance throughout the length of this project. I would like to thank the other members of the examining committee, Dr. L. C. Schooley and Dr. E. Pierce, for their review of this manuscript and subsequent helpful comments. I also wish to thank George Van Horn of the Immigration and Naturalization Service for his tireless work in the construction of the test site; and Pete Rebeil and Tim Feucht for their help in carrying out the experiments. Next, I would like to thank the Immigration and Naturalization Service for their financial support.

I would like to thank my parents and in-laws for the emotional and financial support, which made it possible for me to achieve my goals. And finally, I would like to thank my wife, Nancy, for her assistance, support and love, during these years of graduate study.

TABLE OF CONTENTS

TABLE OF CONTENTS -- Continued

TABLE OF CONTENTS -- Continued

LIST OF ILLUSTRATIONS

LIST OF ILLUSTRATIONS -- continued

LIST OF ILLUSTRATIONS -- continued

LIST OF ILLUSTRATIONS -- continued

LIST OF ILLUSTRATIONS -- continued

LIST OF ILLUSTRATIONS -- continued

ABSTRACT

An experimental analysis of the factors which affect the sensitivity of the Ported Coaxial Cable Sensor (PCCS) system is presented. The measured response profile of the test system is compared against variations of cable separation distance, soil conductivity and permittivity, and magnetic field intensity above the transmitter cable.

These experiments show that higher conductivity and permittivity of the burial medium results in a decrease in the strength of the magnetic field above the transmitter cable, and that this results in a decrease in response number. The results of these experiments are compared with the results obtained from a theoretical analysis of a simplified model.

An experimentally derived relationship between cable separation distance and response number, which is valid for all soil types, can be applied to predictably minimize variations in sensitivity, resulting in a response ratio for each cell which will not exceed 3:1.

CHAPTER 1

INTRODUCTION

1.1 Purpose

The objective of this study is to analyze those factors which affect the sensitivity of the Ported Coaxial Cable Sensor (PCCS) system and to develop a deployment scheme which allows the system to differentiate between human intruders and small animals.

A PCCS system will assist the U.S. Border Patrol in its mission to control the international border and prevent intrusions by providing accurate information on the number and location of intrusions along even remote areas of the border.

The PCCS system is essentially a line-guided radar whose operation is based on the use of two parallel leaky (i.e. ported) coaxial cables that distribute electromagnetic fields along their length. The presence of an intruder above the cable-pair will cause a variation in the amount of energy coupled between the two cables, thus signaling the presence of the intruder.

Previous studies (Harman, 1983; Miller, Flohr, and Lundien, 1984; and Frankel, Van Horn and Carlile, 1984) have shown that the amplitude and structure of the electromagnetic field around the PCCS cables are directly dependent on the electrical properties of the soil in which the cables are buried. That is, as the conductivity and permittivity of the soil increases, the external field strength between the cables decreases causing a decrease in the received signal caused by an intruder.

Variations in the soil cause the sensitivity of the PCCS system to vary as a function of position along the cables. Uneven sensitivity is undesireable as it results in some areas of the system being unable to detect intruders while other areas are so sensitive that even the crossing of small animals can trigger an intruder alarm.

. This report will describe experiments which were undertaken to determine the exact effect of soil variation and cable separation distance on the ability of the PCCS system to detect intruders. This information will be used to find the best method to attain a more even detection sensitivity for the PCCS system. Only by evening out the sensitivity can the PCCS system be effective in differentiating between human intruders and small animals.

1.2 Historical Background

Guided radar techniques have been used in electromagnetic detection sensors for at least 10 years (Patterson and Mackay, 1977; Harman, 1982). Applications have included obstacle detection along railway lines, and intrusion detectors for perimeter security of military bases and prisons (Harman and Mackay, 1976).

In the early 1970's, researchers at Queen's University in Ontario, Canada, developed several prototypes of microprocessor-based intrusion detection sensors which were able to resolve human intruders. Since then, improvements in leaky cable design and signal processing techniques have paved the way for the development of the current GUIDAR (Guided Intrusion Detection and Ranging) PCCS intrusion detection system. The PCCS system described in this report is a GUIDAR system and henceforth the acronym PCCS will signify GUIDAR unless specifically noted.

1.3 Document Organization

This report is organized into six chapters. Chapters 1 and 2 introduce the PCCS system and describe the theory and operation of the working GUIDAR PCCS system. Also discussed is the need to even out the sensitivity of the system in order to have the detector resolve between humans and small animals.

In Chapter 3, a theoretical analysis of electromagnetic wave propagation is given. Special attention is paid to excitation of more than one mode, and the interaction of modes at an interface between soils with different permittivities.

Chapter 4 describes the design and construction of the 200 meter long PCCS test site which was built to facilitate the experiments of this project. The two specially designed test cells are also described.

Chapter 5 is the heart of this report as this chapter describes the design, implementation and test results for all five experiments. The observations and graphical data in Chapter 5 set the stage for Chapter 6 which presents the main conclusions drawn from all the test results, and suggests a deployment scheme which will enable the PCCS system to effectively differentiate between human intruders and small animals. Additional recommendations are also given for improving the performance of the PCCS system.

1.4 Test Periods

The PCCS test site is located on the University of Arizona's Campbell Farm in Tucson, Arizona. Construction of the test site was begun in June 1986 and completed in August 1986. The system electronics were subsequently moved on

site the following month. Between September and December of the same year the system electronics were calibrated, additional test equipment was brought in or fabricated, and the project experiments were planned. All tests were conducted between January 15, 1987 and April 15, 1987.

Several times during this test period heavy rainfall occurred which resulted in postponing the next test for about a week until the ground could completely dry out. Any test that was not completely finished before a postponement was begun anew when the testing resumed.

CHAPTER 2

THEORY AND OPERATION OF PCCS SYSTEM

This chapter describes the theory and operation of the GUIDAR Ported Coaxial Cable Sensor system. The majority of the information presented in this chapter originates from the GUIDAR technical manual (Guided Intrusion Detection and Ranging System, 1981). Also discussed are limitations on the detector system's resolution capability which are caused by variations in the soil in which the PCCS cables are buried.

2.1 Overall System Operation

The Ported Coaxial Cable Sensor (PCCS) is a time- domain, pulsed, line-guided radar system which is designed to detect the presence of a human or vehicle traversing the system by monitoring the disturbances of an electromagnetic field set up between two parallel, buried, leaky coaxial cables. One cable acts as a transmitter and the second, as a receiver.

An RF pulse of energy is sent down the transmit cable. Some of this energy is coupled into the receiver cable and returns to the PCCS receiver where the signal is analyzed to determine if an intruder is present.

When an intrusion is detected, the PCCS system will signal an intrusion alarm and the PCCS system printer will output the time of day, the cell number, and the response number. The cell number locates the intruder(s) within a 33- meter interval while the response number is proportional to the radar cross section, and

thus the size, of the intruder. Thus, the PCCS system enables the operator of the system to know the location and size of an intruder as well as the time of the intrusion.

2.2 System Components

The cables used in the PCCS system are SPIRAX cables which are manufactured by Computing Devices Company of Ottawa, Canada, the makers of the GUIDAR PCCS system. A diagram of the SPIRAX cable is shown in Figure 2.1. The cables are similar to ordinary coaxial cables except that the outer conductor is formed by two helically wound copper tapes. The two tapes are counterwound such that diamond- shaped apertures are distributed evenly around the outer conductor.

In an ordinary, non-ported coaxial cable the electromagnetic field is totally confined between the inner and outer conductors. The dominant eigenmode is the familiar TEM mode. In ported coaxial cables, however, the apertures in the outer conductor allow the electromagnetic energy of an eigenmode to also exist external to the outer conductor. The electromagnetic fields of these eigenmodes die off as a function of increasing radial distance away from the outer conductor (Harman, 1982).

In the PCCS system, there are two parallel, ported coaxial cables. As mentioned above, one of the cables acts as a transmitter while the other cable acts as the receiver. The two cables are each terminated with 50 ohm terminations, which matches the characteristic impedance of the SPIRAX cables. As a result, all the energy propagating downline will be (ideally) absorbed at the terminations without reflecting back. Computing Devices Company suggests that the parallel cable-pair

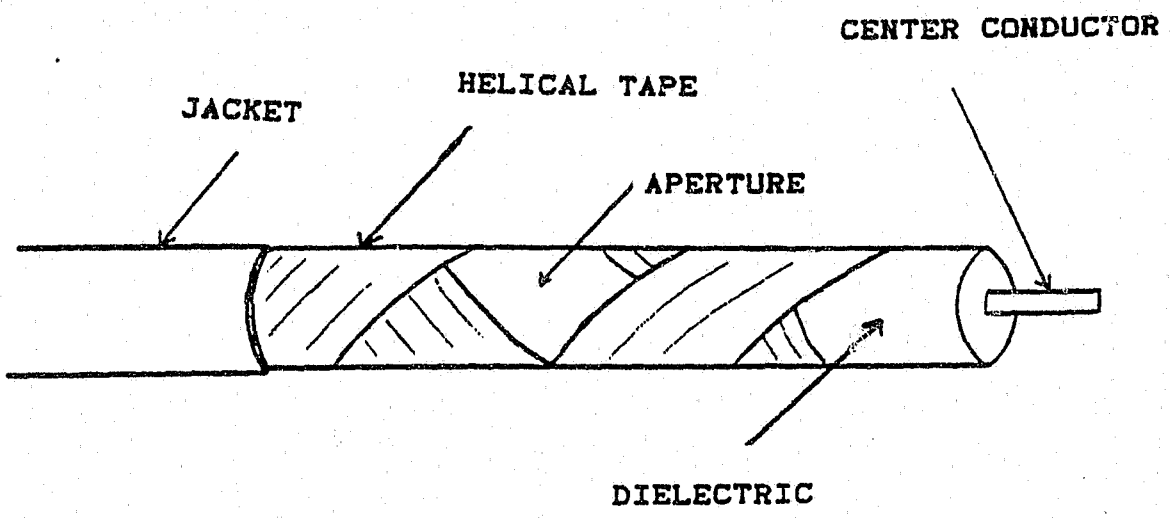

Figure 2.1 SPIRAX Ported Coaxial Cable

should be buried at a depth of 9 inches with the two cables set 5 feet apart.

Besides the ported coaxial cables, the PCCS system consists of the Processor, Detector and Ranging unit (PDR), the Data Acquisition System (DAS), and the printer.

The PDR is the heart of the PCCS system; it contains the transmitter, receiver, amplifier, digitizer, processor, and detector circuits. The transmitter circuit card has switches which allow for varying the frequency, pulse width, and output power. For our tests, the PDR was set to transmit an 800 mW pulsed signal at 63 MHz. The width of the pulse was set to be 450 nanoseconds.

Besides sending out the transmitter signals, the main job of the PDR is to sample the return signal from the receiver cable and to perform the target detection algorithms. The return signal is sampled once every 285.8 nanoseconds. Each sample corresponds to a different 33.33 meter interval (which is termed a cell) on the cable. For each iteration, sixty samples are taken, regardless of the number of cells actually in the deployed system.

The processor then integrates the signal for each cell over 1024 iterations. The processor then extracts the phase and quadrature components of the return signal and uses vector subtraction between the two to determine the target profile (Patterson and Mackay, 1977). The timing scheme for the PDR is listed below.

Sampling interval 285.8 ns X 60 cells	=	17.1 us
Phantom Target Compensation	=	4.0 us
Jitter Delay	=	0.1 us
Time per iteration	=	21.2 us
Preprocessor output 1024 iterations	=	21.7 ms
Read cycle 16.4 us X 60 cells	=	1.0 ms

Single cycle time	=	22.7 ms
2 X Inphase + 2 X Quadrature	=	90.8 ms
Processor computation	=	9.0 ms
Total cycle time	=	99.8 ms

The total cycle time, the time it takes the PCCS to check for the presence of intruders along the entire system, indicates that the PCCS completes about 10 intruder detection cycles per second.

The Data Acquisition System (DAS) interfaces with the PDR; its function is to monitor the performance of the PCCS system and to output the relevant data, such as an intrusion alarm, to the Texas Instruments 743 KSR thermal printer.

Data is transmitted from the PDR to the DAS via a 300-baud serial data port. A thumbwheel switch on the PDR tells the DAS what type of output data is desired. Besides intrusion alarm information, the DAS can report on raw signal data, cell threshold levels, PCCS system parameter settings, and the system profile which indicates the effect the soil is having on the cross-cable coupling.

Data can either be sent to the printer or to a chart recorder or oscilloscope depending on the type of data or the needs of the system operator.

2.3 Theoretical Operation of the PCCS System

The technology of the PCCS system is derived from narrow-band time-domain reflectometry (NBTDR), which is used in industry to test for cable discontinuities (Patterson and Mackay, 1977). NBTDR equipment allows us to measure very small changes in the reflection coefficient of a distributed cable system versus time.

Figure 2.2 shows a pictorial diagram of the main components of the PCCS

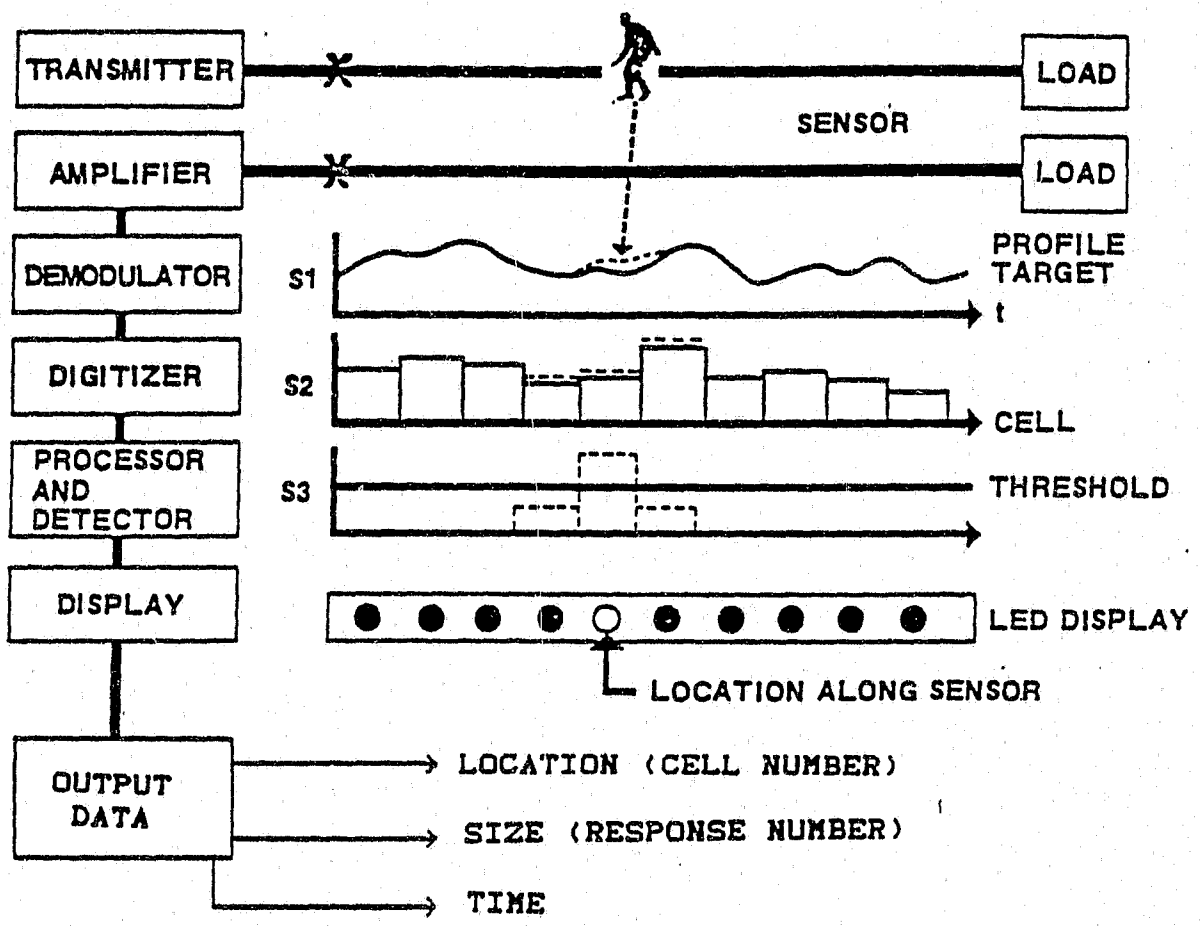

Figure 2.2 PCCS system components

system. The PCCS system consists of two parallel, buried, leaky coaxial cables which define a detection zone along which an intrusion can be sensed. One cable acts as a transmitter and the other as a receiver. The current system configuration allows for two cable- pairs, each one mile long, to be used with one PCCS system processor.

The PCCS system transmitter sends a 450 nanosecond- wide pulse of RF energy (63 MHz) down the transmitter cable. The pulse consists of the system eigenmodes whose electromagnetic fields at the receiver cable will excite eigenmodes on the receiver cable. While most of the energy coupled into the receiver cable travels downline and is absorbed by the cable termination, a small amount of the energy travels in the opposite direction back to the PCCS system receiver where the signal is amplified so that microprocessor-controlled signal processors can perform target detection routines (Harman, 1982).

The amplitude of the demodulated signal obtained from the receiver cable is monitored for changes over a short time period, with the assumption that such changes are induced by an intruder. The demodulated signal, shown as signal S1 in Figure 2.2, is termed the system profile and is relatively static over short time periods. That is, if there is no intruder, the system profile will remain unchanged for every pulse that propagates through the system.

The variation of the system profile, as a function of position along the cable, reflects the effect that variations of the permittivity and conductivity of the soil have on the transmitter electromagnetic field which is coupling to the eigenmodes on the receiver cable.

As shown in Figure 2.2, when an intruder crosses the cable-pair the electromagnetic field between the cable- pair is perturbed, resulting in a corresponding perturbation in signal S1, the system profile. Through time gating

and digitization, signal S1 is quantized into discrete levels and electronically divided into distance intervals called range cells which correspond to locations along the length of the cable-pair. The range cells are represented by signal S2 of Figure 2.2. The location of an intruder can be determined from the time gating since the propagation velocity of the pulse on the receiver cable (2.37×10^8 meters/second) is known.

The distance interval determines the resolution distance with which we can locate an intruder. Since the PCCS samples the return signal from the receiver cable once every 285.8 nanoseconds, the distance intervals are each 33.33 meters long. Thus, the entire length of the PCCS system is electronically divided into a number of 33.33 meter long cells.

The processor in the PDR will then do pulse integration, which adds up the perturbation signal in each range cell for 1024 pulses in order to magnify the perturbation signal caused by an intruder. The magnified perturbation signals are indicated by the dotted lines in S3 of Figure 2.2.

In each range cell a threshold level can be set. Any magnified perturbation signal which rises above the threshold level will cause an intrusion alarm to occur. The variable threshold setting helps to eliminate nuisance alarms by allowing the system to detect a large intruder, such as a person, while allowing small objects, such as animals, to go undetected.

As shown in Figure 2.2, when an alarm occurs the Data Acquisition System (DAS) outputs information (via a printer) recording the time of the intrusion, along with the location (cell number) and size of the intruder (response number).

2.4 Actual Operation of PCCS System

The actual operation of the PCCS system is similar to the theoretical description in the previous section although in the real situation limitations arise which reduce the ability of the PCCS to detect intrusions and screen out nuisance alarms.

The main problem deals with the system profile and the uneven sensitivity that was discussed earlier. Previous studies (Frankel et al, 1984; Miller et al, 1984) have shown that variations in the soil cause the electromagnetic coupling between the transmitter and receiver cables to be uneven as a function of position along the cables. Uneven coupling means that the sensitivity is varying with linear position as well. By uneven sensitivity, we mean that response numbers with differing magnitudes will be obtained when the same intruder crosses the system at different locations. This seriously impairs the ability of the PCCS system to accurately resolve the size of the intruder and to differentiate between humans and small animals.

Theoretically, the variable threshold setting should handle this problem. That is, in a very sensitive region of the system, where the response number for an average sized "standard person" crossing the system is very high, the threshold can be set very high. Similarly, in an insensitive region of the system, where the response number for the standard person is very low, the threshold can be set low.

In practice, however, the soil-caused variations in sensitivity occur over very short distances, while a single threshold level can only be set for each 33.33 meter cell. Therefore, we expect to find both high and low sensitivity regions within the same cell.

Previous response profile tests (Frankel et al, 1984) carried out along areas of the U.S.- Mexican border have shown that most cells do indeed contain high and

low sensitivity regions. Response profile tests are implemented by having the same standard person traverse the cable-pair at every 1 meter interval and then plotting the resulting response numbers as a function of position.

A response profile which varies significantly within the same cell means that if the threshold level for that cell is set too high then human intruders crossing at low sensitivity regions of the cell will go undetected. On the other hand, if the cell threshold level is set too low then small animals crossing the line at high sensitivity regions of the cell will set off false intrusion (i.e. nuisance) alarms.

The "response ratio" is the ratio of the highest response number in a cell to the lowest response number in the same cell, with the response numbers in both cases due to the same standard person crossing the system. In the previously mentioned border area study it was found that the average response ratio did not exceed 6:1 in 85% of the cells. That border area study also concluded that in order to set the cell thresholds so that differentiation between humans and small animals is possible, the reponse ratio should be no greater than 3:1. Therefore, for the PCCS system to be an effective detection device some method must be found which can lower the response ratio in each cell to no higher than 3:1; that is, we need to be able to lower the response profile of the high sensitivity regions while raising the response profile of the low sensitivity regions.

Since the varying response profile is assumed to be the result of the varying conductivity and permittivity of the soil, attempts have been made (Frankel et al, 1984) to lower the response ratio by the method of soil exchange. For example, to raise the response profile for a "dead" or insensitive region, the soil between and around the cables is excavated and the excavated area is then backfilled with sand. Since sand has a low conductivity and permittivity, the electromagnetic field strength between the two cables should be strong, resulting in an increased sensitivity. To

lower the response profile for a sensitive region requires the same excavation, although the replacement soil needs to be taken from an area where the response profile is known to be low.

There are several drawbacks to this method. First of all, the large quantity of soil that would need to be excavated requires the use of heavy earth-moving equipment and is a very time consuming and expensive procedure. Also, the soil to be backfilled would have to be excavated and transported as well. If the PCCS system is deployed in a remote and isolated location this will further exacerbate the logistics problem.

Second, any program involving the large-scale excavation of soil (and the piling of excess soil) will negatively impact on the environment and the natural aesthetics of the deployment area. This would be especially important should the PCCS be deployed across many miles of open countryside.

The third drawback to the soil exchange method is that there is no way to easily control or predict the effect that the soil exchange will have on the response profile. For example, backfilling an insensitive area with sand will raise the response profile, but the amount of the increase cannot be controlled or predicted. Thus, we could find that after a soil exchange the response profile might have changed by too little or too much. To lower a response profile which is too high is even more problematic since it requires finding a backfilling soil with the correct conductivity and permittivity necessary to reduce the response profile to the desired level.

If the PCCS is to be an effective intrusion detector then we need to find a relatively easy method which will allow us to change the response profile in a predictable way so that the response ratio is never greater than 3:1. The method we recommend in this paper is to adjust the cable separation distance, that is, vary the distance between the transmitter and receiver cables in order to increase or decrease

the detector sensitivity. This method will be discussed in Section 5.6 and in Chapter 6.

2.5 Advantages of PCCS Over Other Sensor Types

Since the early 1970's the U.S. Border Patrol has used a variety of electronic sensors to monitor remote areas of the international border against intrusions (Frankel et al, 1984). These sensors detect intrusions by sensing seismic, infrared or electromagnetic signals which are induced by intruders. Some examples of seismic sensors are:

1) Seismic point sensor. This device consists of a buried geophone which detects the vibration caused by a passing person, animal or vehicle. Its range of detection for a human intruder is about 50 feet.

2) Buried line intrusion detector. This device is made up of a buried grid of wires which respond to soil motion caused by vehicles or footsteps. The intruder must be on the ground surface directly above the grid to be detected. A typical grid is 20 to 40 meters in length.

3) Maid/Miles line intruder detector. This device uses a buried coaxial cable which detects variations in the soil pressure above the cable. It is used in lengths of 100 meters.

Examples of infrared or optical sensors are:

4) Infrared "line" sensor. This surface mounted device detects the change in infrared intensity caused by intruders who walk across the devices field-of-view. This device can detect human intruders at a range of up to 50 meters, line-of-sight.

5) Infrared imaging sensor. This device enables Border Patrolmen to observe

the surrounding terrain at night. The device creates an infrared-based image which is visible through a binocular-like eyepiece. It has a maximum range of detection of 2 miles, line-of-sight, assuming clear weather.

6) Low-light TV cameras. These cameras are being tested by the Border Patrol and are to be used for close range observation in the vicinity of well travelled areas such as port-of-entry inspection stations.

Examples of electromagnetic detection sensors are:

7) Magnetic point sensor. This device acts as a buried metal detector and, therefore, can detect vehicles and in some cases people who are carrying ferrous metal objects. Its maximum detection range is nominally several meters for people and about 10 meters for vehicles.

8) An AN/PPS-15 personnel detection radar. This is a short-range radar which can detect people, animals or vehicles in motion within a one mile, line-of-sight range.

As can be seen, most of the commonly used buried sensors are limited by having a very short detection range. The infrared, optical and radar sensors have a larger detection range but are limited by the requirement that the intruder be in the "line-of-sight" of the sensor's field of view. When trying to detect people in vegetated, rolling terrain this line-of-sight requirement becomes quite constraining and thus limits the usefulness of such devices.

The advantages of the PCCS system are apparent. First, the detection zone is linear which makes it the appropriate choice for monitoring intrusions across a border or security perimeter.

Second, the PCCS system can currently be deployed to monitor a 2 mile line. Not only is the PCCS system able to detect crossings over a large continuum,

without gaps in coverage in space or time, but the system can be operated night and day regardless of the weather.

Since the PCCS can detect an intrusion anywhere that the cable-pair is deployed, the PCCS detection capability can extend to any type of terrain, regardless of the topology.

Another feature of the PCCS system is its ability to pinpoint the location of an intrusion within a 33.33 meter cell. Such spatial resolution is important because of the far-reaching detection zone of the PCCS.

The last advantage of the PCCS system is one that has yet to be realized in actual applications. That is the ability of the PCCS to resolve the size of the intruder, and therefore, to be able to differentiate between human intruders and small animals. Considering that the PCCS system is being considered for deployment in remote border areas that have abundant animal life, it is obvious that the PCCS system can only be truly effective if this differentiation ability can be realized. Assuming that it can, the PCCS emerges as a cost effective, all-weather intrusion detector that can be used to pin-point the location of intruders over vast, remote areas of the border without unnecessary alarms which are due to the crossing of small animals.

CHAPTER 3

THEORETICAL ANALYSIS OF EM PROPAGATION ON TRANSMITTER CABLE

Before building the actual PCCS system test site a theoretical analysis of electromagnetic wave propagation in a buried, leaky, coaxial cable was undertaken in order to gain insights into EM wave behavior in a subsurface environment and to give us indications of phenomena to expect in the real system.

Particular emphasis was placed on identifying propagating modes and on understanding what effect the electrical properties of the soil had on them. It was also desired to know the characteristics of each mode and to see how these modes interacted with one another at the interface between soils of differing permittivities.

3.1 Cylindrical Earth Model

In the real PCCS system the ported coaxial cable is buried 9 inches below ground surface as shown in Figure 3.1.

Because the concentric regions within the cable are cylindrical while the air-soil interface is planar we see that the resulting field distributions will not be symmetric with respect to the axis of the cable. Thus, a mathematical model which uses the geometry of the real system will be quite complicated, although soluable (Wait, J.R., 1973; Richmond, 1981).

As a first step towards a theoretical understanding of EM wave propagation in a buried, leaky, coaxial cable a simpler theoretical model was developed which is

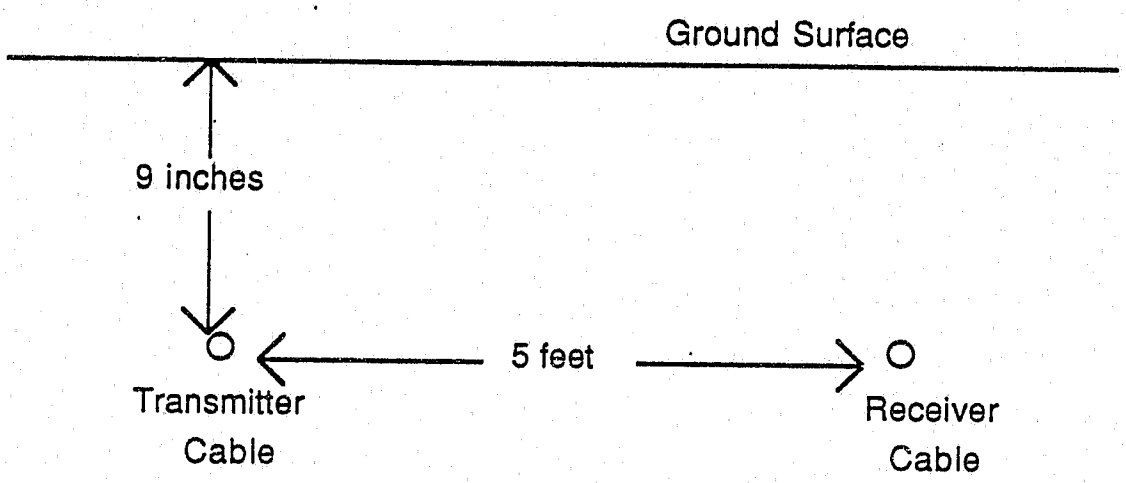

Figure 3.1 Deployment Configuration of PCCS Cable-pair

called the "cylindrical earth" model. A sketch of the model, along with the manufacturer's values for parameters, is shown in Figure 3.2. In that Figure, a is the radius of the inner conductor, b is the radius of the outer conductor, c is the radius of the cable's protective jacket, d is the radial distance to the air-soil interface, ε_{r1}, ε_{r2}, ε_{rsoil}, are the relative permittivities of the dielectric filling, cable jacket and soil, respectively, and Z_t is the transfer impedance, discussed below, of the ported coaxial cable.

The model gets its name from the fact that the soil forms a concentric cylinder around the z-directed coaxial cable. In this model the air-soil interface is not planar but rather is also cylindrical.

The cylindrical earth model was chosen for reasons of simplicity. The cylindrical shape of all regions signifies cylindrical symmetry which results in an absence of azimuthal variation (i.e. $d/d\phi = 0$, where ϕ is the azimuthal cylindrical coordinate). To further simplify matters we assume that all regions are lossless; that is, $\sigma = 0$.

Although this model is a simplification of the real problem and does not follow the actual geometry we feel that this model contains the "physics" of the real problem and therefore conclusions drawn from the results of the modeled problem are applicable to the actual situation. The quantitative results, of course, would not be applicable.

The dimensional parameters of the coaxial cable and the permittivities of the cable's internal dielectric and jacket were selected to represent those of the actual SPIRAX ported coaxial cable that is used in the GUIDAR PCCS system.

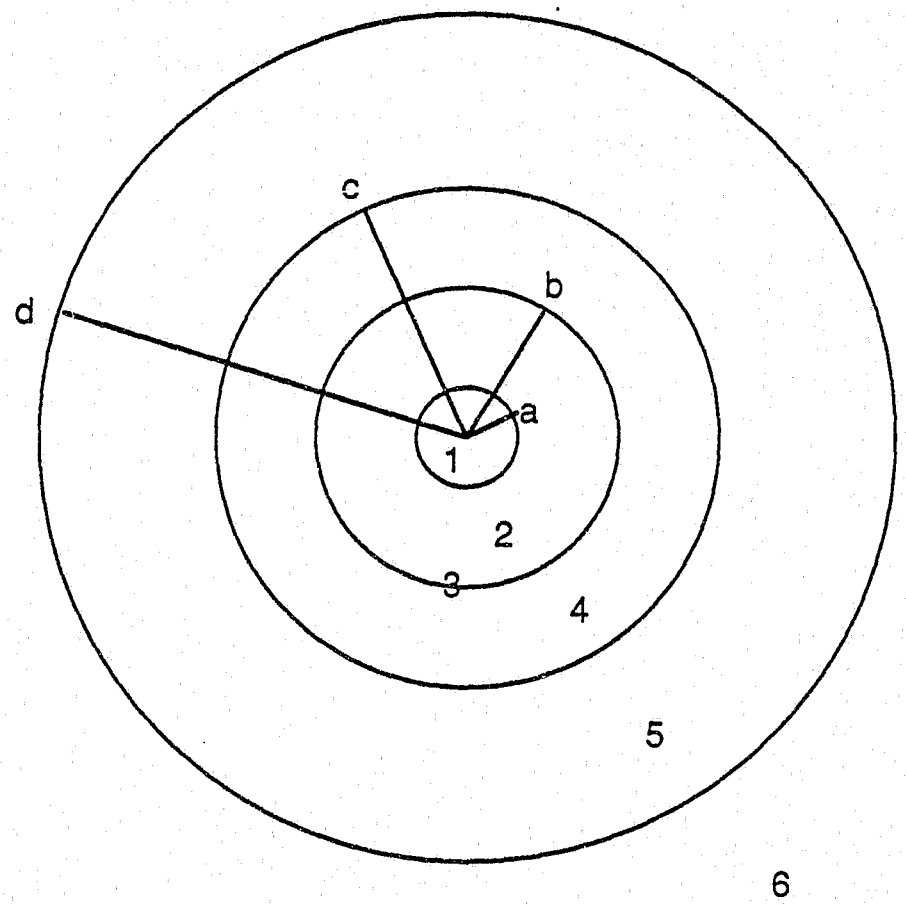

Parameters	Regions
a = 0.090 in,	1. inner conductor
b = 0.25 in.	2. dielectric
c = 0,33 in.	3. outer conductor
d = 9.0 in., 18.0 in.	4. jacket
L_t = 80 nH/m	5. soil
	6. air
f = 60 MHz	

Figure 3.2 Cylindrical Earth Model-- cross-sectional view. Relative permittivity of dielectric and jacket, 1.6 and 2.2, respectively.

The apertures in the outer conductor of the coax are modeled by the transfer impedance, Z_t, which characterizes the cable's ability to couple energy between the interior and exterior of the cable (Fernandes, 1979; Hill and Wait, 1980). Since the apertures are distributed evenly around the cable, and since the wavelength is large compared to the aperture size, it is assumed that this interior to exterior coupling does not vary with z or ϕ (i.e. axially or azimuthally). The transfer impedance not only serves as an impedance parameter but also is expressed in a form which readily lends itself to boundary value formulations.

The transfer impedance, Z_t, was first defined by Schelkunoff (1934) in an attempt to characterize the interior to exterior electromagnetic coupling that occurs even when the outer conductor of a coaxial cable is a solid tubular shield. This is due to the outer conductor being an imperfect conductor with a defined skin depth.

Delogne and Safak (1975) have extended the concept of transfer impedance to cover intentionally "leaky" coaxial cables which have been developed to meet the needs of modern communications and guided radar security applications. The transfer impedance is defined as the axial electric field, E_z, in the thin outer conductor of a coaxial cable divided by the current, I, flowing through that conductor. An assumption of the model is that E_z does not vary radially within the outer conductor, as if that conductor were very thin compared to the skin depth. Thus, E_z is continuous from the inside to the outside of the conductor. We thus obtain

$$Z_t = \frac{E_z}{I} \Big|_{r=b} \tag{3.1}$$

where b = radius of outer conductor.

In the case of a coaxial cable's outer conductor, the surface current density, J_S, can be expressed as

$$J_S = n \times (H_2 - H_1) \tag{3.2}$$

where n is the normal unit vector, and H_1 and H_2 are the magnetic fields on either side of the outer conductor at r = b. Equation 3.2 can be used to obtain the current flowing through the outer conductor as

$$I = 2\pi r[H_{\phi 2}(r) - H_{\phi 1}(r)] \Big|_{r=b} \tag{3.3}$$

where $H_{\phi 1}$ is the ϕ-component of the magnetic field in the dielectric, and $H_{\phi 2}$ is the o/-component of the magnetic field exterior to the outer conductor, both evaluated at r = b.

It therefore follows that the transfer impedance of the outer conductor is

$$Z_t = \frac{E_z(r)}{2\pi r\left[H_{\phi 2}(r) - H_{\phi 1}(r)\right]} \Big|_{r=b} \tag{3.4}$$

For boundary condition applications this can be rewritten as

$$H_{\phi 2}(b) - H_{\phi 1}(b) = \frac{E_z(b)}{2\pi b Z_t} \tag{3.5}$$

To find Z_t explicitly for a SPIRAX ported coaxial cable we use M. Maki's (1984) formulation as follows:

$$Z_t = Z_d + jwL_t \tag{3.6}$$

where Z_d is the diffusion impedance, ω is the angular frequency, and L_t is the inductive component of the transfer impedance. Z_d varies with the skin depth of the outer conductor and thus varies with frequency.

At increasingly higher frequencies the skin depth becomes increasingly small, thus the conductor becomes a better shield to block energy leakage and electromagnetic coupling. Therefore, at high frequencies Maki shows that Z_d becomes negligible, and we are left with the inductive ($j\omega L_t$) term to evaluate Z_t. This agrees with the findings of Wait and Hill (1977).

For SPIRAX ported coaxial cable, Maki has developed a formula (Maki, 1984) for evaluating Z_t at high frequencies:

$$Z_t \approx j\omega L_t \tag{3.7}$$

where

$$L_t = \frac{\pi\mu A^{3/2} e^2}{6n\left[E(e) - (1 - e^2)K(e)\right]} \qquad \text{for } \theta < 45^\circ \qquad (3.8)$$

A = fractional coverage of apertures in outer conductor

n = number of copper tapes in outer conductor

$$e = \sqrt{1 - \tan^2\theta}$$

θ = pitch angle of wound copper tapes in outer conductor

and K(e) and E(e) are complete elliptic integrals of the 1st and 2nd kind, respectively.

Using this formulation (equation 3.8) for the SPIRAX cable used at the PCCS test site, yields a value of

$$Z_t = 80 \text{ nH/m} \qquad (3.9)$$

3.2 Eigenmodes of the Cylindrical Model

In the real PCCS system the transmitted, pulsed signal is sent to the ported coaxial cable via a "lead-in" section of non-ported coaxial cable. Since this "lead-in" is a standard coax, this implies that the electromagnetic wave in the "lead-in" is propagating in a TEM field configuration. A TEM wave is azimuthally symmetric (i.e. $d/d\phi = 0$) and only the E_r and H_ϕ field components are present.

At the cable transition between the "lead-in" coaxial cable and the ported coax, the TEM wave will excite modes with the same azimuthal symmetry, and similar field components. An azimuthally symmetric TM wave is similar to a TEM wave except for the addition of E_z, the axially directed component of the electric field. It is well known that strong coupling will occur between two modes with similar electromagnetic field configurations. Thus, we would expect that the TEM wave propagating in the "lead-in" cable is transformed into a TM wave (with azimuthal symmetry) in the ported cable (Harman, 1982). It is for this reason that we assume only TM waves with azimuthal symmetry in our model.

To find the eigenmodes in the cylindrical model, we, as usual, solve the wave equation in each dielectric region. The z-dependence of all field components is $e^{-\gamma z}$, where γ is the complex propagation constant for the eigenmode, and

$$\gamma = \alpha + j\beta \tag{3.10}$$

The radially dependent part of the TM field components (E_r, E_z and H_ϕ) for each concentric region can be represented by either Bessel functions (J_n and Y_n) or Modified Bessel functions (I_n and K_n) depending on whether the magnitude of the assumed propagation constant, β, is smaller or larger than the wave number, k, in each dielectric region, where

$$k = \omega\sqrt{\mu\varepsilon} = \frac{\omega}{c}\sqrt{\varepsilon_r} \tag{3.11}$$

where μ is the permeablility, ε is the permittivity, and ε_r is the relative permittivity.

We may find β by solving the standard boundary value problem. In the usual way, E_z and H_ϕ are continuous at all boundaries except at r = b where the transfer impedance condition (equation 3.5) is applied. This process leads to a determinental equation for γ and the known constants of the system. This equation will have the form

$$G(\gamma, a, b, c, d, \varepsilon_{r1}, \varepsilon_{r2}, Z_t, \sigma_{soil}, \varepsilon_{rsoil}) = 0 \qquad (3.12)$$

Solving this equation for γ will yield a set of complex propagation constants, γ's,

$$\gamma_1, \gamma_2, \gamma_3 \cdots$$

all of which correspond to the azimuthally symmetric TM modes (the eigenmodes) that the wave guiding structure will support. Because $\sigma_{soil} = 0$, we have two cases:

Case 1) $\gamma_n = j\beta_n$, which corresponds to propagating modes; and

Case 2) $\gamma_n = \alpha_n$, which corresponds to cut-off modes.

The cut-off modes are assumed to have little stored energy in them, and will therefore be neglected. We thus concentrate on the propagating TM modes and their corresponding propagation constants, $\beta_1, \beta_2, \beta_3$, etc. Once the propagation constants are known, the coefficients in the field component expressions can be determined thus giving us the explicit field component expressions.

It should be noted that in the computational analysis done for the cylindrical earth model, the soil was assumed to be lossless, that is, $\sigma_{soil} = 0$. When we were interested in the effects of lossy soil we used the approximation

$$\alpha \approx \frac{W_L}{2W_T} \quad \text{meters}^{-1} \tag{3.13}$$

where

$$W_T = \frac{1}{2}\int_S \text{Re } E \times H^* \, ds \quad \text{watts} \tag{3.14}$$

$$W_L = \frac{1}{2}\int_S E \cdot J^* \, ds = \sigma_{soil}\int_S \frac{1}{2}|E|^2 \, ds \quad \frac{\text{watts}}{\text{meter}} \tag{3.15}$$

and $$J = \sigma E \tag{3.16}$$

This approximation (3.13) is valid as long as σ_{soil} does not significantly perturb E and H from their $\sigma_{soil} = 0$ values. For some very lossy eigenmodes, this approximation may be poor. Since quantitative results are not important for our purposes, we ignore the poor approximation.

3.3 Three Eigenmodes of Propagation

Following the analysis described above, the Cylindrical Earth Model was found to support 3 distinct propagating mode types. We call these 3 mode types the Transmission Line mode, Goubau mode, and Surface Wave mode. Figure 3.3 shows the β vs. frequency variation for all 3 mode types for a relative soil permittivity of 25.

Eigenmode 1 is called the Surface Wave mode and is the mode corresponding to the propagation constant, β_1 . This mode type is unique in that it has a cut-off frequency. That is, the mode only exists for frequencies above f cut-off. Furthermore, both Figures 3.3 and 3.4 show that there is a hierarchy of Surface Wave modes, each being characterized by a higher cut-off frequency.

Figure 3.4 shows the β vs. frequency variation for a relative soil permittivity of 50. Notice that increased permittivity results in lowering the cut-off frequencies for the higher order Surface Wave modes. Therefore, at f = 60 MHz

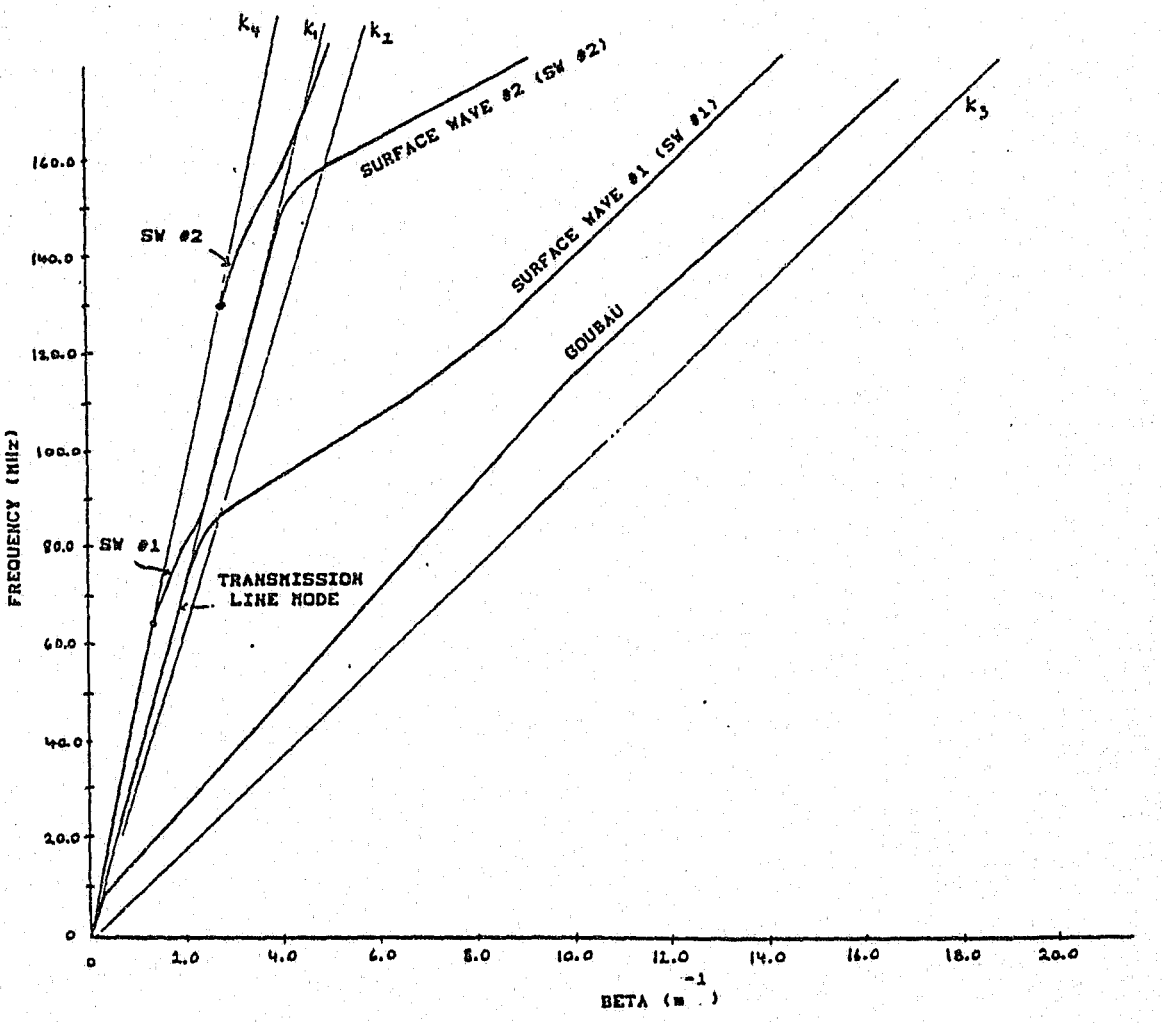

Figure 3.3 Frequency versus propagation constant for three mode types supported by Cylindrical Earth Model. Relative permittivity of the soil is 25. k is wave number in corresponding region denoted by subscript.

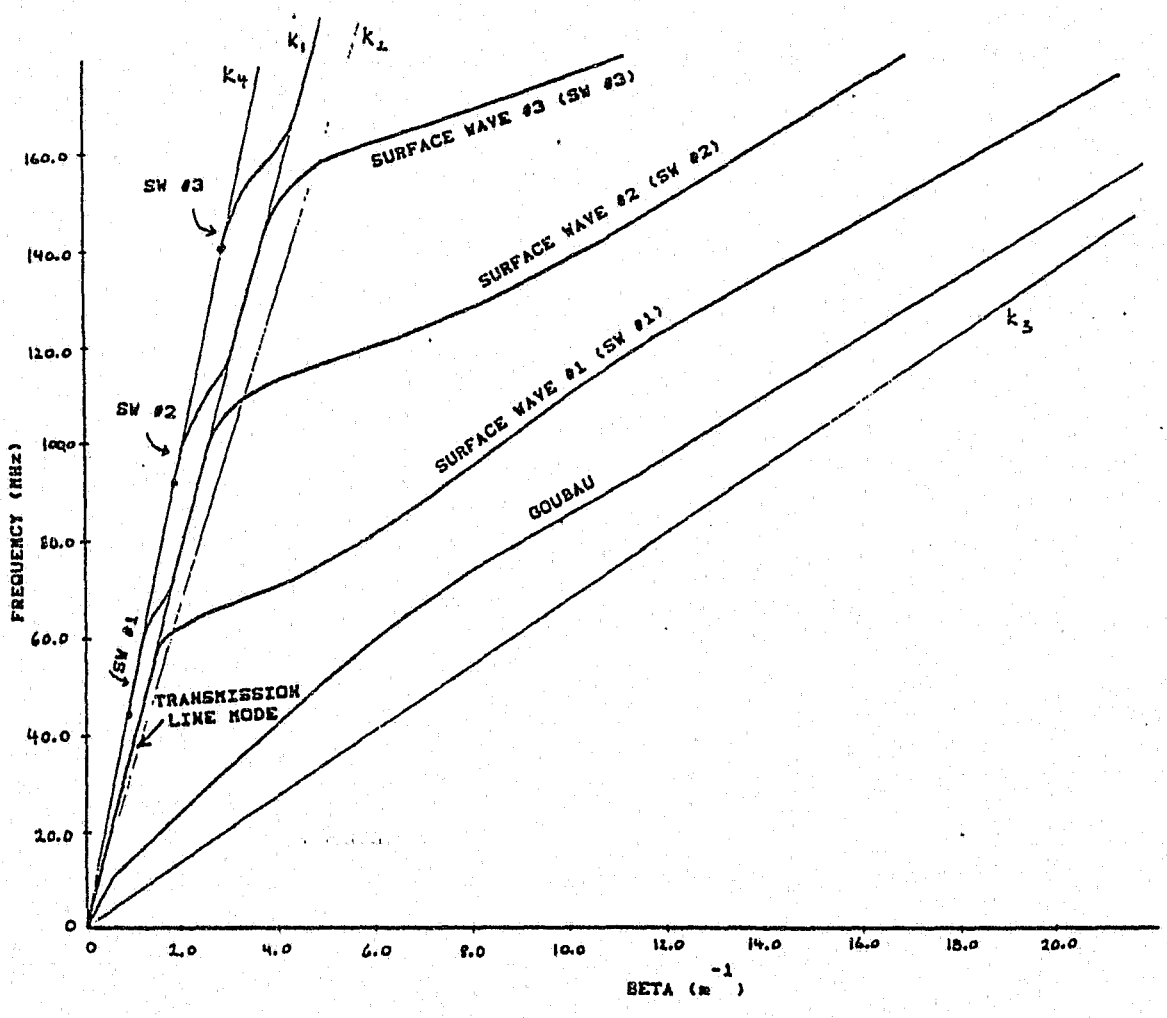

Figure 3.4 Frequency versus propagation constant for three mode types supported by Cylindrical Earth Model. Relative permittivity of the soil is 50. K is wave number is corresponding region denoted by subscript.

and $\varepsilon_{rsoil} = 50$, there will be a propagating Surface Wave mode while for $\varepsilon_{rsoil} = 25$, the Surface Wave will be in a cut-off condition.

Figure 3.5 shows the energy density of the Surface Wave mode as a function of radial distance from the inner conductor. The origin of the graph represents the outer edge of the inner conductor, b represents the outer edge of the dielectric filling, c is the outside of the cable's protective jacket, and d is the air-soil interface.

We see that the energy density of the Surface Wave mode decreases as a function of radial distance away from the inner conductor. It is interesting to note that for propagation in the soil (between points c and d in Figure 3.5) the energy density in the soil becomes greater when the wave enters the lower permittivity of section 2.

Eigenmode 2 is called the Goubau mode and is the mode characterized by the propagation constant, β_2. As shown in Figures 3.3 and 3.4, the Goubau mode, unlike the Surface Wave mode, has a zero cut-off frequency. That is, the Goubau mode will exist at all frequencies. In addition, regardless of the frequency, there will only be a single, unique Goubau mode and not a hierarchy of Goubau modes. Figure 3.6 shows that most of the energy in the Goubau mode is concentrated exterior to the outer conductor with the energy density maximum in the jacket of the cable. The energy density then drops down in the soil and falls off quite rapidly in the air region.

This mode is named after G. Goubau because it was he who showed that

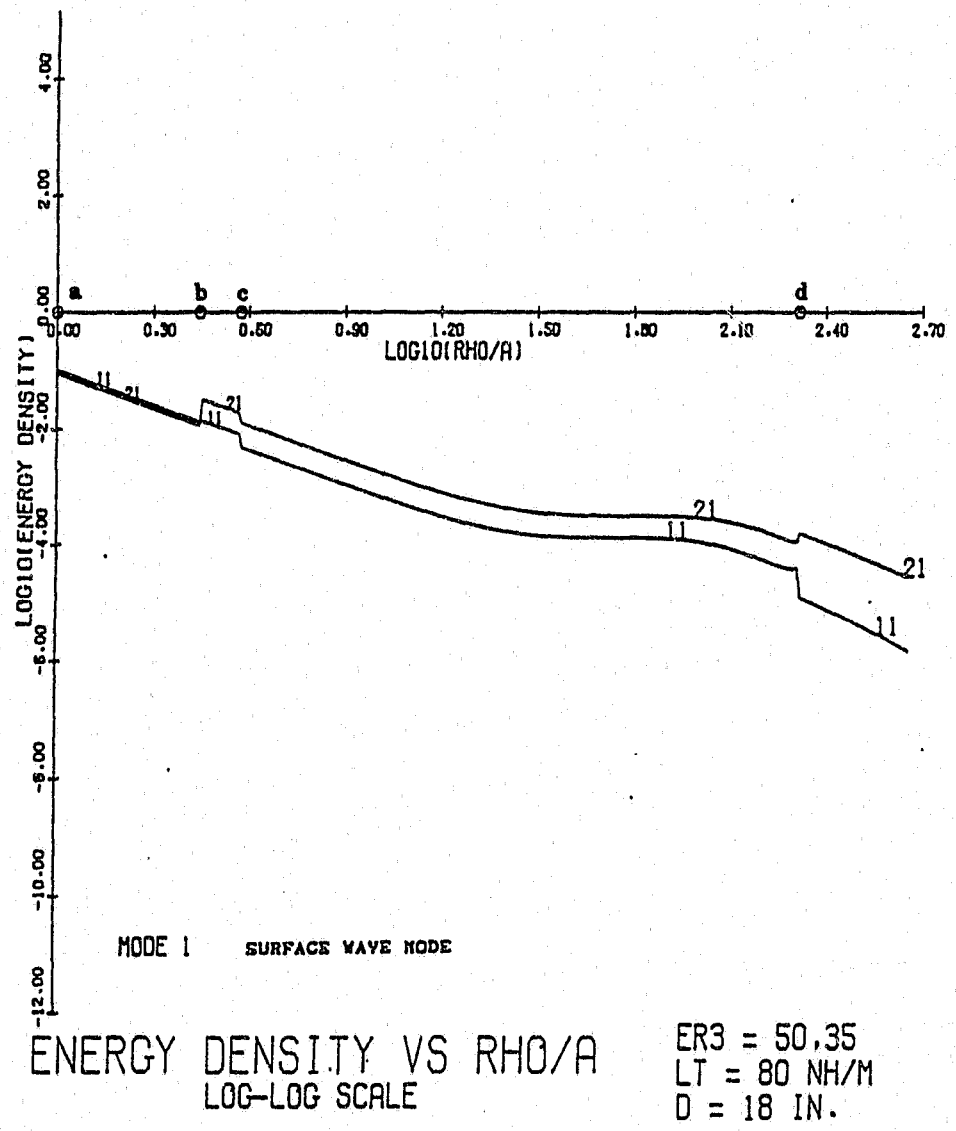

Figure 3.5 Energy density versus radial distance from inner conductor of ported coaxial cable for Surface Wave in Cylindrical Earth Model. Rho/A is radial distance normalized to radius of inner conductor, a. a to b is cable's dielectric filling; b to c is protective jacket; c to d is soil region; beyond d is air region. Curves 11 and 21 are for soils with a relative permittivity of 50 and 35, respectively.

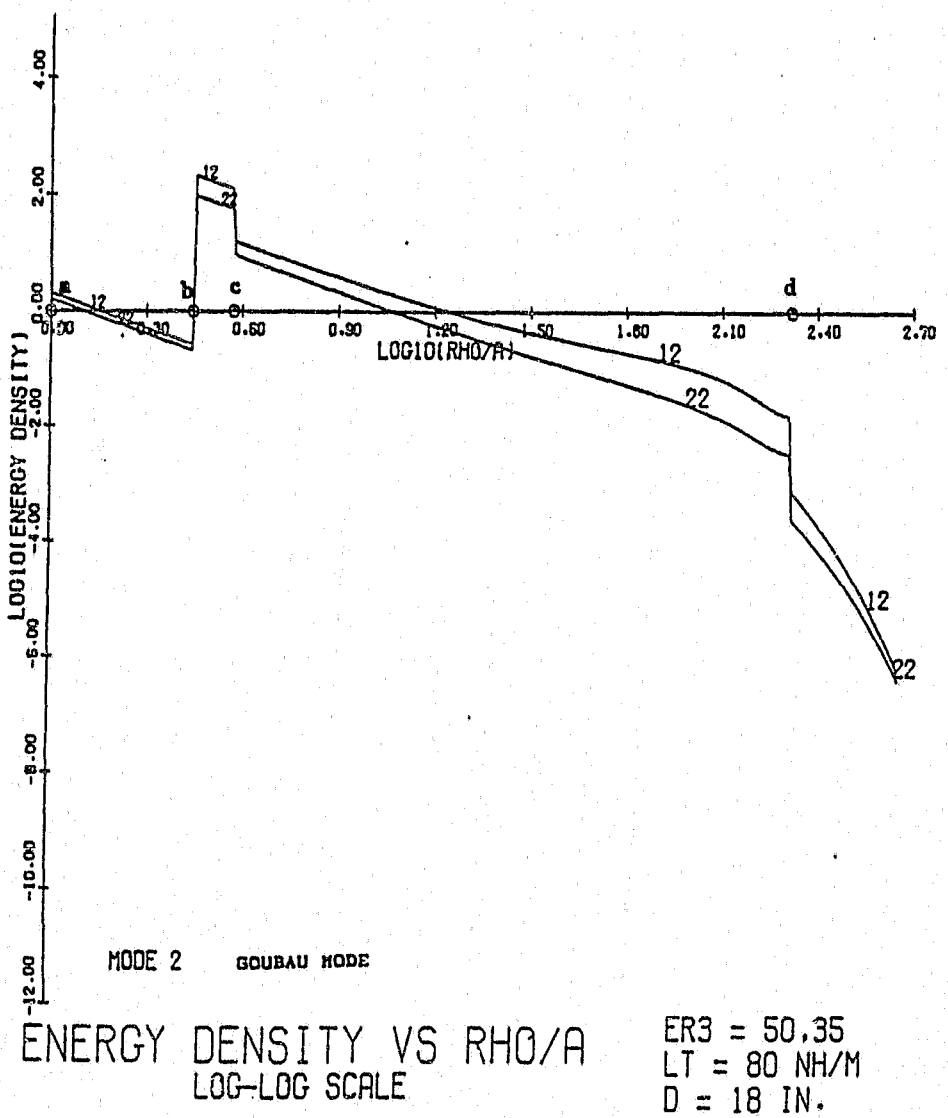

Figure 3.6 Energy density versus radial distance from inner conductor of ported coaxial cable for Goubau mode in Cylindrical Earth Model. Rho/A is radial distance normalized to radius of inner conductor, a. a to b is cable's dielectric filling; b to c is protective jacket; c to d is soil region; beyond d is air region. Curves 12 and 22 are for soils with a relative permittivity of 50 and 35, respectively.

surface waves could be guided by a thin dielectric coating on a conducting wire (Goubau, 1950).

Eigenmode 3 is the Transmission Line mode and is characterized by a propagation constant, β_3, which is very close to the wave number, k, where

$$k = \omega\sqrt{\mu\varepsilon}$$

for the dielectric filling region of the coaxial cable. This mode is called the Transmission Line mode because, as Figure 3.7 shows, most of the energy in the mode is found within the coaxial cable. In fact, in a non-ported coaxial cable this mode becomes the usual TEM mode.

Like the Goubau mode, the Transmission Line Mode has a zero cut-off frequency. Also, there is no hierarchy of Transmission Line modes; that is, for all frequencies there exists only one Transmission Line mode.

It is interesting to observe, in Figures 3.3 and 3.4, that the w vs. β curves for the Transmission Line and Surface Wave mode characteristics never cross. Near 60 MHz the Transmission Line mode becomes the Surface Wave mode and vice versa. This is repeated at higher frequencies at points where the curves would be expected to cross.

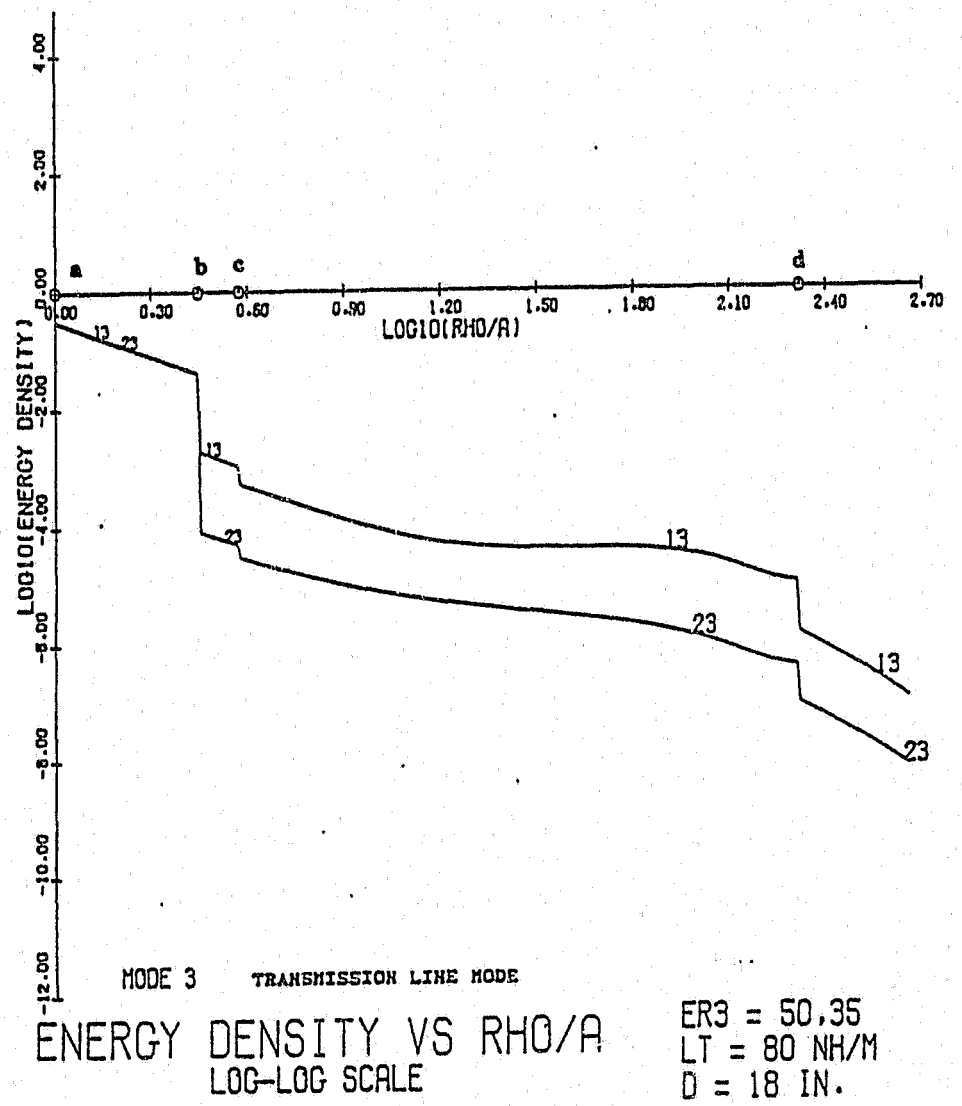

Figure 3.7 Energy density versus radial distance from inner conductor of ported coaxial cable for Transmission Line mode in Cylindrical Earth Model. Rho/A is radial distance normalized to radius of inner conductor, a. a to b is cable's dielectric filling. a to b is protective jacket; c to d is soil region; beyond d is air region. Curves 13 and 23 are for soils with a relative permittivity of 50 and 35, respectively.

3.4 Coupled Mode Theory

In subsequent sections it will become necessary to show that the Transmission Line mode, Surface Wave mode, and Goubau mode all obey the following orthonormal relations:

$$\int_S \frac{H_{\phi i} H_{\phi j}}{\varepsilon P_i P_j} ds = \delta_{ij} \quad \text{and} \quad \int_S \frac{\omega^2 \varepsilon E_{ri} E_{rj}}{P_i P_j \beta_i \beta_j} ds = \delta_{ij} \qquad (3.17\ a,b)$$

where i,j = modes, for i,j = 1 (Surface Wave mode), 2 (Goubau mode), 3 (Transmission Line mode); ε is the permittivity, and δ is the Kronecker delta, with

$$\delta_{ij} = 1 \text{ for } i = j \qquad (3.18a)$$

$$\delta_{ij} = 0 \text{ for } i \neq j \qquad (3.18b)$$

P is the axially dependent part of the field component of the subscripted mode, e.g., $e^{-j\beta z}$. Thus, H_ϕ/P_i is a function dependent only on r; hence the integrands in (3.17 a, b) are only functions of r. Note that ε is a function of r also, where

$$\varepsilon = \varepsilon_1 \quad \text{for } a < r < b$$
$$\varepsilon = \varepsilon_2 \quad \text{for } b < r < c$$
$$\varepsilon = \varepsilon_{soil} \quad \text{for } c < r < d$$

and $\varepsilon = \varepsilon_0$ for $r > d$

The integrals in (3.17 a,b) are surface integrals where the surface s is the entire cross-section of the model system from $r = 0$ to r approaching infinity.

A mathematical proof of these orthogonality relations will be found in Appendix A of this thesis.

3.5 Coupled Mode Theory at Interface

We now wish to examine the behavior of the dominant TM Transmission Line mode as it propagates in the positive z-direction and is incident on an interface between two soil sections with different permittivities as shown in Figure 3.8.

When discussing EM field components or model parameters for the two-soil-section model, the following convention will be used: the component or parameter will be double-subscripted; the first subscript will indicate the soil section, the second subscript will indicate the mode.

As the TM Transmission Line mode passes through the interface, the wave is scattered into all possible TM modes in each soil section. In soil section 1 the scattered waves are reflected waves while in soil section 2 they are transmitted waves.

We will neglect any cut-off modes because they contain very little energy, and their amplitudes will be small compared with the amplitudes of the propagating modes.

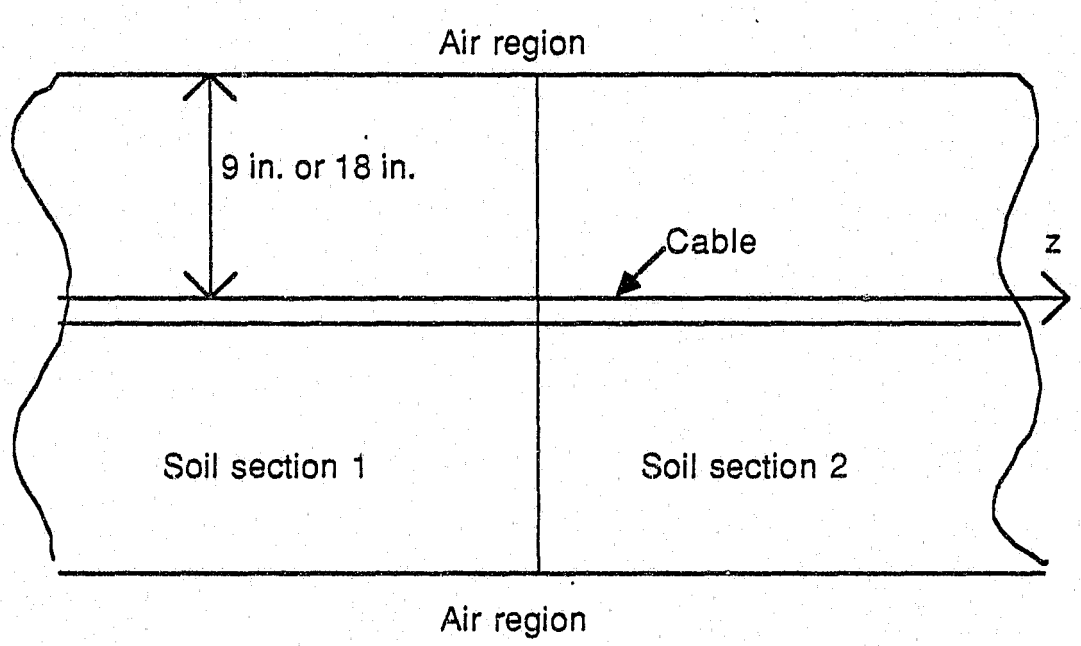

Figure 3.8 Axial view of two-section model

Therefore, we assume that the incident TM Transmission Line mode will set up reflected and transmitted Transmission Line, Surface Wave, and Goubau modes in each soil section. Such a situation is shown in Figures 3.9 and 3.10, for the radial electric field and the azimuthal magnetic field, respectively.

The rest of this section will describe this situation mathematically and will solve for the reflection and transmission coefficients (Γ_1, Γ_2, Γ_3, T_1, T_2 and T_3) for each mode. In order to solve for these coefficients we will need to apply the orthogonality relationship of the different modes that was discussed in the previous section.

3.5.1 Reflection and Transmission Coefficients

For the TM case (with azimuthal symmetry), we have only three field components: E_r, E_z, and H_ϕ. Figure 3.9 shows the reflected and transmitted components of the different modes which result when the radial electric field is incident on the interface between the two soil sections. Note that the radial electric field is tangential to the interface.

For $z < 0$,

$$E_{r1} = AE_{r13} + \Gamma_1 E_{r11} + \Gamma_2 E_{r12} + \Gamma_3 E_{r13} \qquad (3.19)$$

For $z > 0$,

$$E_{r2} = T_1 E_{r21} + T_2 E_{r22} + T_3 E_{r23} \qquad (3.20)$$

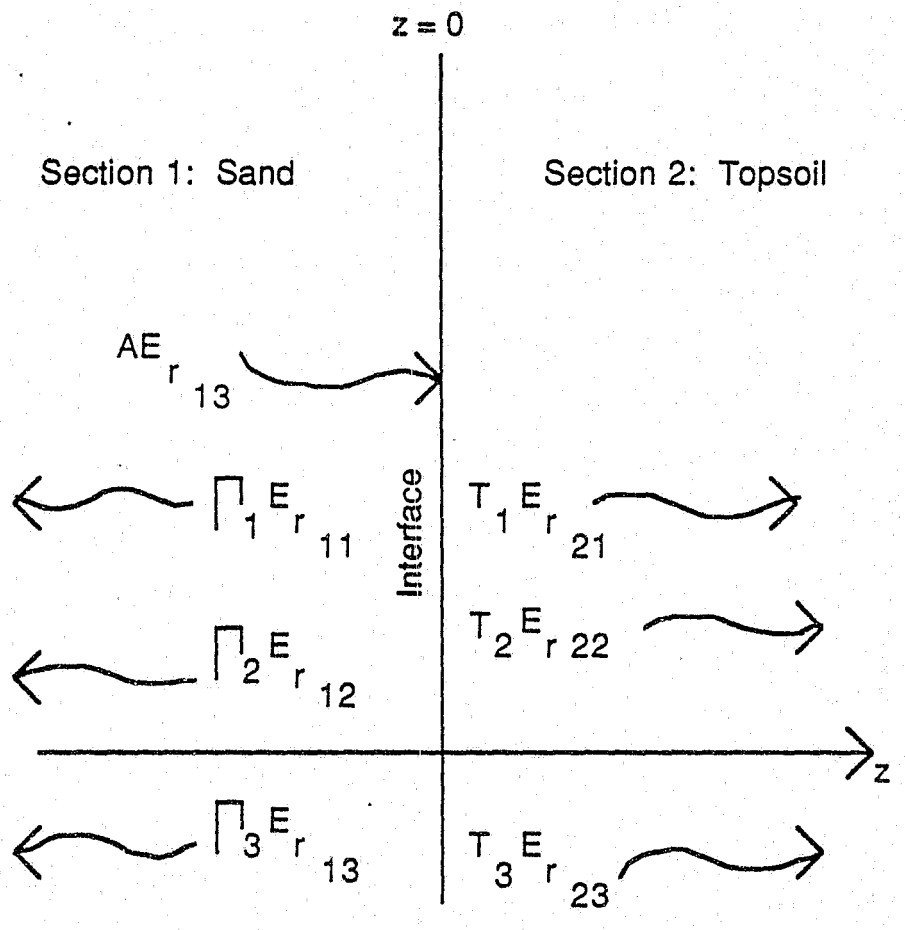

Figure 3.9 Reflected and transmitted components of multimode radial electric field, at interface between two soil sections (first subscript), for three modes (second subscript).

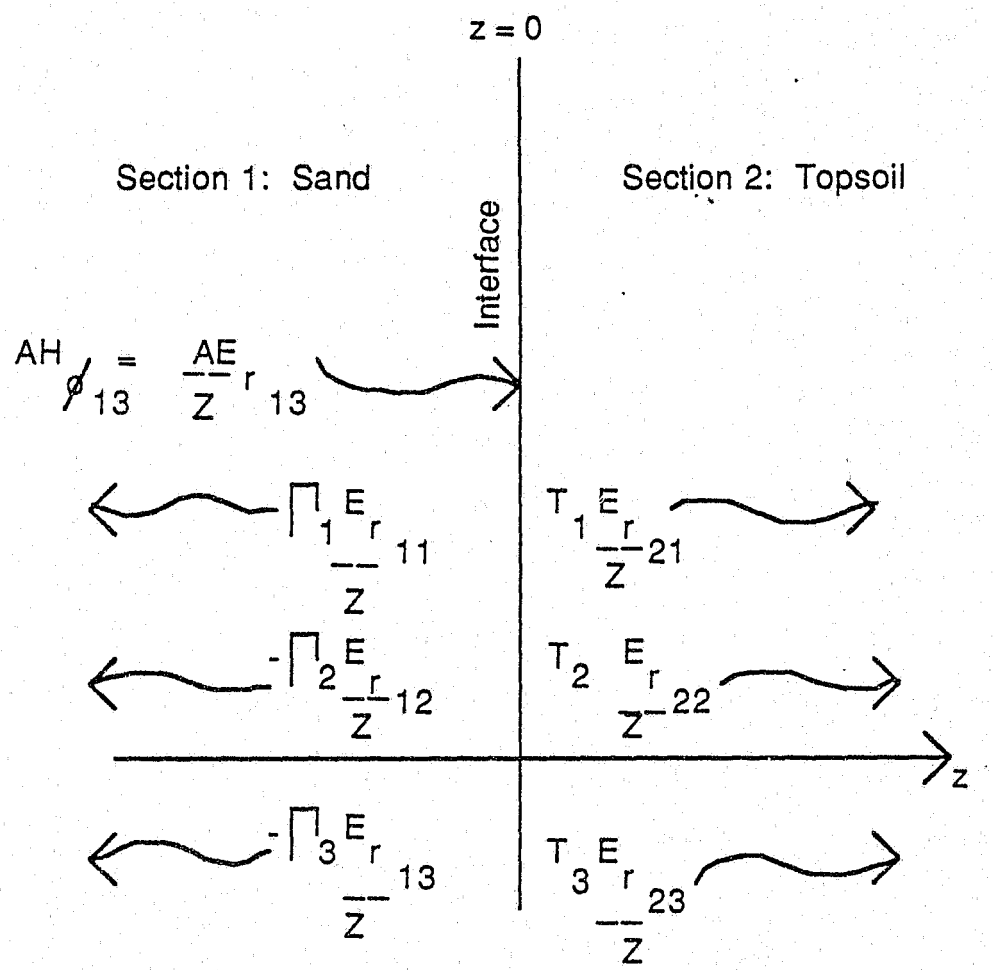

Figure 3.10 Reflected and transmitted components of multimode radial magnetic field, at interface between two soil sections (first subscript), for three modes (second subscript).

Now, for the TM case we use Maxwell's Equations to obtain

$$\frac{E_r}{H_\phi} = \begin{cases} \dfrac{\beta}{\omega\varepsilon} & \text{for a wave in the +z direction} \quad (3.21) \\ \dfrac{-\beta}{\omega\varepsilon} & \text{for a wave in the -z direction} \quad (3.22) \end{cases}$$

If we define $\beta / \omega\varepsilon = Z$ for the TM case, then we can write

$$H_\phi = \pm E_T / Z \qquad (3.23)$$

where the plus sign is for a +z directed wave and the minus sign is for a -z directed wave.

Thus, for the magnetic field, we have the following configuration of reflected and transmitted components as shown in Figure 3.10.

Thus, for $z < 0$,

$$H_{\phi 1} = A\frac{E_{r13}}{Z_{13}} - \Gamma_1\frac{E_{r11}}{Z_{11}} - \Gamma_2\frac{E_{r12}}{Z_{12}} - \Gamma_3\frac{E_{r13}}{Z_{13}} \qquad (3.24)$$

and for $z > 0$ we have

$$H_{\phi 2} = T_1\frac{E_{r21}}{Z_{21}} + T_2\frac{E_{r22}}{Z_{22}} + T_3\frac{E_{r23}}{Z_{23}} \qquad (3.25)$$

Let

$$E_r = R(r)\, e^{\pm j\beta z} \tag{3.26}$$

$$H_\phi = \frac{R(r)}{Z} e^{\pm j\beta z} \tag{3.27}$$

We assume that the radially dependent part of the field component, R(r), is known for all eigenmodes in soil section 1 as denoted by R_{11}, R_{12} and R_{13}.

We also assume that R(r) is known for all eigenmodes in soil section 2 as denoted by R_{21}, R_{22} and R_{23}.

We further assume, from orthogonality, that

$$\int_{a_1}^{\infty} \varepsilon_m R_{mi} R_{mj} 2\pi r\, dr = 0 \qquad \text{for } i \neq j \tag{3.28}$$

Let $R'_{mn} = A_{mn} R_{mn}$ (3.29)

where A_{mn} is the amplitude of the incident wave, so that

$$\int_{al}^{\infty} \varepsilon_m R'^{2}_{mn} 2\pi r\, dr = A^2_{mn} \int_{al}^{\infty} R^2_{mn} 2\pi r\, dr \equiv 1 \tag{3.30}$$

Therefore,

$$A_{mn} = \left[\int_{a1}^{\infty} R_{mn}^2 2\pi r \, dr \right]^{\frac{-1}{2}} \tag{3.31}$$

Thus, for m = 1,2 and n = 1,2,3 there are 6 A's. Use R'_{mn} henceforth and drop the prime. Then we obtain

$$\int_{a1}^{\infty} \varepsilon_m R_{mi} R_{mj} 2\pi r \, dr = \delta_{ij} \tag{3.32}$$

Since E_T is continuous at z = 0 it follows from equations 3.19, 3.20 and 3.26 that

$$R_{13} + \Gamma_1 R_{11} + \Gamma_2 R_{12} + \Gamma_3 R_{13} = T_1 R_{21} + T_2 R_{22} + T_3 R_{23} \tag{3.33}$$

Also, since H_ϕ is continuous at z = 0 we have

$$\frac{R_{13}}{Z_{13}} - \Gamma_1 \frac{R_{11}}{Z_{11}} - \Gamma_2 \frac{R_{12}}{Z_{12}} - \Gamma_3 \frac{R_{13}}{Z_{13}} = T_1 \frac{R_{21}}{Z_{21}} + T_2 \frac{R_{22}}{Z_{22}} + T_3 \frac{R_{23}}{Z_{23}} \tag{3.34}$$

$$\text{Note that } Z_{m,n} = \frac{\beta_{m,n}}{\omega \varepsilon_m} \tag{3.35}$$

If we multiply each term in (3.33) by $\varepsilon_2 R_{2n}$ (where n = 1, 2, 3) and integrate over s (the cross-sectional surface of the concentric regions) we obtain $T_n =$

$$\int_s \varepsilon_2 R_{13} R_{2n}\, ds + \Gamma_1 \int_s \varepsilon_2 R_{11} R_{2n}\, ds + \Gamma_2 \int_s \varepsilon_2 R_{12} R_{2n}\, ds + \Gamma_3 \int_s \varepsilon_2 R_{13} R_{2n}\, ds \tag{3.36}$$

Note that orthogonality has eliminated two terms on the right side. If we now multiply each term in (3.34) by R_{2n} (where n = 1, 2, 3), integrate over s, and use (3.35), we get

$$\int_s R_{13} R_{2n} \frac{\omega \varepsilon_1}{\beta_{13}}\, ds - \int_s \Gamma_1 R_{11} R_{2n} \frac{\omega \varepsilon_1}{\beta_{11}}\, ds - \int_s \Gamma_2 R_{12} R_{2n} \frac{\omega \varepsilon_1}{\beta_{12}}\, ds$$

$$- \int_s \Gamma_3 R_{13} R_{2n} \frac{\omega \varepsilon_1}{\beta_{13}}\, ds = T_n \frac{\omega}{\beta_{2n}} \tag{3.37}$$

(3.36) can be regrouped as

$$\Gamma_1 \int_s \varepsilon_2 R_{11} R_{2n}\, ds + \Gamma_2 \int_s \varepsilon_2 R_{12} R_{2n} ds + \Gamma_3 \int_s \varepsilon_2 R_{13} R_{2n} ds$$

$$- T_n = -\int_s \varepsilon_2 R_{13} R_{2n} ds \tag{3.38}$$

or, using more compact notation,

$$\Gamma_1 a_{1n} + \Gamma_2 a_{2n} + \Gamma_3 a_{3n} - T_n = -e_n \qquad (3.39)$$

(3.37) can be regrouped as

$$\Gamma_1 \int_s R_{11} R_{2n} \frac{\omega\varepsilon}{\beta_{11}} ds + \Gamma_2 \int_s R_{12} R_{2n} \frac{\omega\varepsilon_1}{\beta_{12}} ds + \Gamma_3 \int_s R_{13} R_{2n} \frac{\omega\varepsilon_1}{\beta_{13}} ds$$

$$+ T_n \frac{\omega}{\beta_{2n}} = \int_s R_{13} R_{2n} \frac{\omega\varepsilon_1}{\beta_{13}} ds \qquad (3.41)$$

(3.40)

or

$$\Gamma_1 b_{1n} + \Gamma_2 b_{2n} + \Gamma_3 b_{3n} + T_n \frac{\omega}{\beta_{2n}} = h_n \qquad (3.41)$$

Equations 3.39 and 3.40 can be written in matrix form as:

$$\begin{bmatrix} a11 & a21 & a31 & -1 & 0 & 0 \\ a12 & a22 & a32 & 0 & -1 & 0 \\ a13 & a23 & a33 & 0 & 0 & -1 \\ b11 & b21 & b31 & \omega/\beta_{21} & 0 & 0 \\ b12 & b22 & b32 & 0 & \omega/\beta_{22} & 0 \\ b13 & b23 & b33 & 0 & 0 & \omega/\beta 23 \end{bmatrix} \begin{bmatrix} \Gamma_1 \\ \Gamma_2 \\ \Gamma_3 \\ T_1 \\ T_2 \\ T_3 \end{bmatrix} = \begin{bmatrix} -e_1 \\ -e_2 \\ -e_3 \\ h_1 \\ h_2 \\ h_3 \end{bmatrix} \qquad (3.42)$$

This matrix equation can be solved for the reflection and transmission coefficients because integrands of all integrals contain known quantities.

3.6 Interference Patterns

Once the reflection and transmission coefficients for the total radially-directed electric field and total azimuthally-directed magnetic field (Equations 3.19, 3.20, 3.24 and 3.25) have been determined, we then have explicit expressions for the total radial electric field and azimuthal magnetic field for both soil sections. We can then investigate how the 3 modes interact with one another at the interface between the two soils.

From Figures 3.3 and 3.4 we saw that in a soil with a relative permittivity lower than 30, only the Transmission Line and Goubau modes will exist at frequencies near 60 MHz. Figure 3.11 shows the interaction of these two modes at the interface, for the case where the relative permittivity of the soil is 25 for section 1, 12 for section 2, and the conductivity of the soil is 10 mmhos/meter.

Notice that the interaction between the two modes causes an interference pattern at the interface. For this case, the distance between adjacent extrema on the interference pattern is about 6 meters. After about 20 meters the interference pattern dies out (as the Goubau mode dies out) leaving only the slowly attenuating Transmission Line mode.

Figure 3.12 shows the interference pattern which occurs at the interface between soils with relative permittivities of 50 and 35. At 60 MHz, these permittivities will support a Surface Wave mode, in addition to the Transmission Line and Goubau modes. In this case, the slow attenuation of the Surface Wave

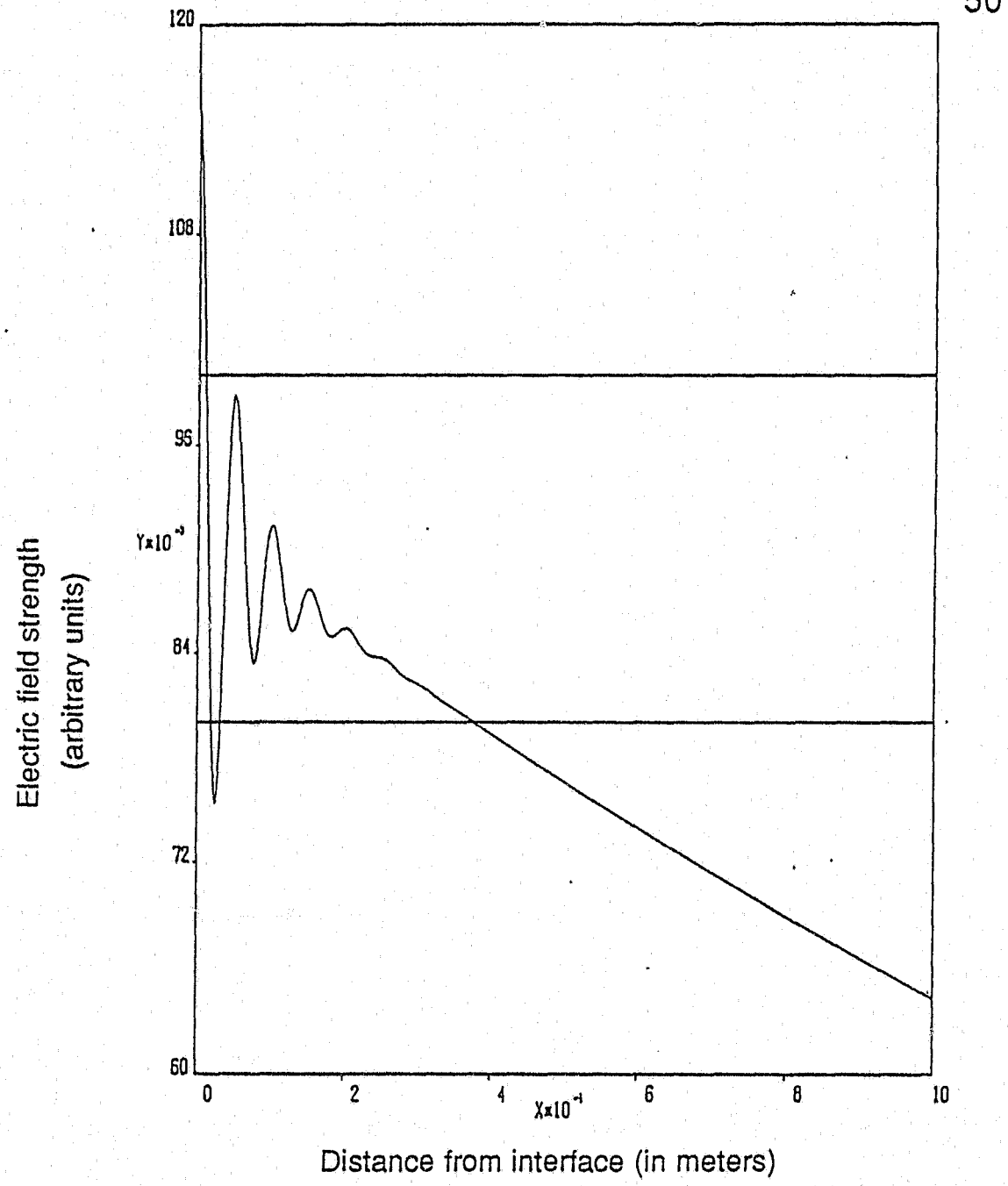

Figure 3.11 Interference pattern resulting from interaction between Transmission Line mode and Goubau mode at interface between two soil sections in Cylindrical Earth Model. d = 9 inches, f = 60 MHz, L_t = 80 nH/m, and relative permittivity of soil is 12.

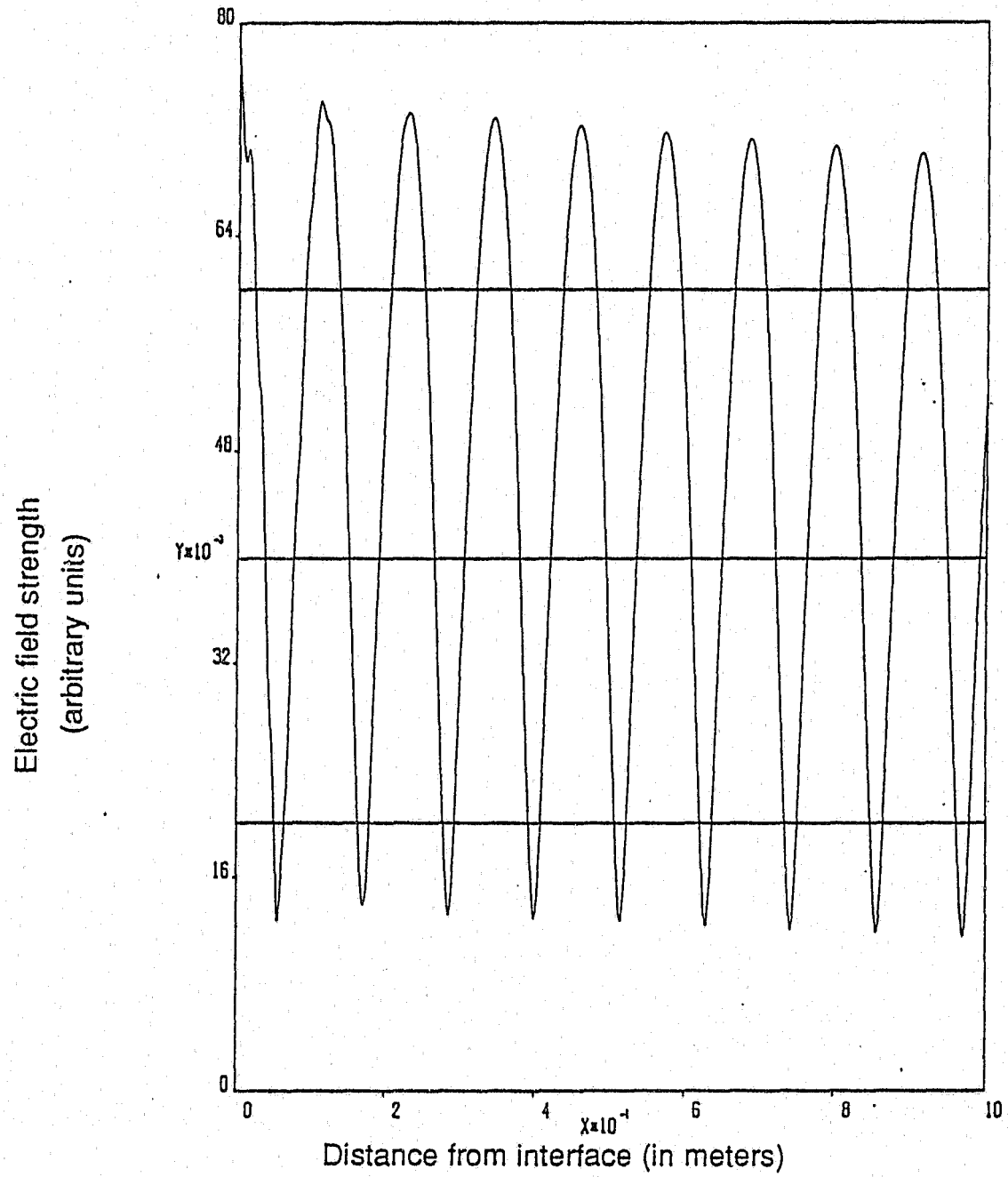

Figure 3.12 Interference pattern resulting from interaction between Transmission Line mode, Goubau mode, and Surface Wave mode at interface between two soil sections in Cylindrical Earth Model. d = 18 inches, f = 60 MHz, L_t = 80 nH/m, and relative permittivity of soil is 35.

mode causes the interference pattern to exist over a much greater distance compared to the previous (two-mode) case. The reflection and transmission coefficients for this case were found to be

$$\Gamma_1 = -.0341 \qquad T_1 = .189$$

$$\Gamma_2 = .0297 \qquad T_2 = .083$$

$$\Gamma_3 = -.0289 \qquad T_3 = .930$$

where the subscripts 1, 2, and 3 represent the Surface Wave, Goubau, and Transmission Line modes, respectively. These numbers show that the Transmission Line mode is the least affected by the soil interface, which is not surprising since most of the energy in the Transmission Line is within the cable.

For the first case, where the interface was between soils with relative permittivities of 25 and 12, the reflection and transmission coefficients were found to be

$$\Gamma_2 = -.00983 \qquad T_2 = .045$$

$$\Gamma_3 = -.00072 \qquad T_3 = .997$$

where the subscripts 2 and 3 represent the Goubau and Transmission Line modes, respectively. In this case, as in the three mode case, we see that the Transmission Line mode is the least affected by the interface.

It should be noted that the above two cases were contrived so that the same number of modes existed on either side of the interface. For the situation where a

different number of modes existed on either side of the interface it would be necessary to "balance" the situation by introducing one or more non-propagating (i.e. cut-off) modes discussed earlier in Section 3.2. For non-propagating modes we found that

$$\gamma = \alpha_n \tag{3.43}$$

An interesting observation is the behavior of the ratio between the attenuation constant, α, and the conductivity of the soil, σ_{soil}, as a function of changing soil permittivity. Using Equations 3.13-15 we can write

$$\frac{\alpha}{\sigma_{soil}} = \frac{\frac{1}{2}\int |E|^2 ds}{\int_S \mathrm{Re}\, E \times H^* \, ds} \tag{3.44}$$

Figure 3.13 plots Equation 3.44 as a function of permittivity for a frequency of 60 MHz. In this plot α is the attenuation constant for the Transmission Line mode.

Notice that the attenuation decreases as the relative permittivity of the soil rises. This possibly indicates that as the relative permittivity increases, the electromagnetic fields become more concentrated within the cable, and therefore, are not as susceptible to the attenuative effects of the soil.

The last data point on Figure 3.13 indicates that the attenuation starts to increase substantially as the relative permittivity of the soil increases past 35. It is interesting to note that according to Figures 3.3 and 3.4 the Transmission Line mode

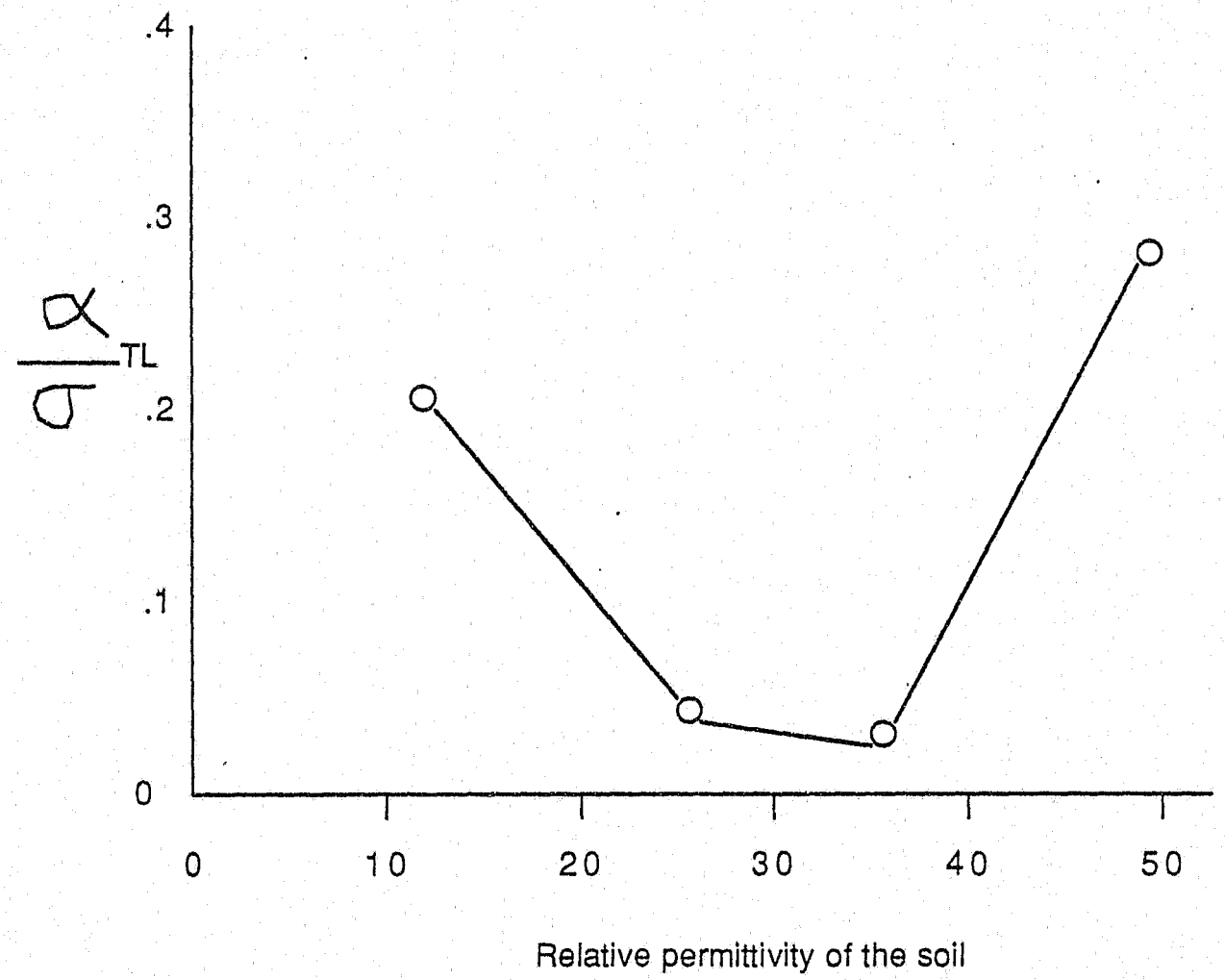

Figure 3.13 Alpha over sigma as a function of the relative permittivity of the soil. Alpha is the attenuation constant of the Transmission line mode; sigma is the conductivity of the soil.

is transformed into the Surface Wave mode when the relative soil permittivity increases above the mid-30's for a frequency around 60 MHz. Recall that the Surface Wave mode has a high percentage of its energy outside the cable and, therefore, one would expect the attenuation to be higher.

3.7 Application to PCCS

The previous sections introduced the Cylindrical Earth Model, showed how the original TEM wave is transformed into a TM Transmission Line mode (with azimuthal symmetry) at the non-ported to ported cable transition, discussed how different mode types could be excited at the interface between soils of different permittivities, and investigated how these modes could interact with each other.

In the actual PCCS system the air-soil interface is planar, not cylindrical; nevertheless, the model shows that the excitation of multiple modes leading to interference patterns can occur in the cylindrical case, which suggests that periodic oscillations in the electromagnetic field which are observed in the real (planar) case could be the result of similar mode interactions.

Also, in the real PCCS system we do not have an interface between two differing homogeneous soils. Rather, the soil is non-homogeneous which means that the permittivity and conductivity are continuously changing in all directions. The simple single-step permittivity model that we used could be extended into a higher order model which would represent the continuous variation of the soil permittivity by using many discrete step-changes in permittivity.

Since the soil is constantly changing, it is assumed that the generation of (and interaction between) the different modes is continually occurring, resulting in

the rapid variations in response number that have been observed in this and other (Frankel et al, 1984) PCCS experimental test projects.

Since the native soil in which the PCCS cable is designed to be buried is non-homogeneous it seems that the rapid variations in response number are inescapable, save for a scenario in which the entire burial path of the PCCS system is filled with transplanted homogeneous soil. Such a scenario is not considered possible due to the constraints of time, money and environmental concerns.

Since an interference pattern is created at the interface between soils whose permittivities significantly differ from one another, this indicates that although backfilling sand into a "dead" region (described in Section 2.4) would raise the response profile for that region, there would be exceptionally high and/or low response numbers near the edges of the transplanted sand region due to interference patterns created by the sudden transition in soil permittivities.

In a previous PCCS experiment (Frankel et al, 1984, pp. 119 and 122) the response profile for a low sensitivity region was raised by the soil exchange method. Figures 3.14 and 3.15 show the response profiles of the cell before and after the insensitive area (between crossing 16 and 21) was backfilled with sand. Figures 3.14 and 3.15 show that while the response profile of the insensitive region did rise after being backfilled with sand, there were rapid variations in the response profile at the edges of the backfilled sand region. These extreme variations can be seen between positions 15 and 16 where the response numbers ranged from 10,200 to 14,652 and also between 20 and 21 where the response ranged from 5,600 to 11,600.

The creation of these interference patterns gives one more reason why

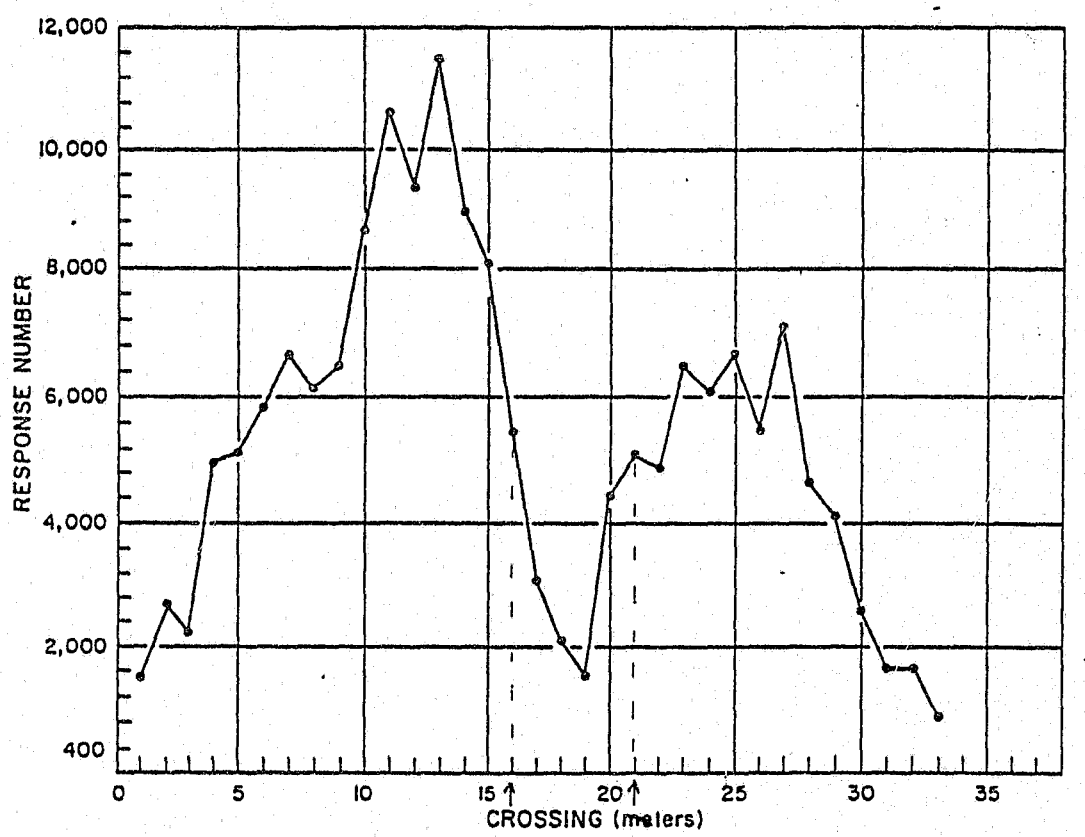

Figure 3.14 Response number profile for Cell B - 36 of a previous study (Frankel, et al, 1984). This cell has a region of low sensitivity between crossings 16 and 21.

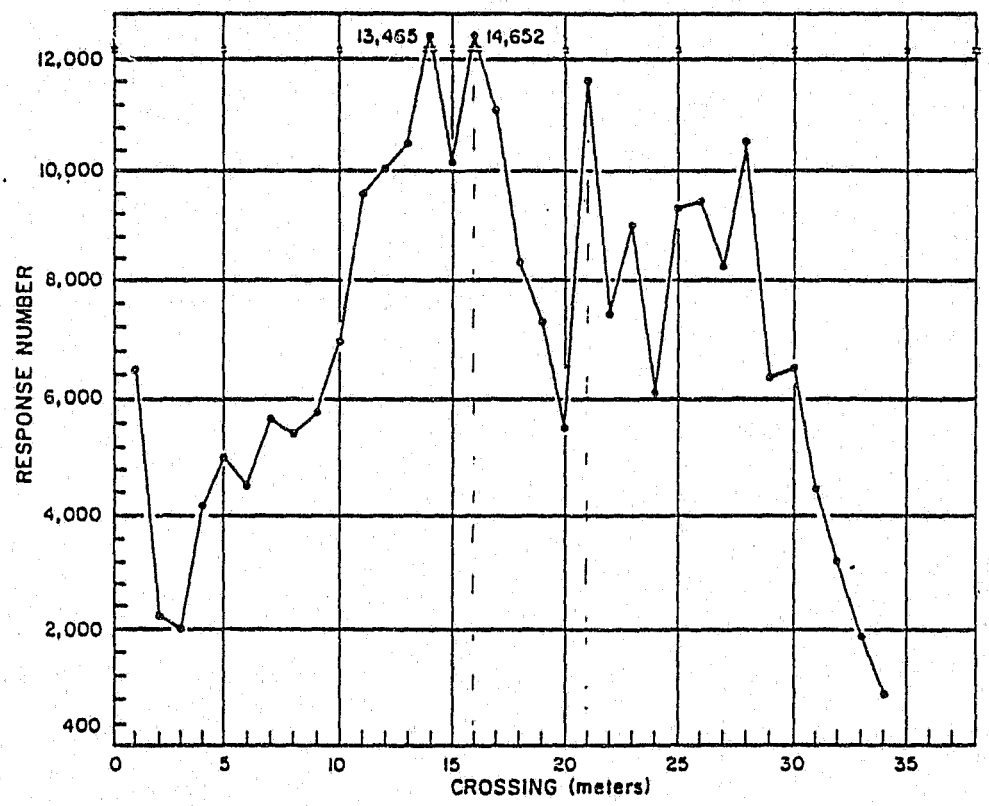

Figure 3.15 Response number profile for cell shown in Fig. 3.14 after soil between crossings 16 and 21 had been replaced with wash sand.

replacing native soil in the PCCS system burial path is not the best way to affect the response number profile of a cell.

3.8 Excitation of the Receiver Cable

The previous sections of this chapter have dealt with wave propagation on the transmitter cable. We have seen that electromagnetic fields due to the eigenmodes on this cable extend through the soil and exist at the location of the receiver cable. In this section we will discuss qualitatively how these fields couple to the receiver cable. We shall state the results first, and then present a brief summary of how the calculation of the coupled modes could be put on a firm quantitative basis.

It is presumed that the only eigenmode of interest on the receiver cable is the TM Transmission Line mode with no azimuthal variation, because this is the only mode that can strongly couple to the TEM mode which exists in the unported part of the receiver cable. It is this returning TEM mode which carries the signal that may indicate the presence of an intruder. We will consider two cases of coupling to the TM Transmission Line mode on the receiver cable: the first is the coupling by transmitter fields in the absence of an intruder, and second, by transmitter fields scattered from the intruder.

3.8.1 No Intruder Case

Suppose that the intruder is absent, and that the transmitter and receiver cables are in a perfectly uniform soil, i.e., a soil in which there are no spatial variations of permittivity or conductivity. On the transmitter cable, we could have

several eigenmodes propagating, all of which are TM with no azimuthal variation. Consider any eigenmode; because the cables are identical, this same eigenmode can exist on the receiver cable. The transmitter eigenmode will couple strongly to the same receiver eigenmode (see Section 3.8.3). Now, the transmitter eigenmode propagates towards the cable's matched termination, and in a uniform soil, no energy is reflected back. Because of phase cancellation the excited eigenmode on the receiver cable will likewise only propagate towards the cable termination, while zero energy propagates backwards toward the PDR. Thus, in a uniform soil, the PDR receives no signal. The system thus described is seen to be a null device.

This system acts in principle like a directional coupler where an incident wave in one arm couples to a wave in a second arm which travels only in the same direction as the incident wave.

In the real world, the variations in soil parameters upsets the null. As we have seen previously, variations in soil parameters will lead to reflections of eigenmodes as well as coupling among eigenmodes; thus, the PDR end of the receiver does not see a null signal, but rather a finite, small signal.

3.8.2 Intruder Present

When an intruder is present, the eigenmodes extending from the transmitter cable will be scattered by the intruder. These scattered fields will exist locally about the receiver cable. Their strength will be approximately proportional to the strength of the transmitter electromagnetic fields at the intruder. Thus, if the intruder is crossing at a place where the transmitter fields are small (e.g., due to a high permittivity, which causes the Transmission Line eigenmode to have its energy

shifted inside the cable) or at a minimum of an interference pattern of two or more eigenmodes, the scattered fields at the receiver will be proportionally small.

These fields will then couple to the Transmission Line eigenmode on the receiver cable. This mode will propagate both towards its termination and towards the PDR.

For a uniform soil, the only signal arriving at the PDR is the Transmission Line eigenmode excited by the fields scattered by the intruder. In a nonuniform soil, this eigenmode (due to the fields scattered by the intruder) must be separated out from the reflected eigenmode(s) due to soil variations. We have discussed in Chapter 2 that this is the function of the PDR.

The null nature of this system should be emphasized. By placing the PDR at the same end of the receiver cable as the location of the transmitter for the transmitter cable, the signal return is due only to soil nonuniformities and scattering from the intruder. If the PDR had been placed where the receiver cable termination is located, the receiver cable's Transmission Line eigenmode due to fields scattered from the intruder would be much too small compared to the receiver eigenmodes coupled through the soil from the transmitter in the absence of the intruder to be detected.

3.8.3 Theoretical Background

The above discussion may be put on a sound quantitative basis by invoking the Induction Theorem of Electromagnetic Theory (Harrington, 1961). This theorem, applied to our configuration, states that the coupling of either the TM eigenmodes on the transmitter to the receiver, or the coupling of the scattered fields to the receiver cable may

be quantitatively predicted by a fictitious magnetic surface current, M_ϕ, in the azimuthal direction, flowing around the soil-jacket interface of the receiver cable. The value of this magnetic surface current is easily calculated if one knows the exciting fields due to the transmitter at the receiver cable in the absence of the receiver cable. In the absence of an intruder, these exciting fields are just the eigenmodes of the transmitter evaluated at the receiver.

When an intruder is present, the scattered fields can also be found in principle from the Induction Theorem: the eigenmodes of the transmitter can be used to calculate fictitious electric and magnetic source currents on the surface of the intruder. These source currents are then used to calculate the scattered fields at the location of the receiver cable. This latter step is very difficult because of the complicated source current configurations and that there is an interface between the medium in which the sources exist (air) and the medium in which we wish to calculate the fields (soil). Nevertheless, in principle, the problem can be solved. This problem could be made easier if the human intruder were replaced by a more tractable shape, e.g., an ellipsoid.

We are now at the point where the coupling of all fields has been represented by an azimuthally-directed magnetic surface current circulating about the jacket-soil interface of the receiver cable. Note that in both cases, this source current is of finite extent. For the case of the eigenmodes of the transmitter in the absence of an intruder, the magnetic source current is approximately the length of the receiver cable, in our case, about 6 cells. In the case of an intruder, the scattered fields are no doubt very local about the location of the intruder.

The case of the excitation of eigenmodes on a cylindrical structure by an azimuthal source current (of finite extent) about its exterior has been treated in great detail

by Stix (1962). In brief, Stix shows that if the azimuthal magnetic current is

$$M_\phi = M \exp(-j\beta_o z) \tag{3.45}$$

then all TM eigenmodes with no azimuthal variation will be excited. The eigenmode with its propagation constant, β, closest to β_o will have the largest amplitude, and the amplitudes of the other eigenmodes decrease as their β's diverge from β_o. Backward travelling eigenmodes (modes propagating in the -z direction) can also exist, but their amplitudes are negligible compared to +z travelling eigenmodes.

Since the cables are identical, this tells us that an eigenmode on the transmitter cable will couple strongly to the same eigenmode on the receiver cable and that both will travel in the same direction (+z direction toward the termination) with negligible energy travelling in the reverse direction (-z direction) towards the PDR.

For the case of an intruder, the local fields will probably not have a discernable spatial phase variation. The amplitude variation, however, can be resolved into a spatial Fourier integral with both exp ($-j\beta z$) and exp ($+j\beta z$) terms present. The portion of the Fourier spectrum containing energy with a β near that of the Transmission Line eigenmode of the receiver will couple strongly to that eigenmode. Thus, the Transmission Line eigenmode is excited in the receiver, and travels away from the position of the intruder in both directions, i.e., towards the termination and towards the PDR. It is this Transmission Line eigenmode that is detected and analyzed by the PDR.

Qualitatively, we can see that the strength of the Transmission Line eigenmode which returns to the PDR is due to, first, the strength of the Transmission Line electromagnetic fields at the intruder (i.e., the Transmission Line fields that we have calculated above, and that we have measured in Section 5.5), and second, the ability of the intruder to scatter these fields (i.e., the size of the intruder and his chemical composition).

CHAPTER 4

TEST SITE

4.1 Introduction

A PCCS test system was installed and experiments were conducted at the University of Arizona's Campbell Experimental Farm in Tucson, Arizona. The ported coaxial cable-pair of the PCCS system was 200 meters in length; that is, it consisted of six 33 1/3 meter cells. As noted in Chapter 2, a distance of 33 1/3 meters corresponds to the resolution capability of the PCCS system which is a function of the rate at which the return signal is sampled. The instrumentation for the PCCS was located in a one-room transportable structure adjacent to the cable-pair. A sketch of the site layout is shown in Figure 4.1.

The following sections describe the cable deployment procedure, the design and purpose of the two "special purpose" test cells, and the installation of the system electronics.

4.2 Buried Cable Installation

It was decided to deploy the cable-pair in a straight line path that was designed to keep the ported coaxial cables as far away as possible from any possibly disruptive objects that were on the farm site, such as buried sewer pipes, irrigation ditches, or piles of "fill- dirt" (Wait, 1978/9; Parra, 1984). A City of Tucson "Blue Stake" search confirmed that there were no buried conductors in the area.

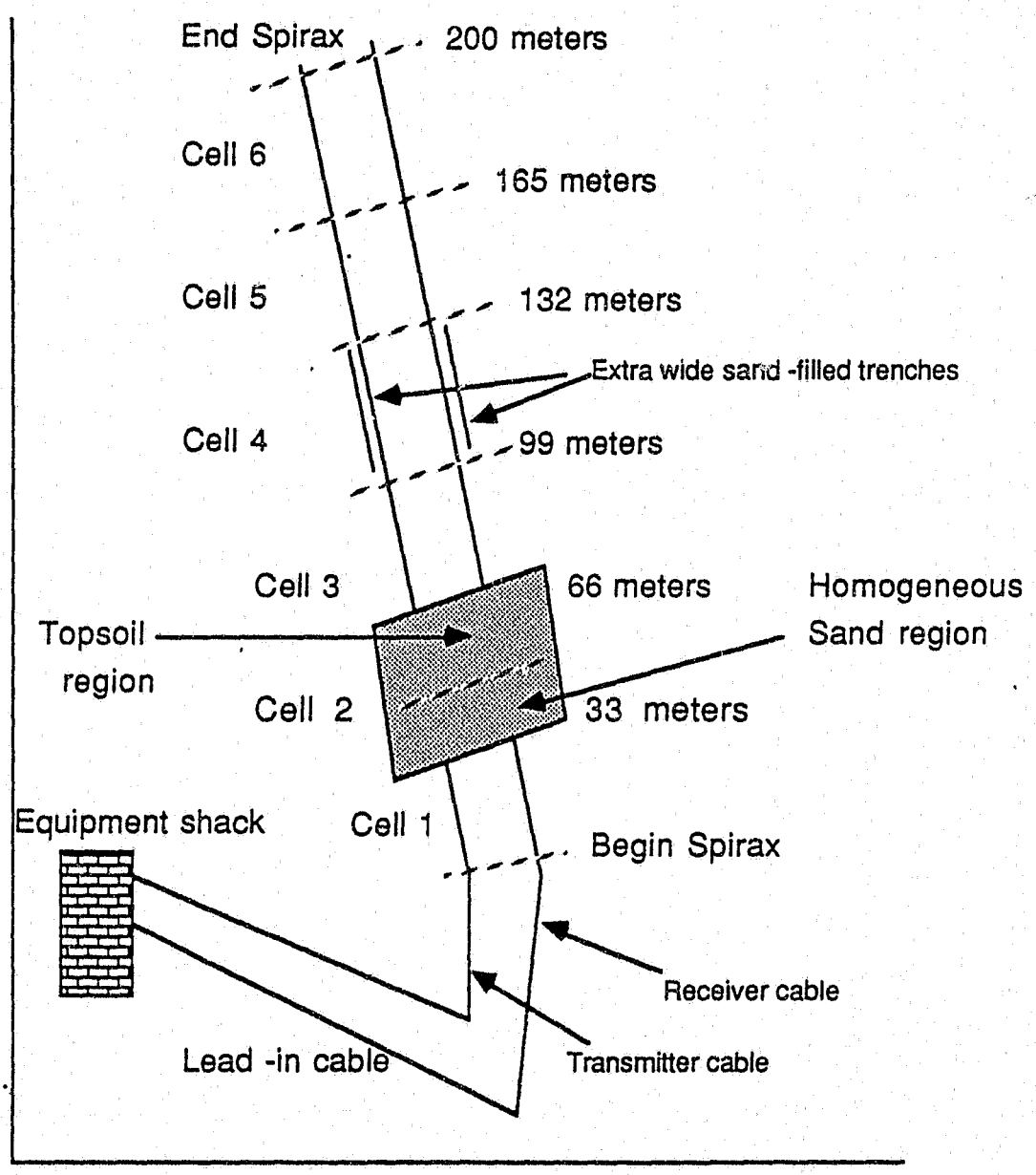

Figure 4.1 Plan of PCCS test site, Campbell Farm, University of Arizona, Tucson, Arizona.

As shown in Figure 4.1, the PCCS was deployed along the far side of the farm property in a north-south orientation. The ground surface was flat and the surface soil appeared to consist of hard-packed topsoil with many small rocks.

The trenching process was begun by first cutting two parallel, shallow, guide trenches with a tractor-mounted 2-shovel furrowing attachment. The two shovels were set 5 feet apart. A trench digging machine called a "ditch witch" was then used to cut a 7-inch wide, 9-inch deep trench over each guide trench. Every effort was made to keep the two trenches parallel but slight variations of an inch or two occurred several times when the ditching attachment hit a buried rock. Figure 4.2 shows a cross-sectional view of the two cable trenches. The method of trenching that was employed was based on the procedures outlined in Chapter 3 of the Final Report of the Evalutation of the PCCS by Frankel, Van Horn, and Carlile, 1984.

After the two trenches were cut, the special test cells in Cells 2 and 4 were excavated. These test cells will be described in the next section.

When all the trenching and excavation was completed the cables were deployed into the ground by pulling them from two tractor-mounted cable reels and laying them by hand into the trenches. The cables were then buried using a road grader to refill the trenches with the original excavated soil. A worker walked alongside the road grader picking out rocks from the fill soil before they could be buried with the cables.

After the cables were deployed the entire site was measured and red spray paint was used to mark off the site into 1-meter increments. Mark 0 indicates where

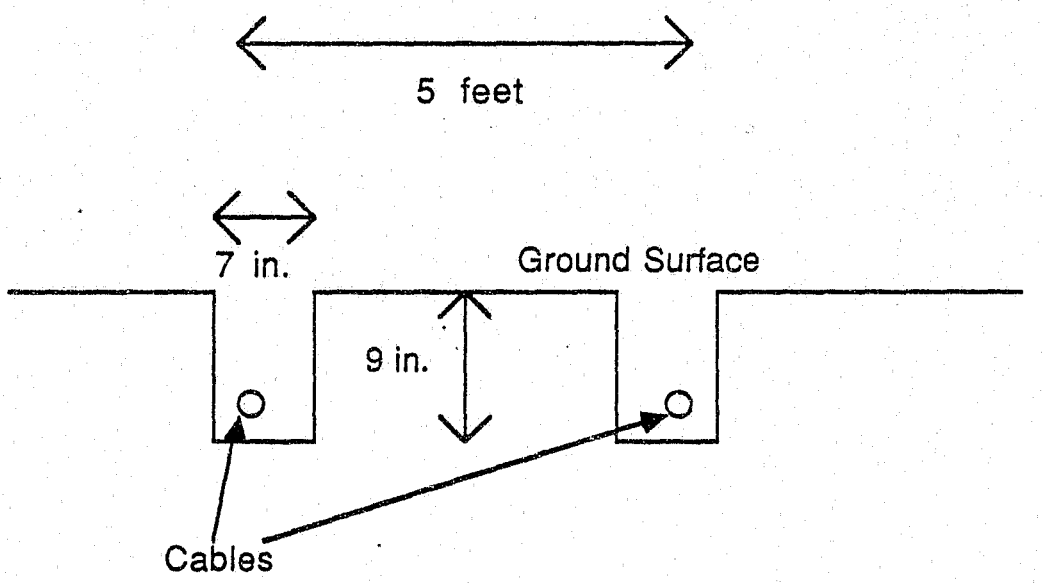

Figure 4.2 Cross-sectional view of cable trenches.

the lead-in cables transition into ported coaxial cables and mark 200 indicates the terminated end of the cables.

4.3 Special Test Cells

In designing this test site it was decided that two of the 33 1/3 meter (109 foot) cells would be specially excavated test cells. Cell 2 is a fully excavated cell featuring an interface between two homogeneous back-filled soil types. Cell 4 is a partially excavated cell in which the cables are buried in extra wide sand-filled trenches.

4.3.1 Fully Excavated Test Cell

Cell 2 is a cell which has been fully excavated, and then backfilled with two different homogeneous soils. The half of the cell which is closest to the PCCS transmitter (the north half) is back-filled with homogeneous wash sand while the other half of the cell is back-filled with relatively homogeneous topsoil; therefore, at the middle of the cell there exists an abrupt interface between the two different soil types. Figures 4.3 and 4.4 show end-on and map views of cell 2.

The reason for having such a test cell is twofold. First, since both halves of the cell contain homogeneous soil we can more easily separate out and observe the effect that non-soil factors (such as cable separation distance) have on the response number profile.

Second, the existence of an abrupt interface between two different, homogeneous soil types provides the optimum soil configuration in which to test for

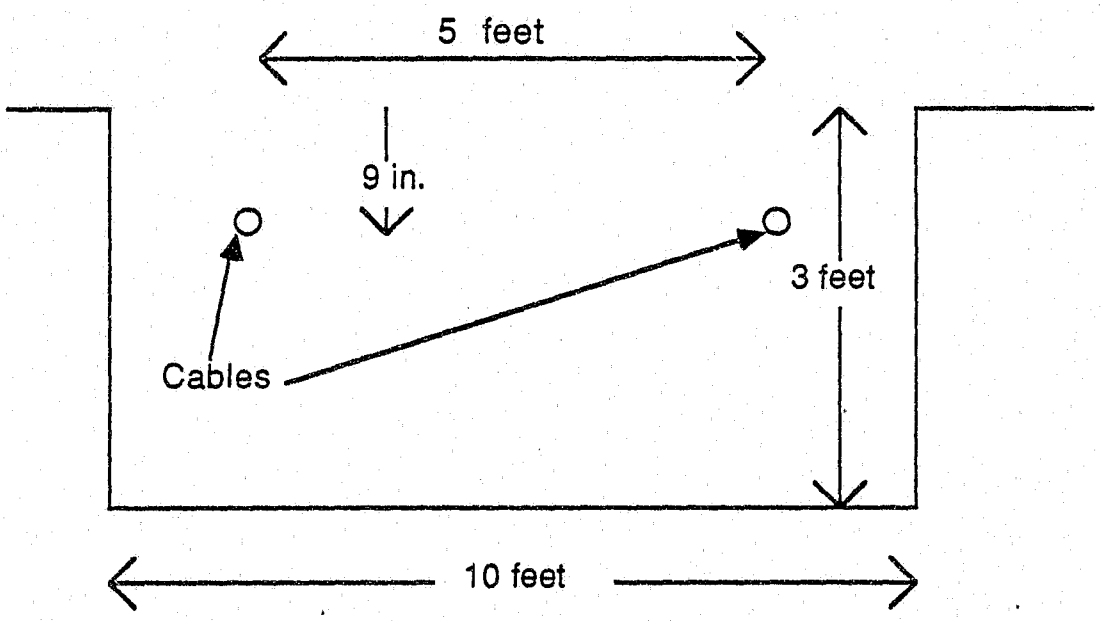

Figure 4.3 Cross-sectional view of cell 2. Cell was totally excavated and then backfilled with homogeneous sand in one half, and topsoil in the other half.

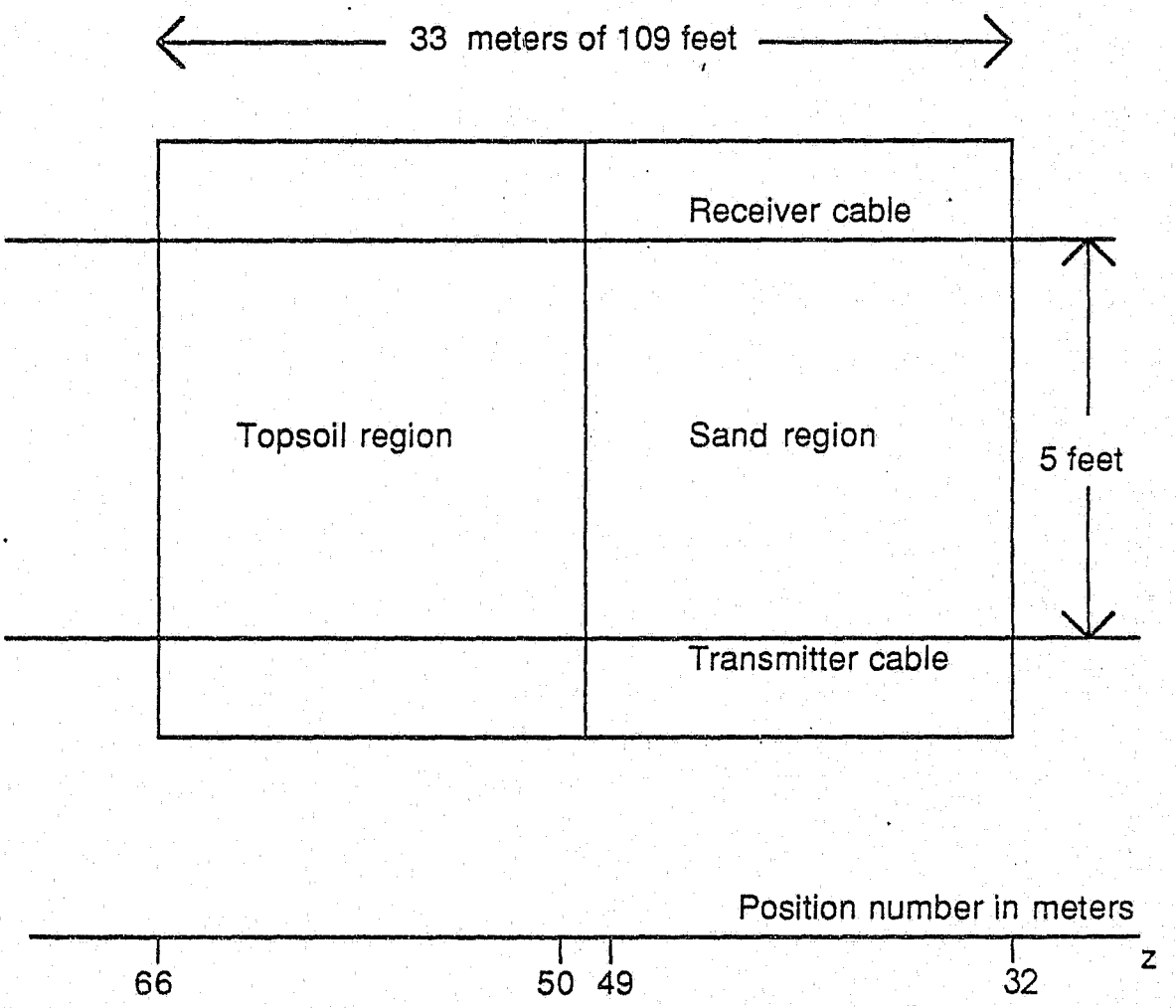

Figure 4.4 Map view of cell 2, showing sand and topsoil regions. (Not to scale).

the existence of interference patterns in the electromagnetic field which are predicted by the theory of coupled modes, introduced in Chapter 3.

The cell was constructed by first removing all the original soil. This was accomplished by using heavy earth moving equipment such as front loaders and dump trucks. As the cell was being excavated many different soil types were encountered the deeper we went. At ground level the soil was hard-packed topsoil with many small rocks. Below this was a layer of caliche followed by a layer of large, smooth river rocks. The test site is located near the banks of a normally dry river bed so this indicates that the river bed has shifted position over time. After about 2 feet down we hit a silty or powdery layer with many small pebbles. Beneath 2 1/2 to 3 feet down we hit sand which continued down to a depth of at least 4 feet. How much further the sand layer went is not known since we stopped excavating at a depth of 4 feet.

After all the original soil was removed, a large trench remained which was 109 feet long, 10 feet across, and 4 feet deep. These dimensions were chosen (Lundien, private communication) so that the electromagnetic fields of the eigenmodes of the transmission cable will not be effected by the native soil external to the trench. A road leading to the bottom of the nearby river bed was bulldozed, and using a front loader and a dump truck, sand from the river bed bottom was transported to the trench. The sand was then back-filled into the north half of the trench (i.e. between position markers 33 and 49) until the trench bottom was only 9 inches below the ground surface.

Again using the front loader and dump truck, topsoil from the farm was transported to and back-filled into the south half of the trench (i.e. between position

markers 50 and 66) until this side of the trench was also filled to within 9 inches of the ground surface. Care was taken so that the interface between the sand region and topsoil region was as abrupt as possible.

At this point the transmitter and receiver cables could be laid in the trench 5 feet apart and then buried with the remaining sand (in the north half) or the remaining topsoil (in the south half).

4.3.2 Partially Excavated Test Cell

Cell 4 is a partially excavated cell in which the cables are buried in extra-wide sand-filled trenches. This contrasts with cells 1, 3, 5 and 6 where the cables are laid in narrow trenches about 7 inches wide which are then filled with the trench's original soil. In cell 4 each trench is about 2 feet wide and 18 inches deep. The trenches are then filled with sand, burying the cables at the standard 9 inch depth. Figure 4.5 shows an end-on view of the trenches in cell 4.

The purpose of the wide sand-filled trenches in cell 4 is to facilitate tests where the cables must be repeatedly uncovered and moved closer together or further apart. Sand is easy to dig up regardless of how long it sits in a trench, while other soil types tend to become quite hard-packed, even after a few days or weeks.

The cell was constructed by first removing all the original soil from two 2-foot wide trenches each centered on the narrow trenches previously cut as described in Section 4.2. This partial excavation was accomplished using a backhoe. After the 2-foot wide, 18-inch deep trenches had been made, a tractor dragged a heavy railroad tie along the bottom of each trench to even out the depth. The original soil was disposed of and the trenches were then partially filled with sand from the

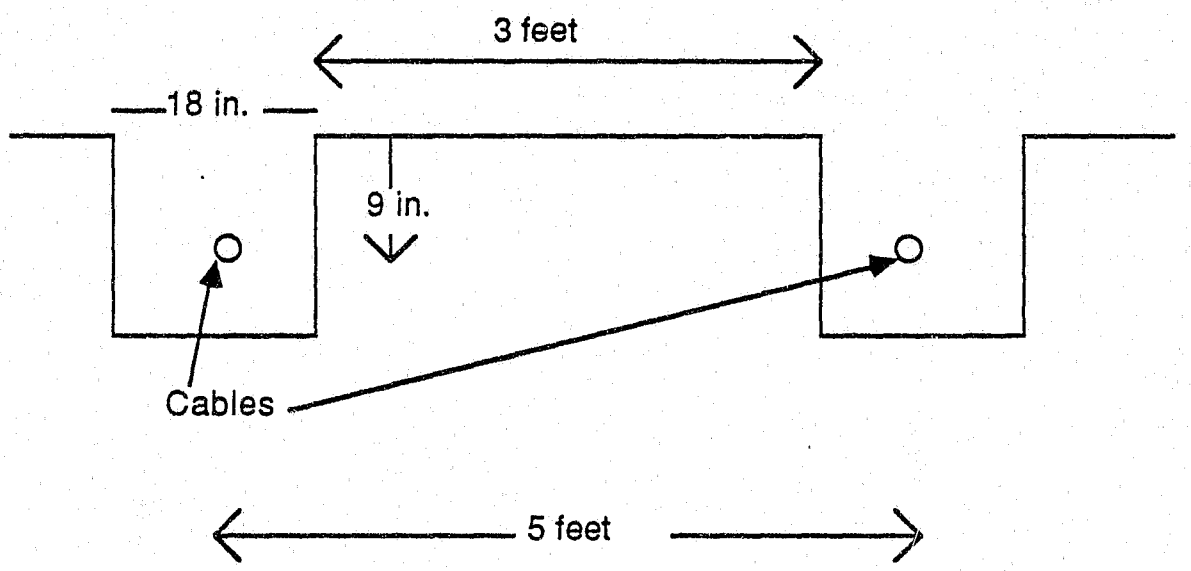

Figure 4.5 Cross-sectional view of wide cells in cell 4. Trenches are sand-filled.

nearby river bed.

When each trench was filled to a depth of 9 inches below ground level the cables were deployed in the trenches. Care was taken to keep the cables about 5 feet apart and the remaining sand was back-filled into the trenches, burying the cables at the standard 9 inch depth.

4.4 Installation of PCCS System Electronics

The electronic equipment that makes up the PCCS system consists of the Processor, Detector and Ranging unit (PDR), the Data Acquisition System (DAS), and the printer. This equipment is housed in an 8-foot by 16-foot, one-room, air-conditioned, transportable structure which is adjacent to the buried coaxial cables at the north end of the test site.

The transmitter and receiver cables are connected to the back of the PDR. These cables are called "lead-in" cables because they are standard (i.e. non-ported) coaxial cables. These lead-in cables exit the equipment room via a conduit and travel underground about 100 feet (see Figure 4.1) until reaching the beginning of cell 1. At the beginning of cell 1 the coaxial cable becomes ported which allows for cross-cable coupling.

The power for the equipment was standard 110 VAC 60 Hz commercial power that was put through a constant voltage transformer. The transformer was augmented by a voltage spike filter. To control static electricity, as well as to protect the equipment from lightning strikes, the PDR, DAS, and printer were all connected to an earth ground.

In addition to the PCCS system equipment, the other test equipment such as the spectrum analyzer, oscilloscope, and electronic cable locator were stored in this room as well.

CHAPTER 5

TESTS

This chapter will describe the design, implementation, and results of the five tests (or experiments) that were performed for this project. Before describing these tests, definitions of PCCS system terminology will be given. Also, the issue of cell boundary demarcation and threshold setting will be discussed.

5.1 Definition and Discussion of Terminology

The following definitions cover some of the terminology used in both the PCCS literature as well as in the following sections describing the project tests. Some of these terms were defined in Chapters 2, or 4 but will be repeated here for convenience.

1) Cable-pair. The two parallel transmitter and receiver cables which are buried about 5 feet apart.

2) Standard person. A person of medium height and build who repeatedly crosses the system at 1-meter intervals to test how the detector sensitivity changes as a function of position along the cable-pair. For reasons of comparison it is important that the standard person be the same person for the entire duration of any one test.

3) Processor, Detector and Ranging unit (PDR). The PDR is the central electronic component of the PCCS system. It contains the transmitter, receiver, amplifier, digitizer, processor, and detector circuits. This device transmits the pulse

signal and then samples the return signal from the receiver cable for signs of an intruder. In some PCCS literature the PDR is called the Processor Display Unit (PDU).

4) Data Acquisition System (DAS). The DAS monitors the PDR and outputs information to a printer, chart recorder, or oscilloscope. When an intrusion occurs, the DAS prints out the time of day, the location (cell number), and the size (response number).

5) Cell. The PCCS system electronically divides the detection zone into distance intervals called cells. When an intrusion alarm occurs, the DAS will print out the number of the cell in which the intrusion occurred. The length of the cell is approximately 33 meters; this length is a function of the rate at which the PDR samples the return signal from the receiver cable. Although the PDR is able to monitor two 48-cell lines, the PCCS test site built for this project has only 6 cells. The cells are numbered from 1 to 6, with cell 1 closest to the PDR.

6) Downline. Downline indicates the direction along the cable-pair away from the PDR, that is, towards the terminated end of the cables.

7) Crossing point or meter mark. The entire detection zone at the test site is marked out in 1-meter increments. Each meter mark is numbered, starting at 0 which indicates the beginning of the detection zone, up to 200 which corresponds to where the cables are terminated. In the response profile test, a person crosses the cable-pair perpendicularly at each meter mark, therefore these marks are sometimes referred to as crossing points.

8) Center line. The center line of the cable-pair is the line which runs parallel to the cable-pair and lies halfway between them, and is located on the surface of the ground.

9) Response number. When an intrusion occurs, the PDR generates a voltage signal which represents the perturbation of the demodulated return signal due to the presence of the intruder. The response number is an integer proportional to the perturbation signal and therefore (ideally) proportional to the size of the intruder. The minimum response number that the PCCS can generate is 400, and the maximum is 32,766 (Frankel et al, 1984).

10) Dead zone. An insensitive region in the detection zone where a person can cross without being detected.

11) Response profile. A plot of the response numbers versus position along the cable-pair; the response numbers are due to the same intruder (or the standard person). 12) Response ratio. The ratio between the highest and lowest response numbers in the same cell, caused by the same intruder.

13) Threshold. The threshold setting defines the smallest response number which will trigger an intrusion alarm. The threshold can be set for each cell, either by the operator or automatically.

5.2 Response number profile test

5.2.1 Test objective

The objective of this test is to determine the response number profile for all cells (meter marks 0 to 200) in the test site when the cable-pairs are crossed by a standard person. This response number profile (also called the sensitivity profile) will be compared with the profiles of other variables in order to determine the degree to which those variables are responsible for variations in the amount of cross-cable coupling.

5.2.2 Implementation

The test site is 200 meters long; that is, it consists of six 33 1/3 meter cells. The ground above the buried cable-pair has been marked off (with paint) in 1- meter increments. The "0 meter mark" is at the beginning of the ported coaxial cable-pair while the "200 meter mark" is at the termination of the cable-pair.

These 1-meter increments mark the points where the standard person will perpendicularly cross the cable-pair. When the standard person crosses the cable-pair the DAS will print out a response number which is a measure of the energy scattered into the receiver cable at the point where the person crossed.

This test was performed by two people, the PCCS operator and the standard person. The exact height and weight of the standard person is not important. What is important is that the same standard person did all the crossings in the experiment. The PCCS operator and the standard person were in communication via hand-held radios.

Upon radioed instruction, the standard person would cross the cable-pair in an East to West direction (the cable-pair was buried in a North-South direction) and stop. After about 15 seconds the standard person would return across the cable-pair, this time in a West to East direction. This method gives the advantage of having two response numbers for each crossing point. These two numbers were averaged together and it was this average that was used to graph the results of this test.

As this basic procedure was repeated at all 200 crossing points, the PCCS operator would record the response numbers together with their corresponding meter mark numbers.

The PDR was operated in the "non-latched" mode and the alarm horn was

disabled. The cell thresholds of the adjacent cells were set to a very high level so as to eliminate sympathetic alarms (discussed below).

The data was graphed as "average response number as a function of position" (as denoted by the appropriate meter mark numbers.) Most of the graphed results can be found in this section while the graphed results for the central area of the test site (meters 26 - 80) will be found in Section 6.2.1. A complete listing in tabular form of the results of this experiment will be found in Appendix B.

5.2.3 Dead regions, sympathetic and multiple responses

In the course of running this experiment it was found that there were about 15 crossing points where the response number for the standard person was below 400, which is the minimum number necessary to trigger an alarm. This means that a person could cross the cable-pair at those points and be undetected by the PCCS system. In the graphed results of this experiment the dead regions are shown by those points with a minimum default value of 400.

Another kind of unwanted response that was initially encountered is the sympathetic response, which is an alarm in one cell caused by a person (or any other large object) crossing the cable-pair in an adjacent cell. These sympathetic responses were eliminated by setting the adjacent cell thresholds very high so as to effectively prevent any alarms from those cells.

The third kind of unwanted response is the multiple response, where the DAS will print out several response numbers for the same cell after the standard person has made a single crossing. These multiple responses could be partially eliminated by raising the cell threshold.

5.2.4 Test Results and Discussion of Data

Figures 5.1 through 5.6 show how the response profile for each cell in the system changes as a function of position. From the graphs we can see that the response profile is far from flat even though it is caused by the same person at each crossing point. This is consistent with previous studies of PCCS performance, although it should be noted that the response numbers and response ratios are much lower at this test site than have been observed elsewhere (Frankel et al, 1984). It is assumed that the variations in the response profile are primarily due to variations in the soil.

In Figure 5.6 we can observe a periodic oscillation in the response profile which occurs in the last 10 meters of the test site (meters 190 - 200). The adjacent peaks of the oscillation occur at 2 meter intervals. We assume that this is an interference pattern caused by the reflection from the cable terminations. Such reflections are minimized by attempting to terminate the cables in their characteristic impedance, but in real systems there is usually a slight discrepancy between the characteristic impedance of the cable and the impedance of the termination due to impedance variations of mass produced components.

In the entire test site the most noticeable variation in sensitivity occurs in cell 2. Figures 5.7 and 5.8 show an expanded view of the section of the test site between meters 26 and 80. Note that cell 2 (the homogeneous sand and homogeneous topsoil test cell) lies between meter marks 33 and 66.

The most obvious feature of the profile is the large "hump" between meter marks 33 and 50. The physical significance of this "hump" is that the sand-filled trench lies between marks 33 and 50. This illustrates that the electrical

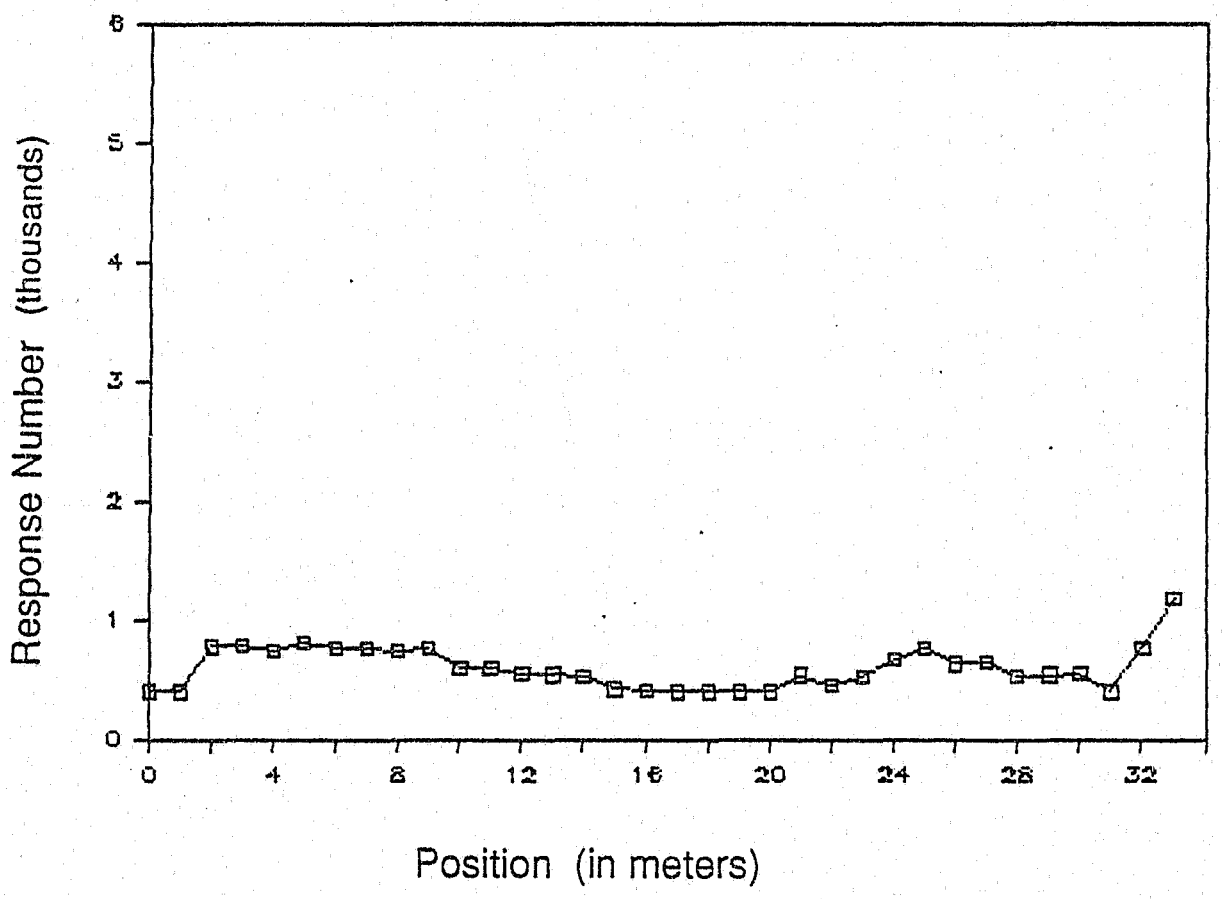

Figure 5.1 Response number profile for cell 1.

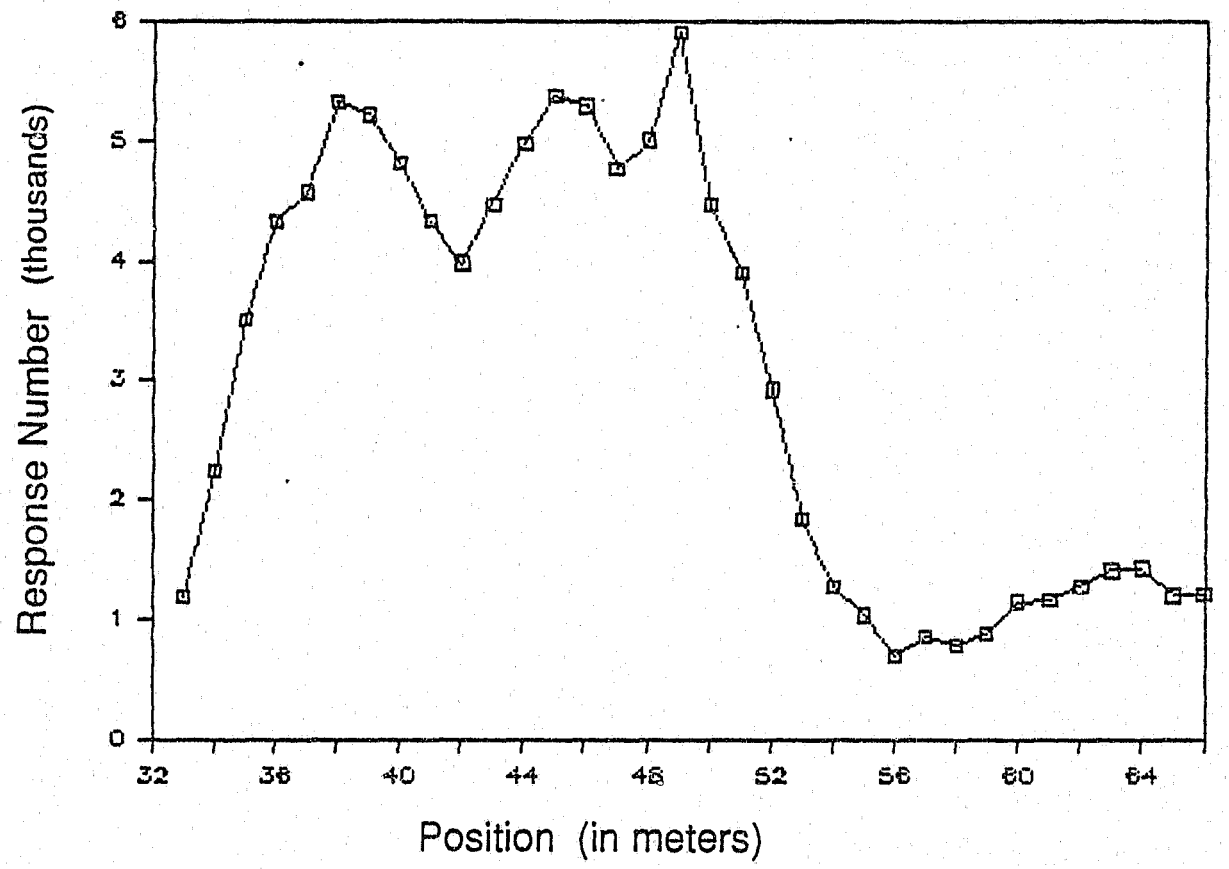

Figure 5.2 Response number profile for cell 2. Sand region lies between positions 33 and 49; topsoil region is between positions 50 and 66.

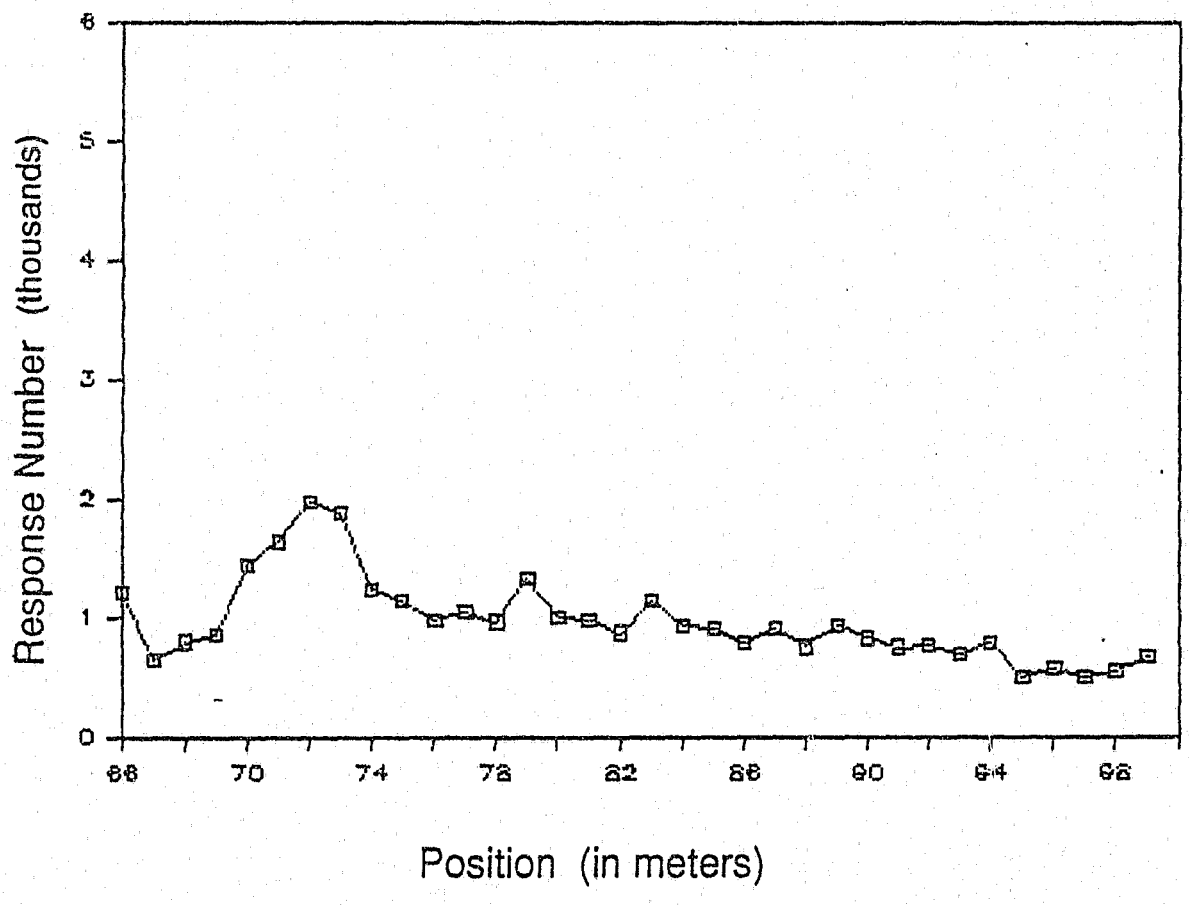

Figure 5.3 Response number profile for cell 3.

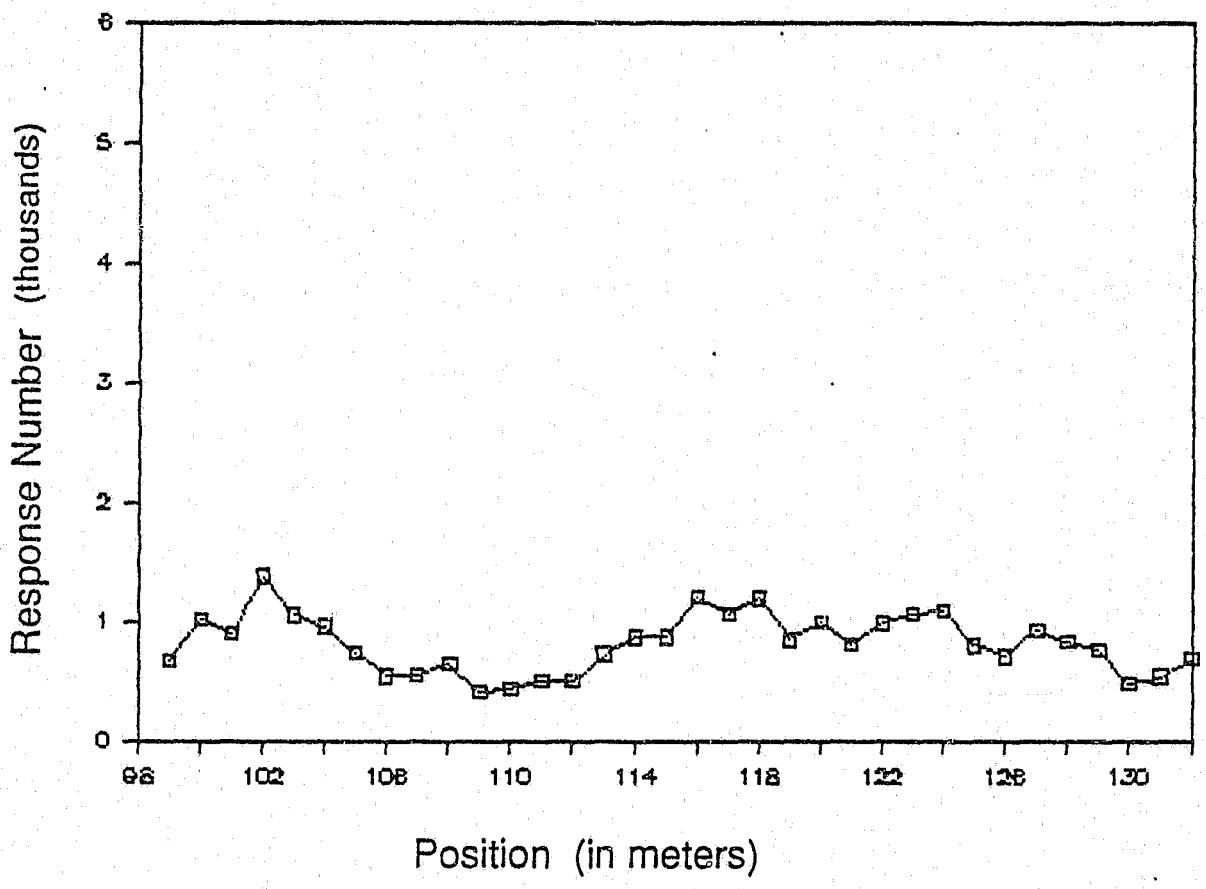

Figure 5.4 Response number profile for cell 4.

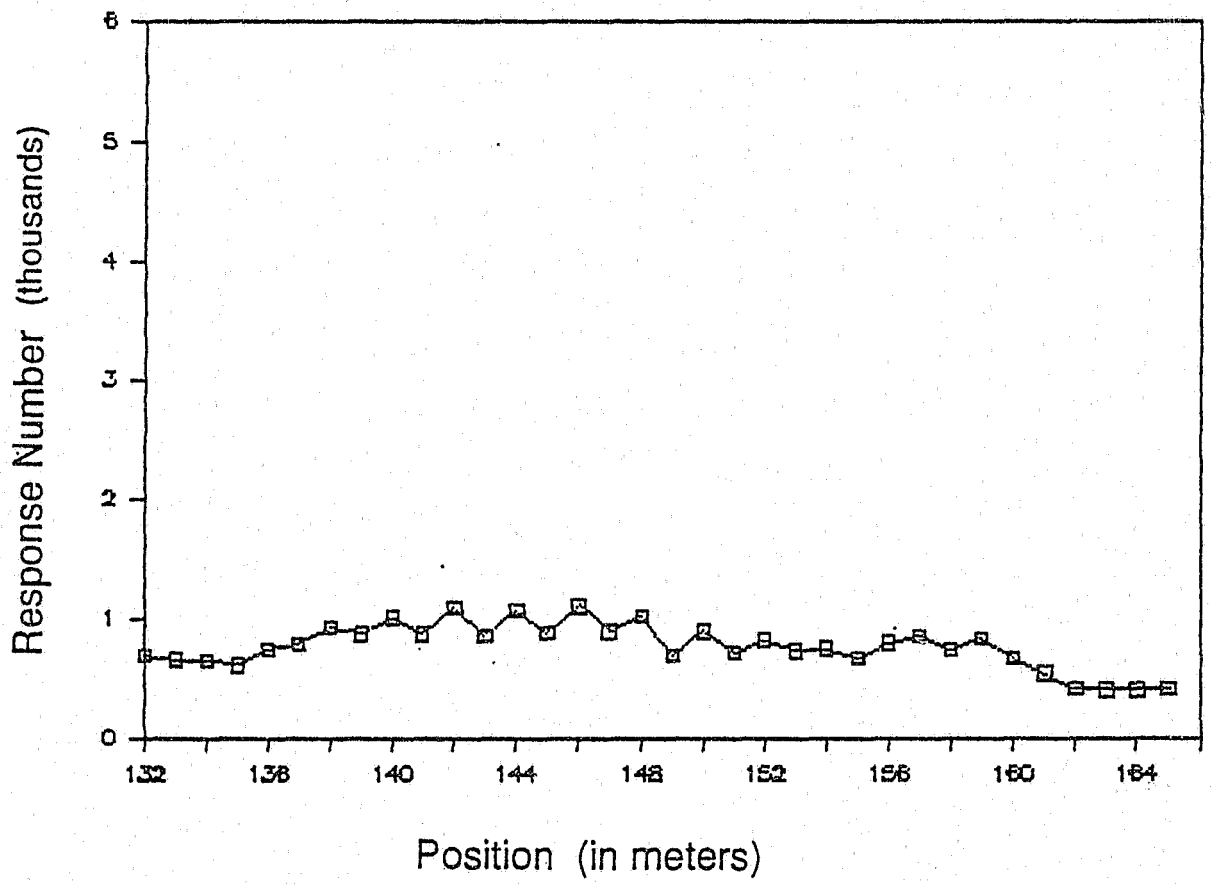

Figure 5.5 Response number profile for cell 5.

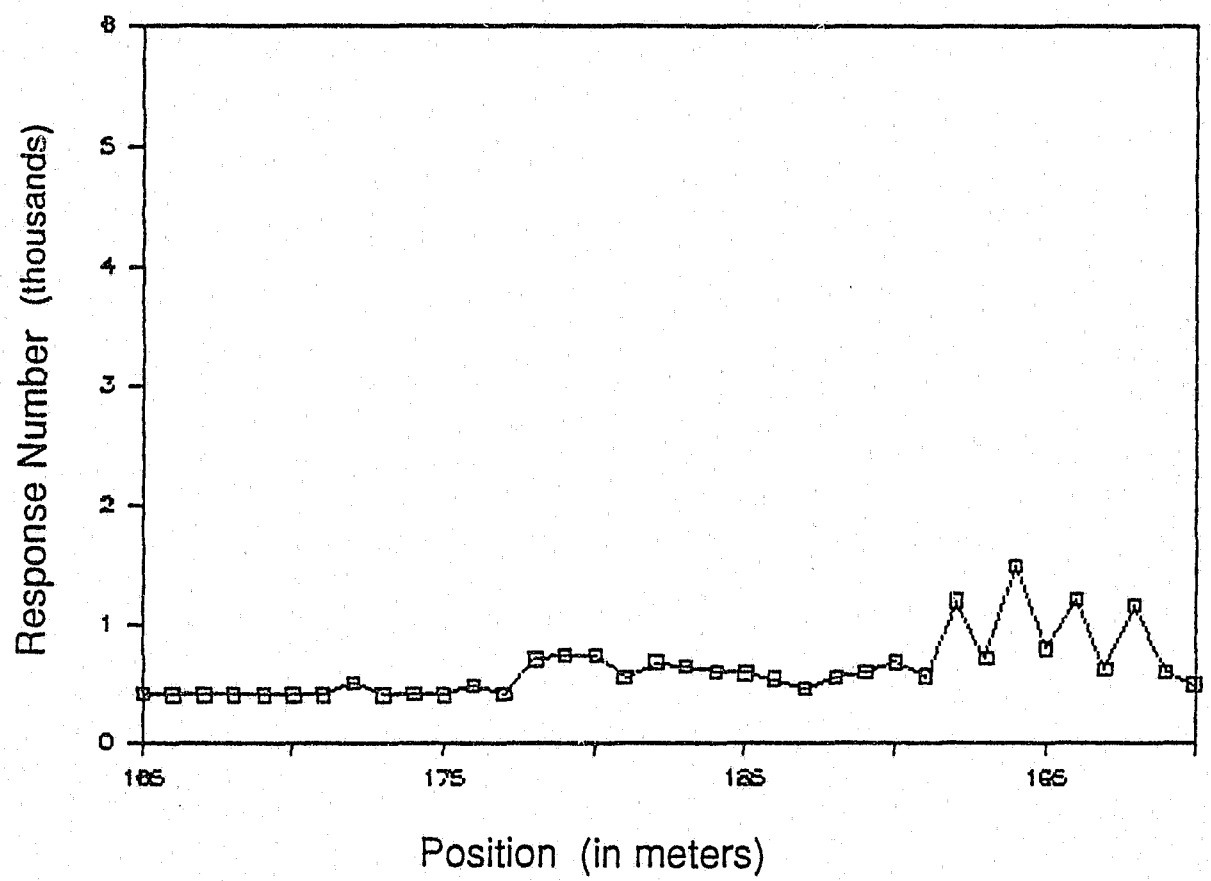

Figure 5.6 Response number profile for cell 6.

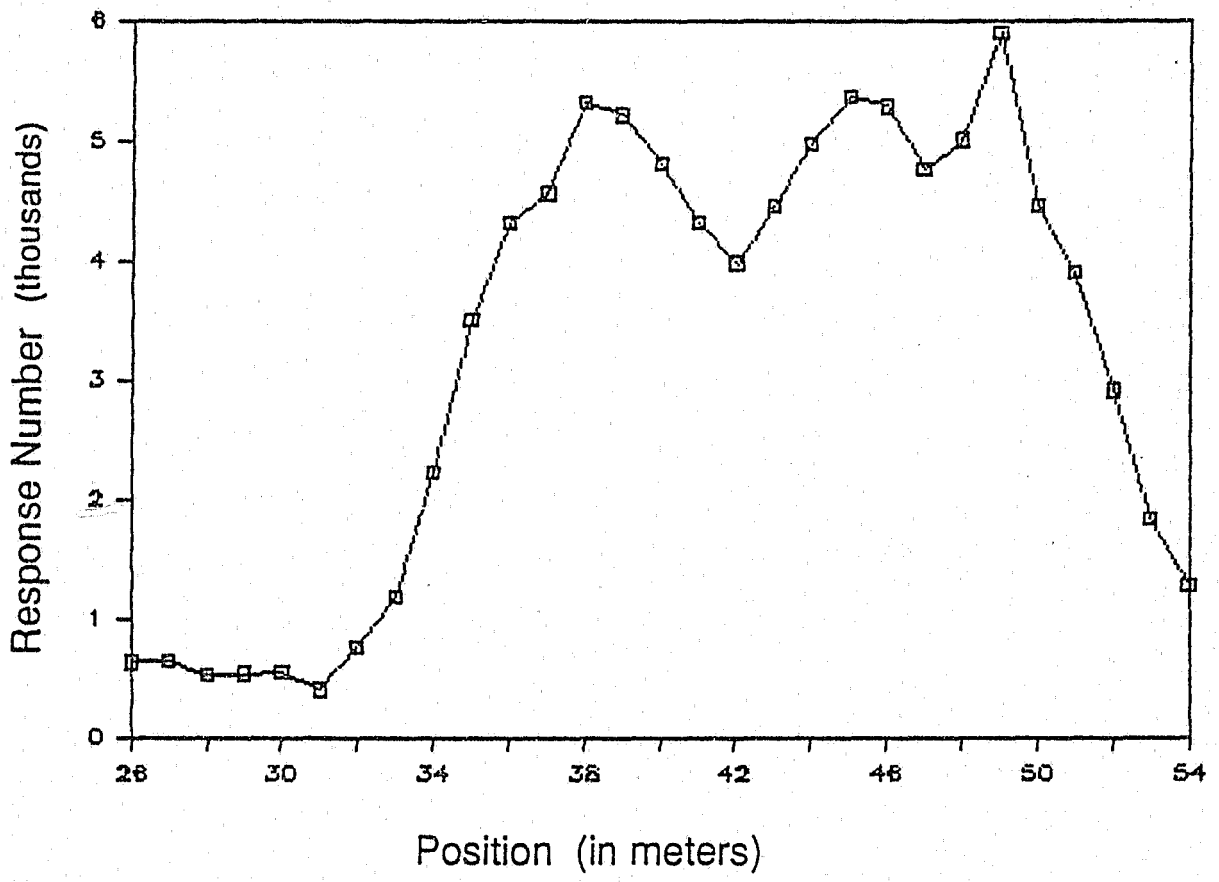

Figure 5.7 Response number profile for positions 26 through 54. Sand region of cell 2 is between positions 33 and 49.

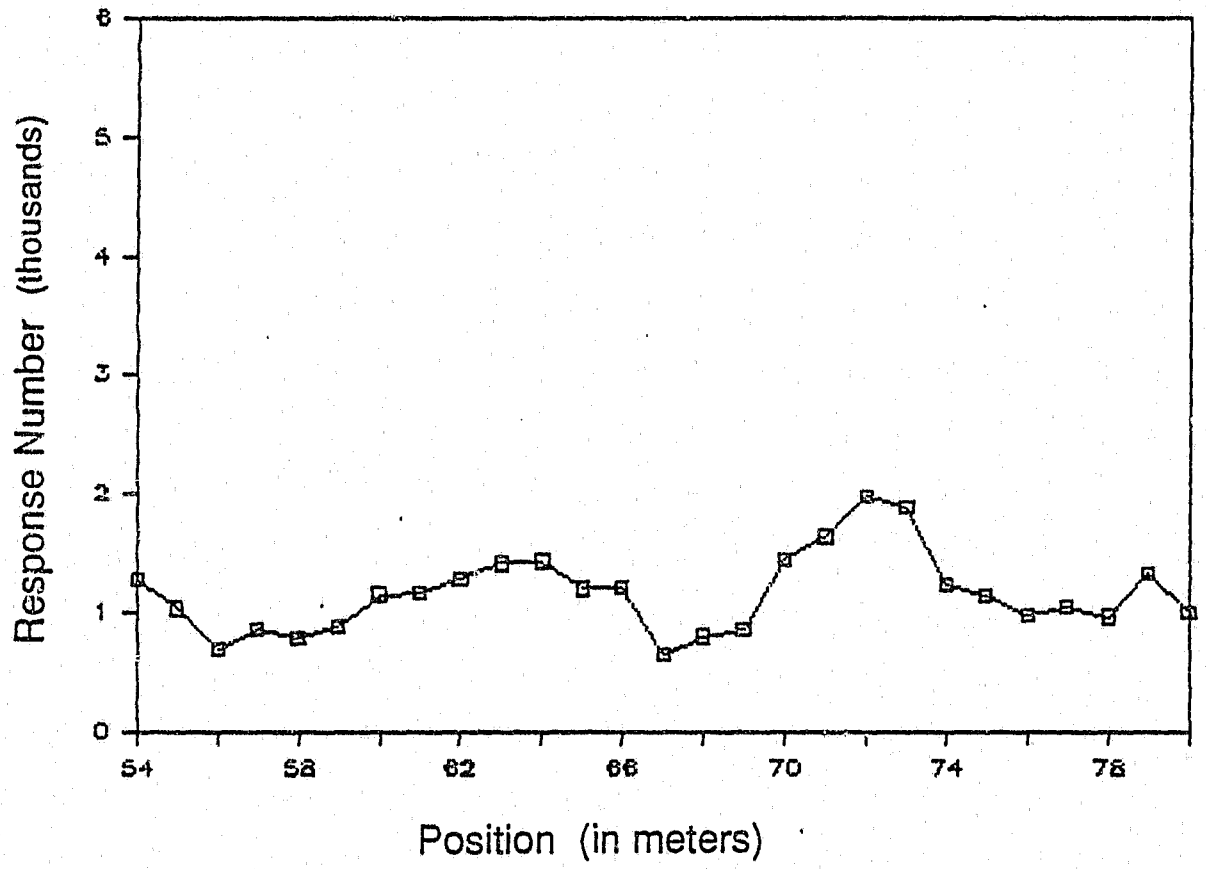

Figure 5.8 Response number profile for positions 54 through 80. Topsoil region of cell 2 is between positions 50 and 66.

characteristics of the soil play an important role in determining the amplitude of the response profile.

The average value of the response number in the middle portion of the sand-filled trench is around 5000. This compares with an average value of around 1000 in the homogeneous topsoil-filled trench which is located between meter marks 50 and 66.

There are several important observations that should be made at this point. First, the sensitivity ratio, the ratio between the maximum response number in the sand trench to the maximum response number in the topsoil trench, is about 6:1. This is highly undesireable as it would make it impossible to distinguish between a person crossing in the low response region and a smaller object (like a dog) crossing in the high response region. Previous studies (Frankel et al, 1984) have concluded that to be able to distinguish between people and small animals we will need to have a sensitivity ratio of no higher than 3:1.

Another important observation is that within a region characterized by a single homogeneous soil type the response profile does vary, but the sensitivity ratio is well within the 3:1 limit.

As a final observation we note that the response profile reaches its lowest values at positions which are near the interfaces between different soil types. For example, the first minima is found at meter mark 31 which corresponds to the interface between the native non- homogeneous soil and the homogeneous sand. The next minima is found at meter mark 56 which is close to the interface between the homogeneous sand and the homogeneous topsoil. The next minima is found at meter mark 67 which is next to the interface between the homogeneous topsoil and the native non-homogeneous soil.

5.2.5 Conclusions

From these observations we conclude that the electrical characteristics of the soil do play a role in varying the sensitivity of the system. It is not yet known, however, if the soil is the dominant factor in affecting sensitivity. Subsequent sections of this thesis will describe experiments which were conducted in order to quantitatively describe how the electrical parameters of the soil vary as a function of position, and to investigate other factors, such as cable separation distance, which may cause the sensitivity to be uneven.

Another area which will be investigated is the behavior of the electromagnetic waves which extend beyond the cable into the soil. Particular attention will be focused on the behavior of this wave as it passes through interfaces between different soil types. The appearance of low response numbers near these interfaces may indicate the presence of interference patterns which were discussed in Section 3.6. Interference patterns are thought to exist due to the interaction of several modes which are excited at the interfaces between different soil types. Subsequent sections will review the results of an experiment that was designed to either substantiate or refute the existence of these interference patterns.

5.3 Cable separation distance test

5.3.1 Test objective

The objective of this test is to find out if the cable separation distance (that is, the distance that the transmitter cable is separated from the receiver cable) varies at each crossing point. If it is found that the cable separation distance does indeed vary then we will graph the variation and try to see if there is any correlation between the cable separation distance and the response number variation.

5.3.2 Implementation

This test was conducted by two persons along the entire length of the test site. With the aid of a Dynatel 500A portable cable locator (made by 3M Corp.), the position of the transmitter and receiver cables at each of the crossing points were marked. The electronic cable locator was found to be accurate to within ±1/2 inch.

Using a tape measure, the distance between them was measured and the cable separation distance was recorded along with the corresponding meter mark number of the crossing point. This process was repeated at all 200 crossing points and the data was graphed as "cable separation distance as a function of position" (as denoted by the appropriate meter mark numbers.)

5.3.3 Test Results and Discussion of Data

Figures 5.9 through 5.14 show the cable separation profiles (i.e. how the cable separation distance changes as a function of position along the cable-pair) for all 6 cells. Figures 5.15 and 5.16 show an expanded view of the cable separation profile for the central section of the test site between meter marks 26 and 80 (cell 2 is between meters 33 and 66). A complete listing in tabular form of the results of this experiment will be found in Appendix B.

Inspection of these cable separation profiles shows that the cable separation does indeed vary as a function of position, and to an extent that was greater than expected. Since the cables were buried in fairly narrow "ditch witch" type trenches (about 7 inches wide) it was naively expected that the cable separation distance would remain fairly constant. Upon examination, however, it is obvious that the cables did not tend to settle to the center of each of the trenches but rather could be anywhere along the width of the trench floor. This being the case we would expect a maximum variation in the cable separation distance of about 14 inches (± 7 inches). This is in fact the variation we found. The maximum cable separation distance was about 70 inches while the minimum was about 56 inches. Although the centers of the trenches were designed to be 60 inches apart, the average cable separation distance was about 63 inches.

The cable separation profiles also show that the maximum rate at which the cable separation distance varies does not usually exceed 2 inches per crossing point. Since each crossing point is 1 meter apart this rate of variation is not unreasonable.

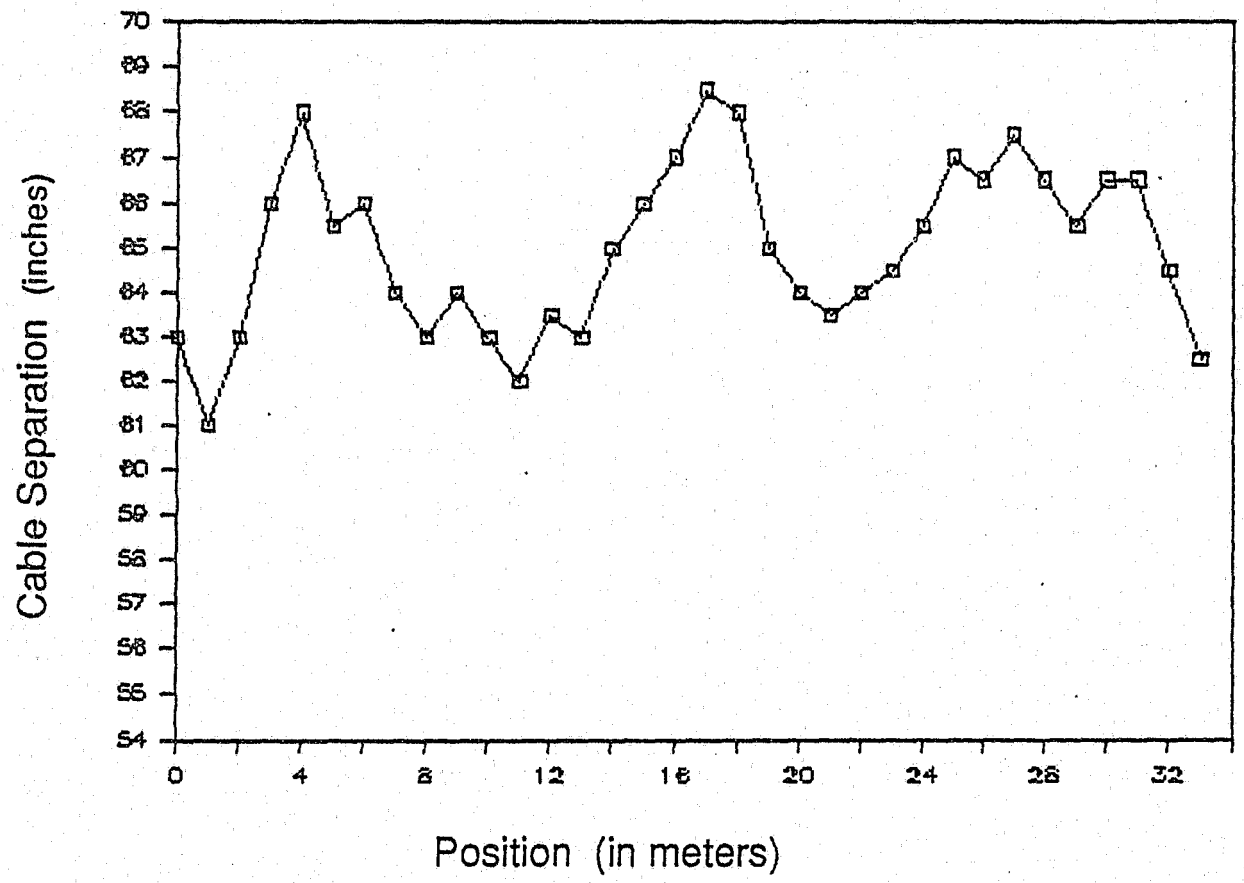

Figure 5.9 Cable separation distance at each position in cell 1.

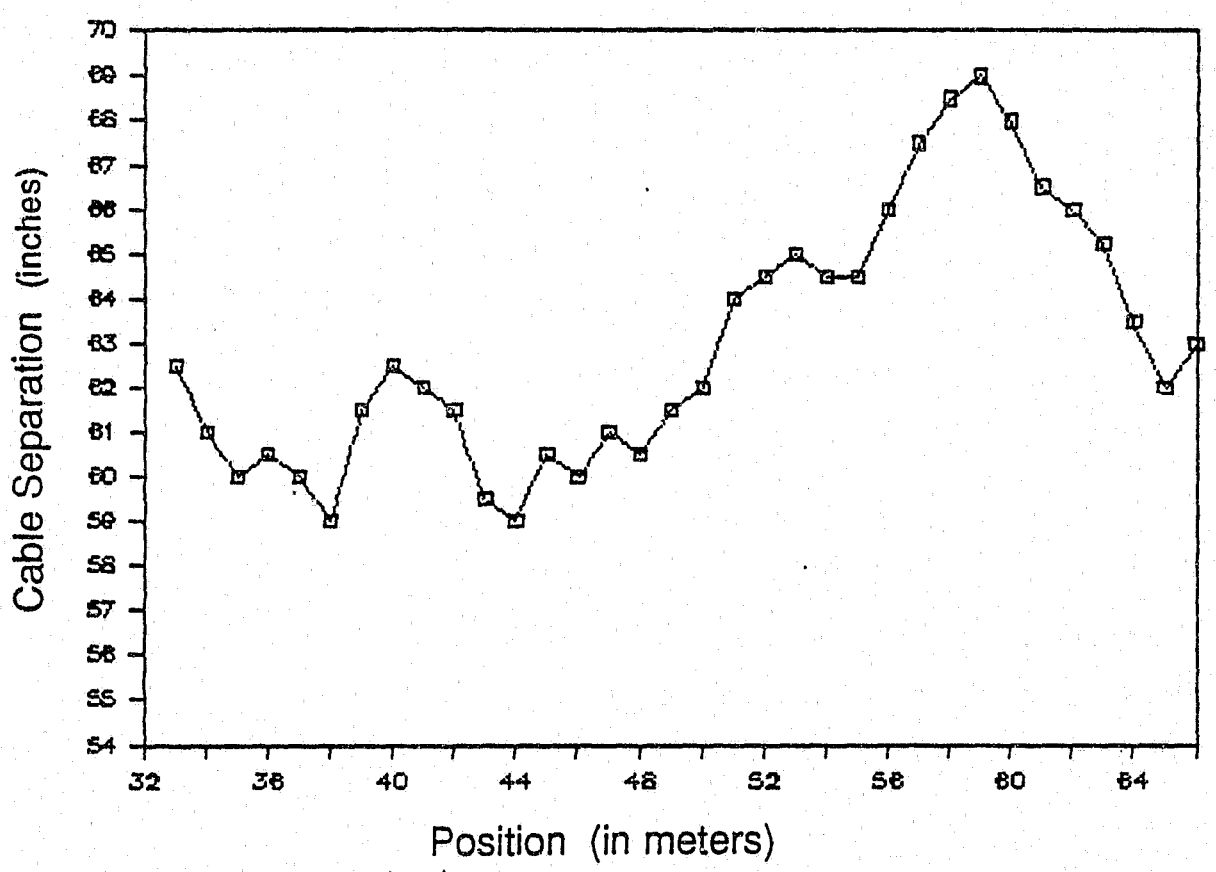

Figure 5.10 Cable separation distance at each position in cell 2.

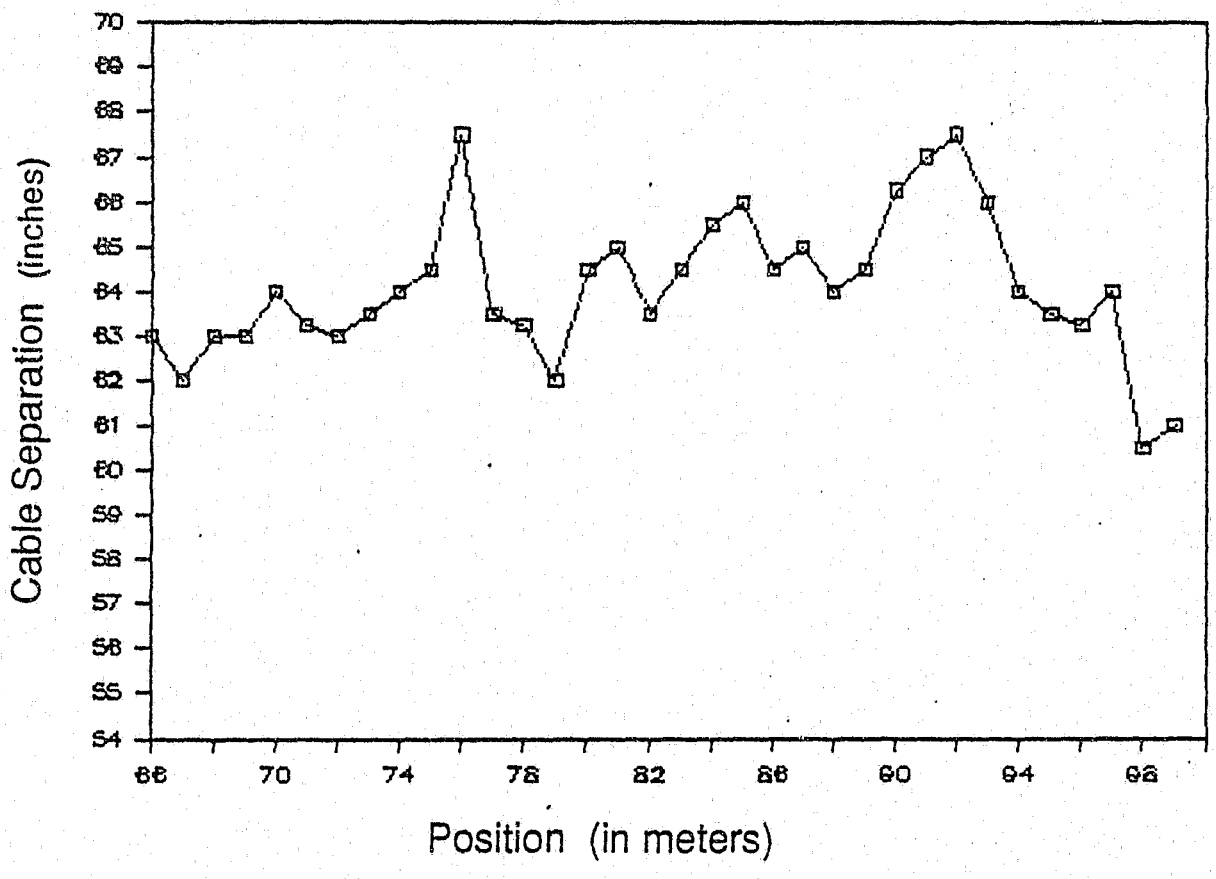

Figure 5.11 Cable separation distance at each position in cell 3.

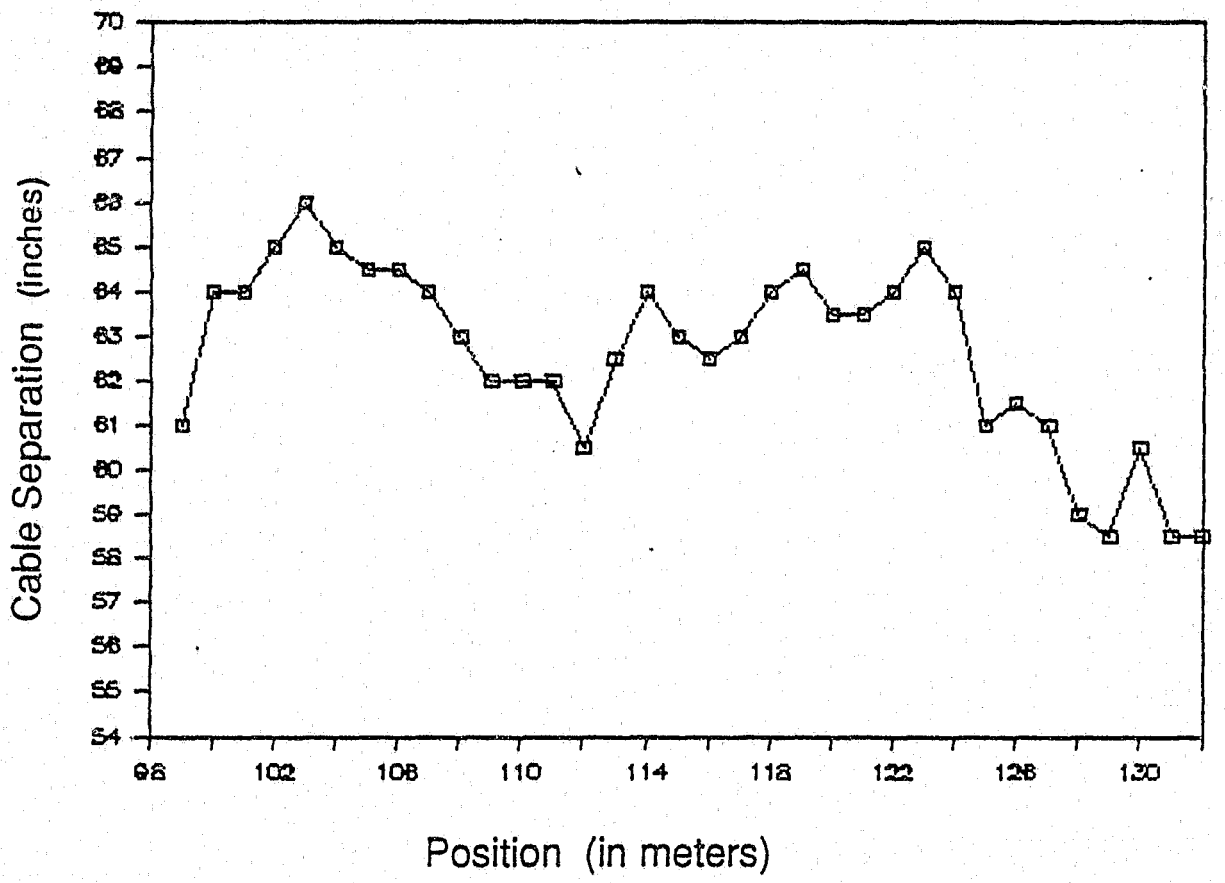

Figure 5.12 Cable separation distance at each position in cell 4.

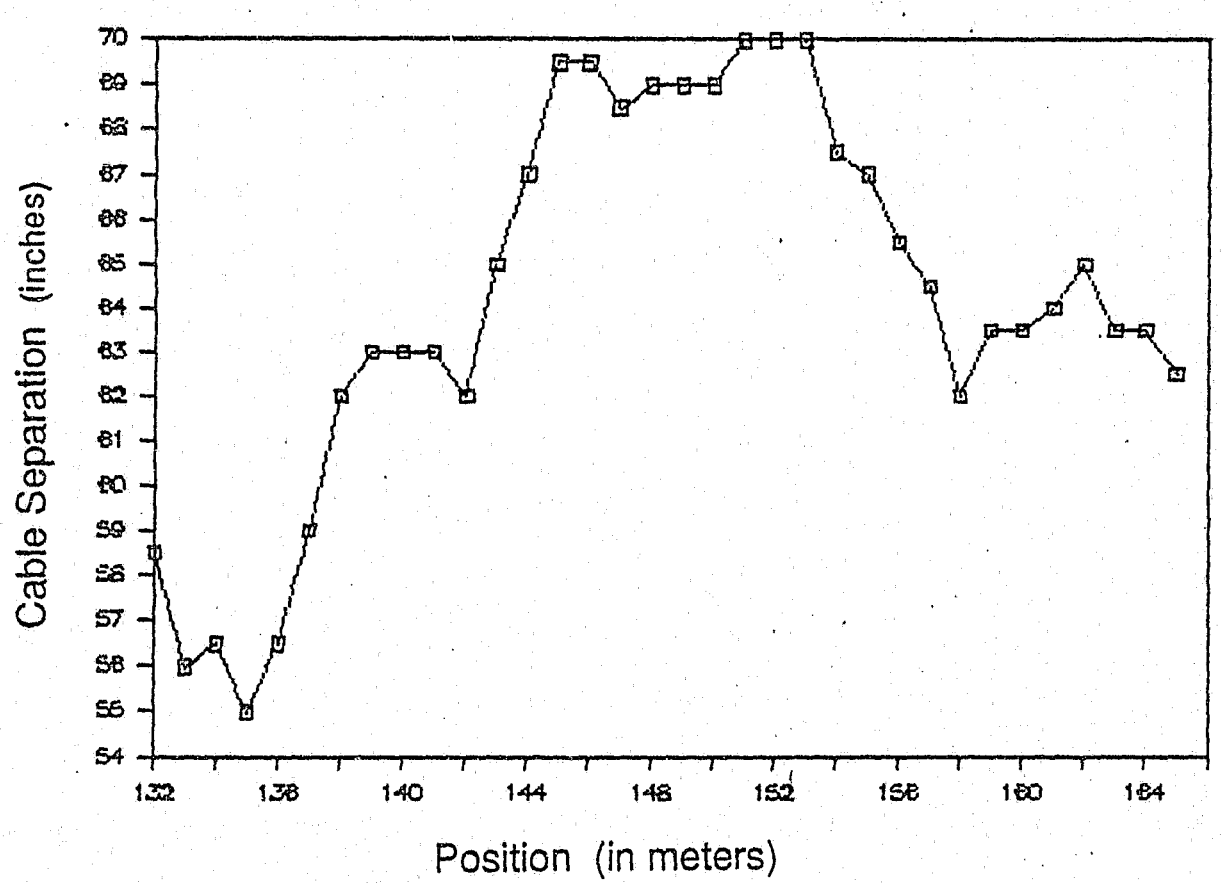

Figure 5.13 Cable separation distance at each position in cell 5.

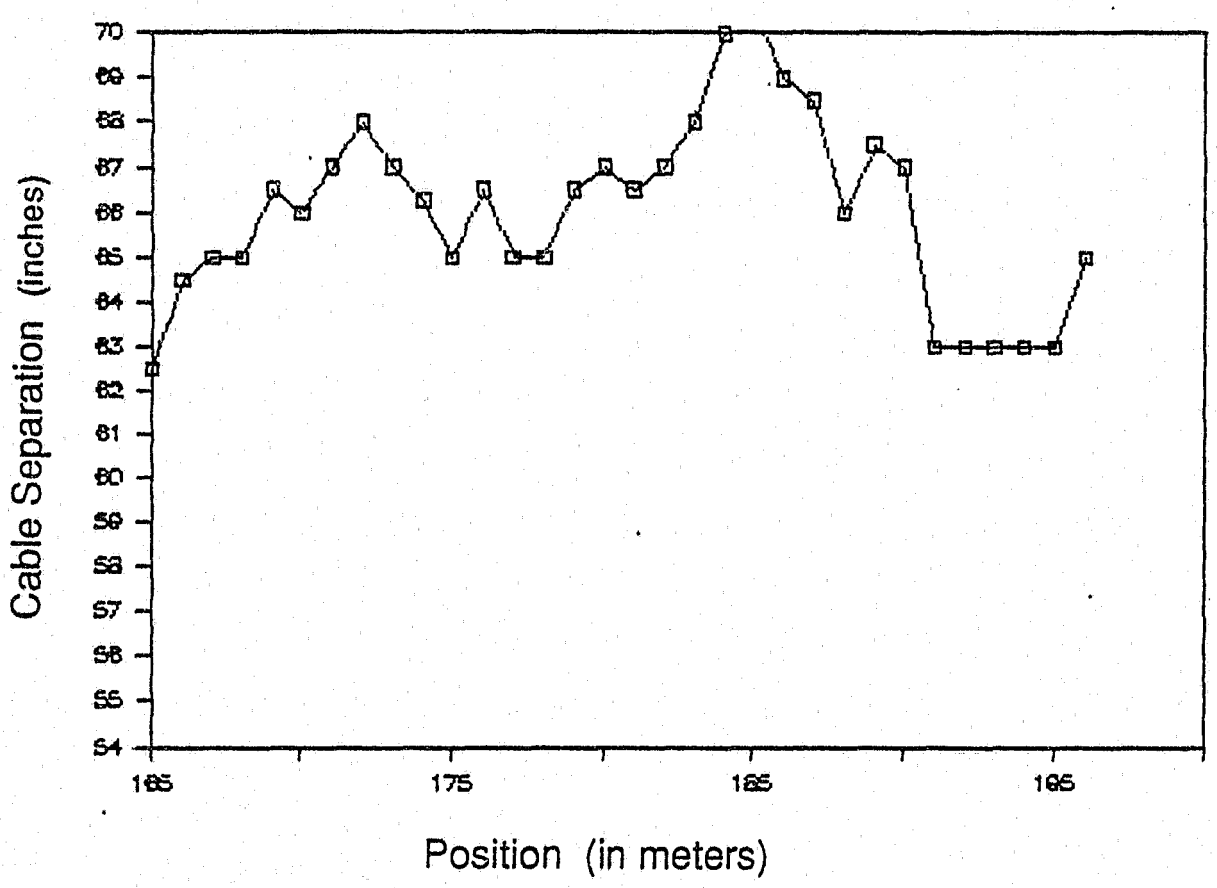

Figure 5.14 Cable separation distance at each position in cell 6.

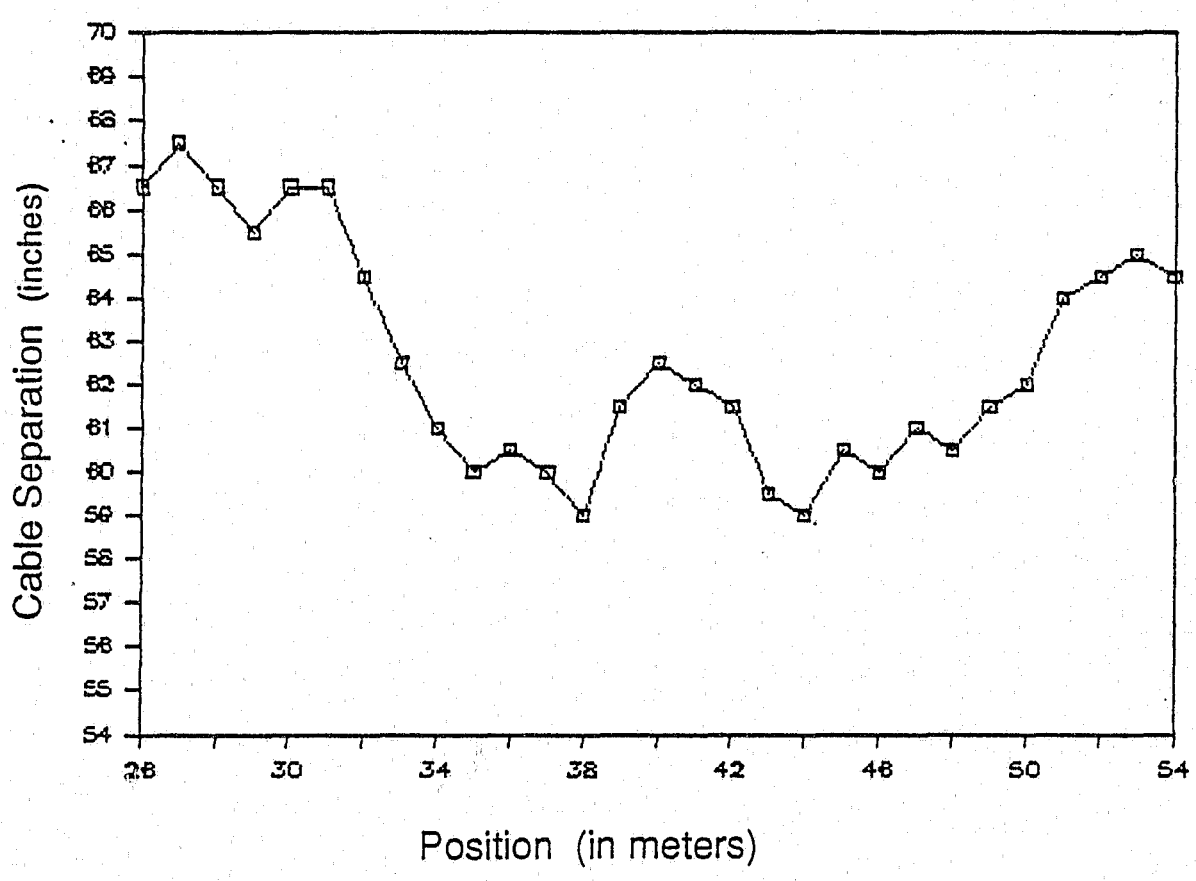

Figure 5.15 Cable separation distance at each position between meter marks 26 and 54.

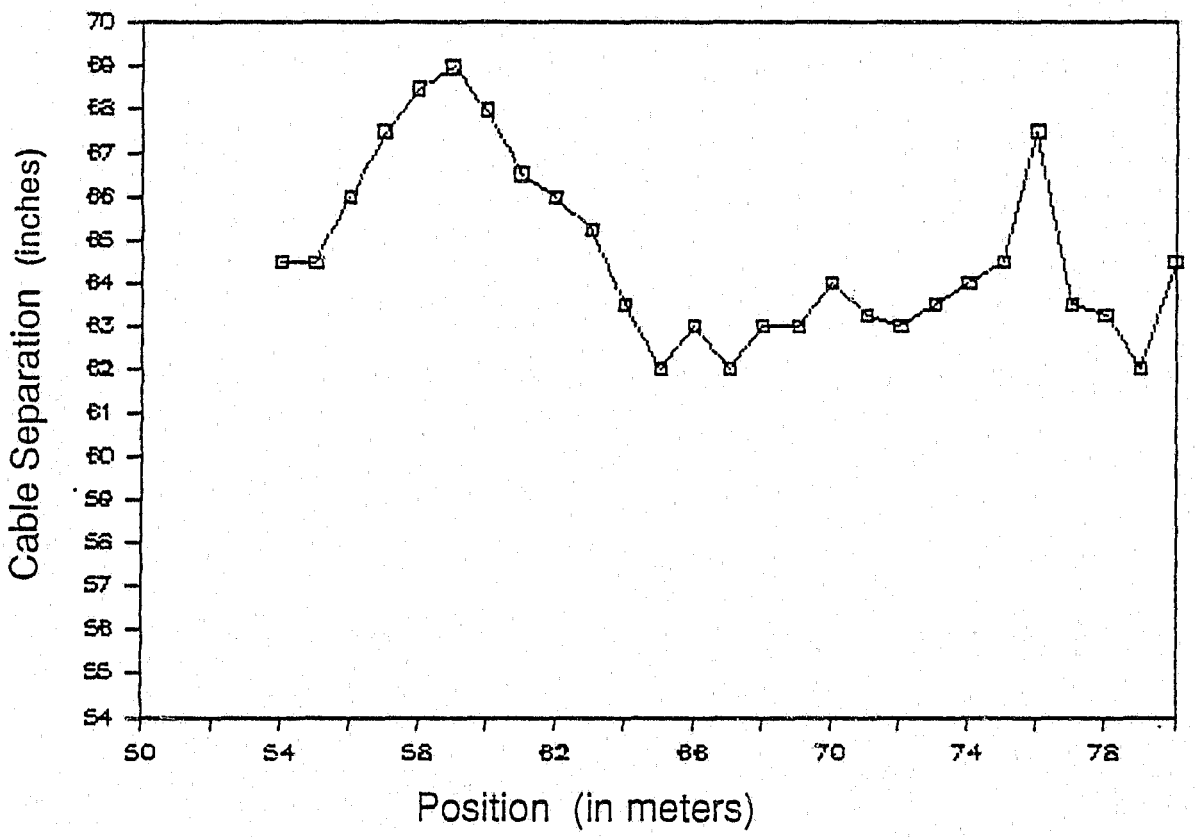

Figure 5.16 Cable separation distance at each position between meter marks 54 and 80.

The largest variation in cable separation distance occurs in cell 5 (Figure 5.13) between meter marks 144 and 156. In this area extremely hard layers of caliche and/or rock were encountered. As described in Chapter 4, the trenches were dug using a "ditch-witch" trench digger. Upon hitting the caliche, the ditch-witch was deflected slightly and as a result the spacing between the trenches increased by several inches.

5.3.4 Conclusion

This experiment shows that the cable separation distance varied at every crossing point and that the variation is larger than expected. Since the variation is significant it needs to be seen whether or not this variation might play a role in affecting the response profile of the system. In subsequent sections we will find that adjusting the cable separation distance is, in fact, an effective way to adjust the sensitivity.

5.4 Soil conductivity and permittivity test

5.4.1 Test Objective

The objective of this test is to determine the relative level and rate of variation of the conductivity and permittivity of the soil as a function of position along the system. These parameters define the electrical characteristics of the soil in that they describe the effect that the soil has on an electromagnetic wave passing

through it. In Chapter 6 the results of this test will be compared with the results of the response profile test to determine whether a correlation between the two exists.

In the soil, the relative permittivity, ε_r, determines, in part, the velocity at which a wave, whose electromagnetic fields extend through the soil, travels through the soil. The conductivity, on the other hand, defines how much energy is absorbed into the soil as the wave propagates through it. Thus, the higher the conductivity the more the wave is attenuated as it passes through the soil.

We are interested in examining the variations in the conductivity and permittivity at each crossing point since it is seen that these parameters play an important role in determining the strength of the transmitted signal that can be scattered into the receiver cable. Since the response profile is a measure of the coupling between the cables, this implies that the variation in the conductivity and permittivity of the soil directly affects the response profile.

Another objective of this experiment is to test the homogeneous sand and homogeneous topsoil in cell 2 to see if they are, in fact, homogeneous. This should also serve as a check on the operation of the soil probe itself (see Section 5.4.2) in that we should see a noticeable difference in the soil probe readouts between the two quite different homogeneous soil types.

5.4.2 Soil probe

In order to carry out this experiment it was necessary to have some way in which to easily measure the conductivity and relative permittivity of the soil. The

nature of this experiment requires that the measuring device (hereafter called the soil probe) be portable, battery powered, and that it should measure the permittivity and conductivity of the soil at the same frequency (63 MHz) that the PCCS system operates at. The requirements for just such a soil probe have been met by a device designed at Ohio State University (Caldecott, Poirier and Svoboda, 1985).

The entire soil probe consists of two main parts which are connected by an RG-58U coaxial cable. First there is the bore-hole probe. This consists of a probe tip made of brass plates and lexan that is at the end of a 1.5 meter aluminum pipe with a T-bar handle at the top. It is this probe tip which is put into a previously made hole in the soil in order to take a soil probe reading. The brass plates in the probe tip act as a capacitor with the surrounding soil acting as the capacitor's dielectric filling.

The second part of the soil probe is a reflectometer, that is, it measures the reflection coefficient seen at the probe tip. The reflection coefficient of this probe tip capacitor is related to the complex admittance of the capacitor, from which the conductivity and permittivity of the soil can be determined (Caldecott et al, 1985). Two digital panel meters output the real and imaginary parts of the complex reflection seen by the reflectometer. In order to convert these outputted numbers into real values of conductivity and relative permittivity one must calibrate the probe to obtain two calibration parameters. These parameters together with the complex reflection coefficient yield the conductivity and relative permittivity (Caldecott et al, 1985).

It should be noted that this measurement is very localized; that is, it measures the conductivity and permittivity within several inches of the the probe tip.

5.4.3 Implementation

It was first necessary to make a 2 inch diameter, 9 inch deep hole in the soil at the desired location of each soil probe test. The hole was made by sledge-hammering a hollow steel pipe into the ground at the test point and then removing it carefully in order to prevent the sides of the hole from caving in. The probe tip was then put all the way into the hole to a depth of 9 inches. This depth corresponds to the depth of the buried PCCS cables.

The soil around the probe tip was then compacted with a heavy steel bar until the readouts on the digital meters stabilized. The compacting of the soil was necessary in order to insure that there were no air gaps around the brass plates in the probe tip which would cause an erroneously low conductivity and permittivity reading.

The soil was, therefore, not truly in situ soil, but was disturbed to some degree at the surface of the probe. The electromagnetic field of the probe senses the soil within a few inches of the probe, and therefore, senses both the soil that is disturbed at the probe surface and the quasi-in situ soil (i.e., only slightly disturbed soil) that is a few inches from the probe.

The readouts from the two digital meters were recorded and converted into conductivity and relative permittivity values using conversion formulas found in the soil probe report (Caldecott et al, 1985). These calculated values were recorded along with the corresponding meter mark number.

After taking a few soil parameter measurements it became apparent that the

conductivity and permittivity of the soil could change considerably over a distance of a few inches. This meant that a single reading could not characterize the soil at a particular crossing point. A new method was needed in order to accurately characterize the soil parameters in the vicinity of a given crossing point.

Additionally it was found that the soil outside of cell 2, that is, all the native soil, was so hard that in some cases the steel pipe could not be driven into the ground to make the hole. In other cases where it was possible to make a hole, the probe would get stuck and some damage occurred in trying to remove it from a test hole. Due to these reasons it was necessary to confine the soil parameter test to cell 2 which contained sand in the first half of the cell and topsoil in the second half.

Before proceeding with this experiment it was necessary to devise a way to accurately characterize the soil parameters at each crossing point. It was determined that since the characteristics of the soil rapidly changed with distance it was necessary to take many readings around a given crossing point and take an average. This average will then characterize the average conductivity and permittivity around that given point.

Due to the laborious and time-consuming nature of taking each soil probe reading it was desired to know the least amount of soil measurements necessary in order to get an accurate average; therefore, a simple test was devised.

Around a crossing point, eighteen soil probe tests were made and the averages of the measured conductivities and permittivities were determined. Six of these points were on the crossing point line which was normal to the cable-pair. The other 12 points were on 2 other lines on either side and parallel to the first line.

These lines were separated by half a meter, thus covering an area 1 meter by 2 1/2 meters.

The next step was to determine the average values using fewer sample points. The sample points chosen were always along or symmetrical to the crossing point line which is normal to the cable-pair. Using this method it was found that 8 to 10 samples were needed to obtain an average value that was within 1% of the average obtained by using 18 samples. Using more than 10 samples was not necessary while using less than 8 samples meant that the average obtained was probably not a realistic average value which characterized the region around the crossing point.

This test was repeated twice at two other locations at the test site and these tests confirmed that a minimum of 8 samples are needed to obtain an average which will characterize an area 1 by 2 1/2 meters. Since the procedure is to characterize the soil parameters in an area corresponding to a crossing point, the configuration of the 8 sample points was: 4 evenly spaced points along the crossing line between the cable-pair, 2 points on the crossing line outside the cable-pair, and 2 points on either side of the crossing line which are each 1/2 meter from the crossing line. This configuration is shown in Figure 5.17.

This configuration was chosen because it came the closest to representing the area crossed by the standard person doing the response profile test. Also, since this test was done at 1 meter intervals it meant that the 2 sample points downline from the crossing point could be used as the 2 sample points upline from the next

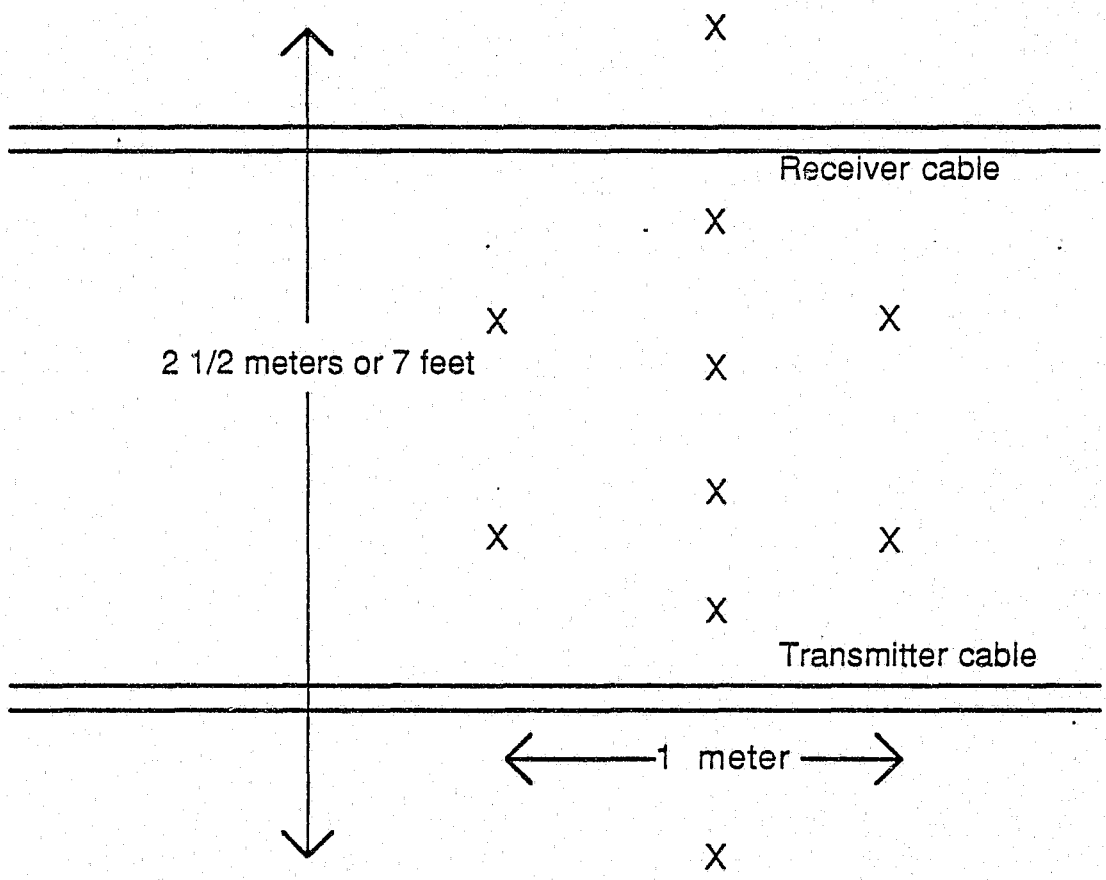

Figure 5.17 Soil sample test, measurement locations.
X's indicate locations of soil measurements.

crossing point. Thus, we could use 10 points to obtain the average while only having to bore 8 holes per crossing point.

Using this testing procedure, measurements were taken starting at the beginning of cell 2 (meter mark 33). The holes were bored, readings were taken, and calculated values for conductivity and relative permittivity were determined. All this data was recorded along with the number of the corresponding crossing point. When all 10 sample points were tested, the averages of the conductivity and relative permittivity were calculated and recorded.

5.4.4 Test Results and Discussion of Data

Figures 5.18 through 5.21 show how the conductivity and relative permittivity of the soil varied as a function of position between meter marks 33 and 65 (i.e. cell 2). The interface between the two homogeneous soil regions is between meter marks 49 and 50. Figure 5.22 shows the loss tangent (at 60 MHz) as a function of position.

In Figures 5.18 through 5.22 the location of the interface between the homogeneous sand and the homogeneous topsoil is easily identified as occurring between meter marks 49 and 50. As was expected the conductivity and permittivity of the sand was much lower than that for the topsoil.

The average conductivity for the sand was around 2.5 mmhos/meter while for the topsoil the average was around 18 mmhos/meter. The average relative permittivity of the sand was about 5 while the average for the topsoil varied around

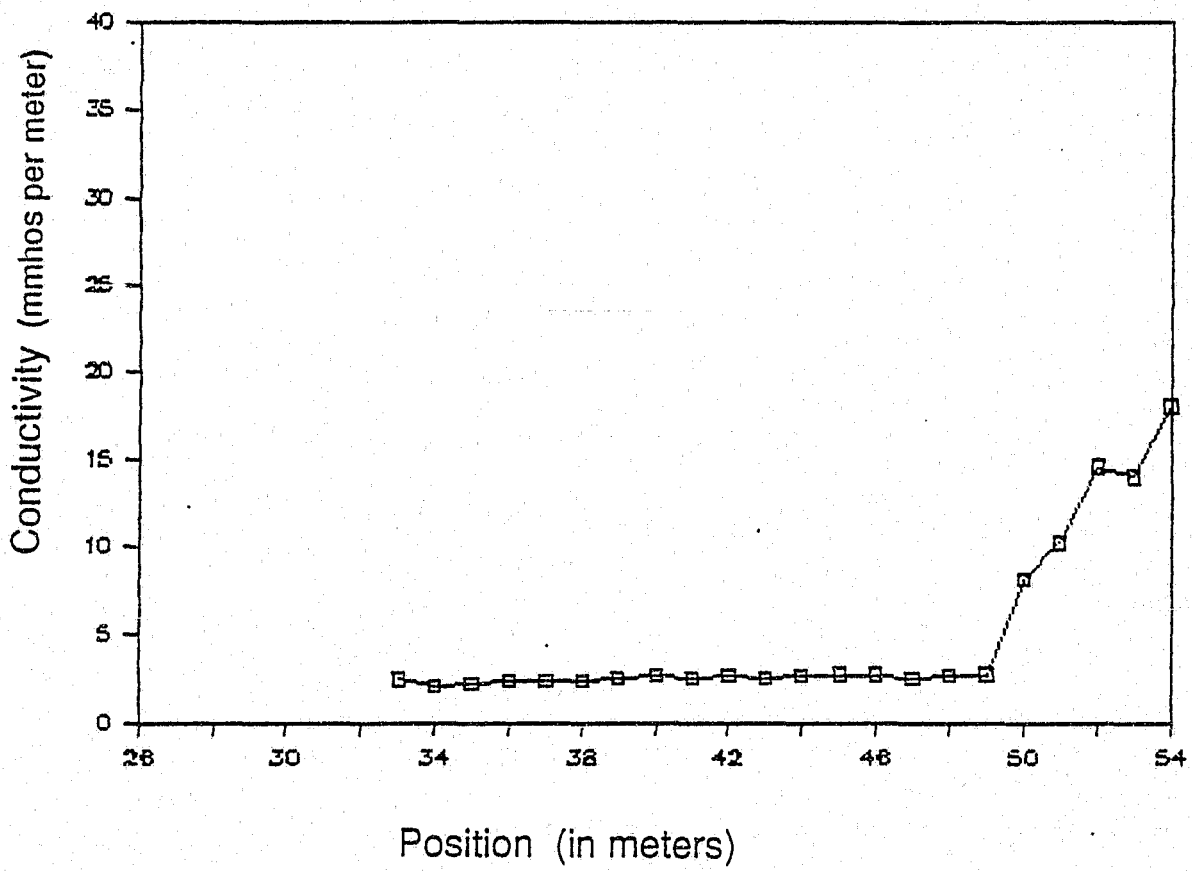

Figure 5.18 Conductivity of the soil at each position between meter marks 33 and 54. Sand region of cell 2 is between positions 33 and 49. Topsoil region is between positions 50 and 66.

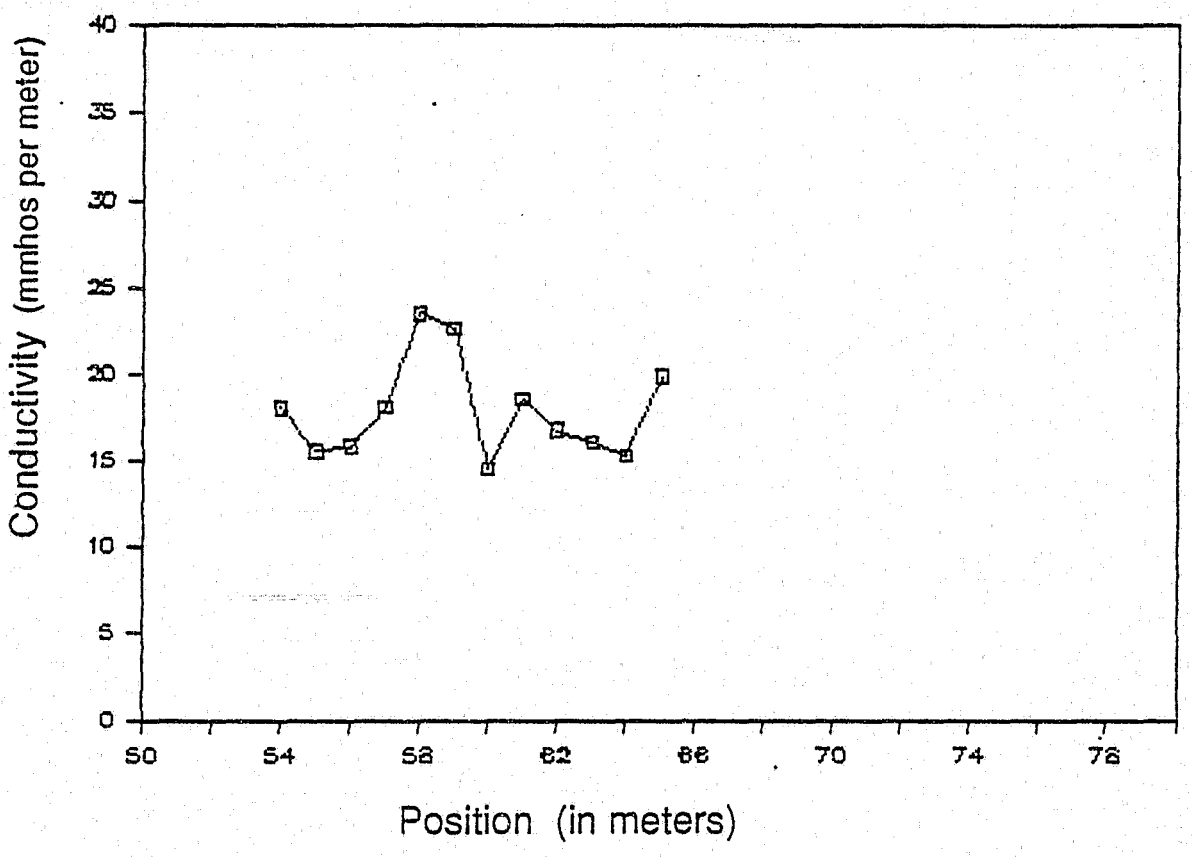

Figure 5.19 Conductivity of the soil at each position between meter marks 54 and 65. Topsoil region of cell 2 is between positions 50 and 66.

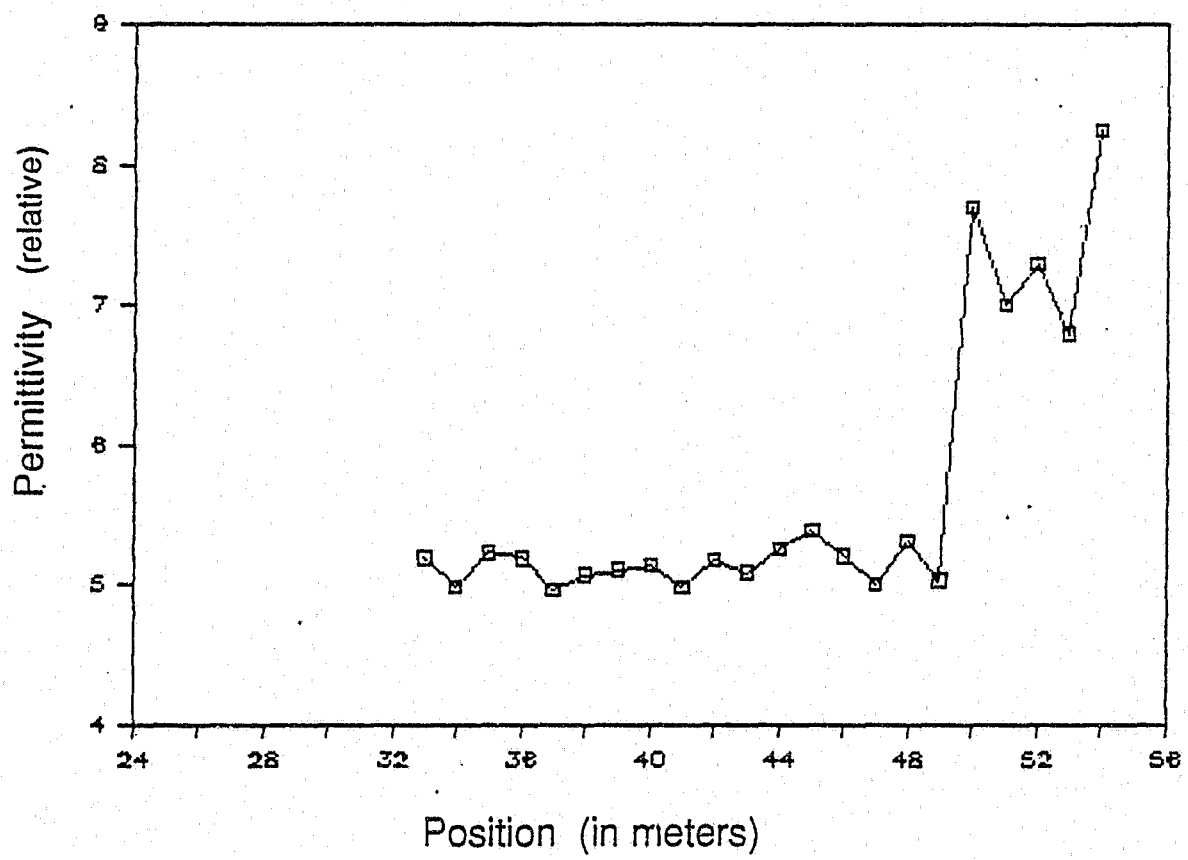

Figure 5.20 Relative permittivity of the soil at each position between meter marks 33 and 54. Sand region of cell 2 is between positions 33 and 49. Topsoil region is between positions 50 and 66.

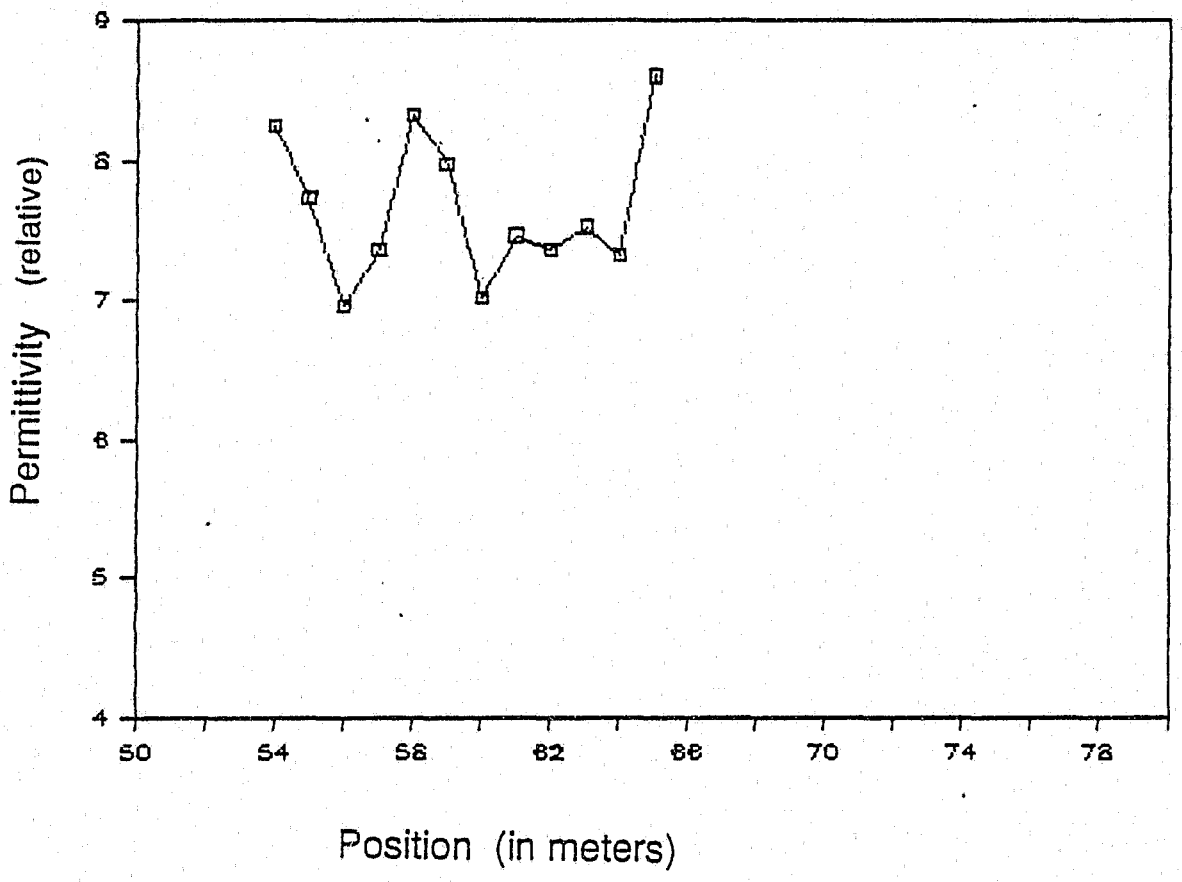

Figure 5.21 Relative permittivity of the soil at each position between meter marks 54 and 65. Topsoil region of cell 2 is between positions 50 and 66.

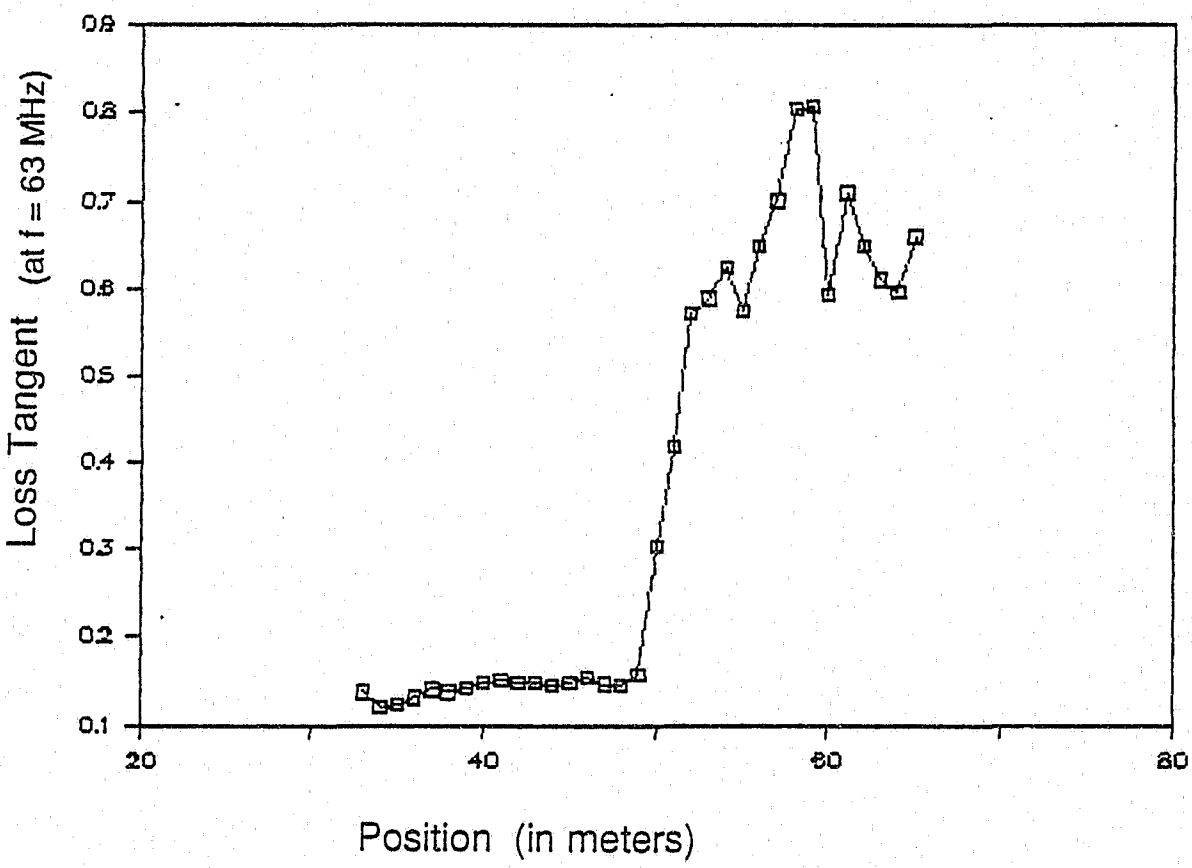

Figure 5.22 Loss tangent of the soil (at a frequency of 63 MHz) at each position between meter marks 33 and 65. Sand region of cell 2 is between positions 33 and 49. Topsoil region is between positions 50 and 66.

an average value of 7.5. In the sand region the profiles for both soil parameters were basically flat while in the topsoil region the profiles vary slightly. It is significant, however, that even though the profile varies in the topsoil region, the variation is always within a range that was can easily be distinguished from the that of the sand.

5.4.5 Conclusions

From these observations we can conclude that, first, the assumption we have made regarding the homogeneous nature of the sand and the topsoil has been validated. It is clear from the flat profiles that the sand is homogeneous. The topsoil region has been shown to be very nearly homogeneous also, although some slight inhomogeneity exists.

Second, we now know that the soil probe is capable of giving us soil parameter data which allows us to differentiate between different soil types. It is also clear that the method of averaging the values obtained from 10 soil samples is yielding good results since the seemingly random data from each measurement averages into well defined ranges for both the sand and topsoil.

Finally, we now have quantitative evidence that the conductivity and the permittivity of the soil does vary as a function of position. Referring back to Figure 5.2 we see that the response numbers are much greater in the sand compared to the response numbers obtained in the topsoil. This experiment seems to indicate that increased conductivity and permittivity does indeed reduce the electromagnetic

coupling between the PCCS cable-pairs, and hence reduces the response number, as was earlier postulated.

5.5 Magnetic Field Intensity Test

5.5.1 Test objective

The objective of this test is to measure the magnetic field on the ground surface directly above the transmitter cable and to investigate the variation in this field as a function of position along the transmitter cable. This information will provide information regarding the behavior of the electromagnetic surface wave as it travels along the outside of the leaky coaxial cable which acts as the guiding structure for the wave.

The results of this test will be used as follows. First, we can determine if the magnetic field profile varies proportionally to the response number profile. Second, the profile will be analyzed to ascertain the presence of interference patterns (Section 3.4) which are theorized to exist at the interface between 2 different soil types.

5.5.2 Theory

It is assumed that the response number is related to the amount of transmitted energy which is scattered into the receiver cable at the point where an intrusion occurs. Since the response number profile varies as a function of position it is assumed that the electric and magnetic field intensities outside the transmitter cable will also vary in a corresponding manner. The existence of such a correspondence will verify the fact that there is a direct relationship between the

magnetic (or electric) field intensity at a location on the transmitter cable and the response number at the same location.

In Sections 3.5 and 3.6, the hypothesis was advanced that due to the interaction of several eigenmodes which were excited at an interface between two media of differing conductivities and permittivities, the resulting constructive and destructive interference between these modes would lead to the existence of an interference pattern of the electromagnetic field on either side of the interface. The current experiment is designed to determine the existence of electromagnetic interference patterns. The magnetic and electric fields at each point will represent the sum of the fields of all modes and thus any interference pattern should be visible as an oscillation of the field intensity versus position plot.

5.5.3 Implementation

This test was conducted using an EE&G MGL-2 (Multi- Gap Loop) B-dot magnetic field sensor with an attached EE&G DLT-96 balun. This magnetic field sensor was used to measure the relative strength of the magnetic field on the ground surface directly above the transmitter cable. The magnetic field is assumed to exist primarily in the plane normal to the axis of the cable. The sensor, or probe, was therefore oriented so that it measured the component of the magnetic field normal to the cable axis and parallel to the ground surface. This type of sensor was selected because it was designed so that it would not perturb the field which it was trying to measure.

In order to begin this experiment it was first necessary to use the electronic

cable locator used in the cable separation test in order to mark the exact position of the transmitter cable at every crossing point location where we had planned to take a magnetic field measurement. The reason for marking the cable location was that the sensor had to be placed directly above the transmitter cable in order to receive the maximum signal strength. Always taking each measurement directly above the transmitter cable insured that any variation in the measured signal was due to an actual attenuation of that signal and was not simply a result of not being directly above the cable.

After the location of the transmitter cable at each measurement point had been marked, the magnetic field sensor was connected to an HP 141 Spectrum Analyzer. The spectrum analyzer was tuned to a center frequency of 63 MHz which is the transmitter frequency for the PCCS system.

As the sensor was put in position directly over the transmitter cable, the measured magnetic field component could be detected by the spectrum analyzer. An HP chart recorder was connected to the spectrum analyzer, and a plot of the magnitude of the signal was recorded along with the meter mark number of the measurement location.

The magnetic field sensor was then moved one meter down to the next location, and the process was repeated. Each time the meter mark number was recorded next to the corresponding plot of the magnetic field.

Since one of the main points of this experiment is to observe the magnitude of the magnetic field in the vicinity of interfaces between different soil types it was decided to take magnetic field measurements from meter mark 26 to meter mark 80. is allows for the observation of the magnetic field at the interface between the

nonhomogeneous native soil and the homogeneous sand at meter mark 33, at the interface between the homogeneous sand and the homogeneous topsoil at meter mark 50, and at the interface between the homogeneous topsoil and the nonhomogeneous native soil at meter mark 66. It also allows for the observation of the magnetic field behavior 7 meters before the first interface and 14 meters after the last interface.

After the running of this experiment the whole process was repeated in order to double-check the initial results and also to ascertain the repeatability of the experiment. After both experiment runs were completed, the chart recorder charts were reviewed and the normalized magnitude of the magnetic field intensities were recorded along with the corresponding crossing point numbers. The results of both experiment runs were averaged and this average value was graphed as a function of position in the final graphs of the results of this experiment.

5.5.4 Test Results and Discussion of Data

Figures 5.23 and 5.24 show how the magnetic field intensity varies as a function of position along the PCCS transmitter cable. These graphs show the section of the test site between meter marks 26 and 80 which includes the homogeneous sand/topsoil test cell (cell 2) as well as the last and first few meters of cells 1 and 3, respectively. A complete listing in tabular form of the results of this experiment will be found in Appendix B.

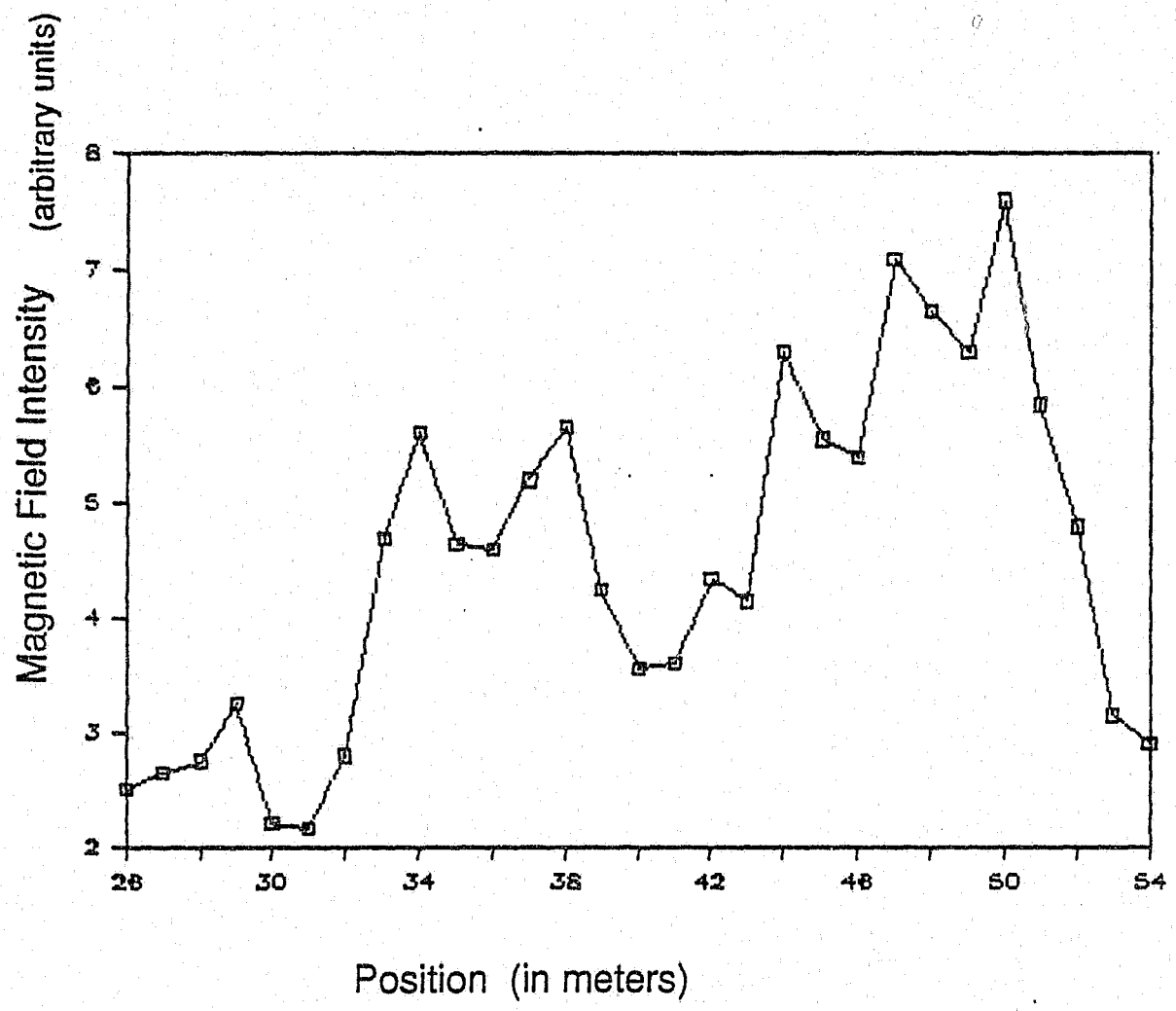

Figure 5.23 Magnetic field intensity at ground surface directly above transmitter cable, for positions 26 through 54. Sand region of cell 2 is between positions 33 and 49. Topsoil region is between positions 50 and 66.

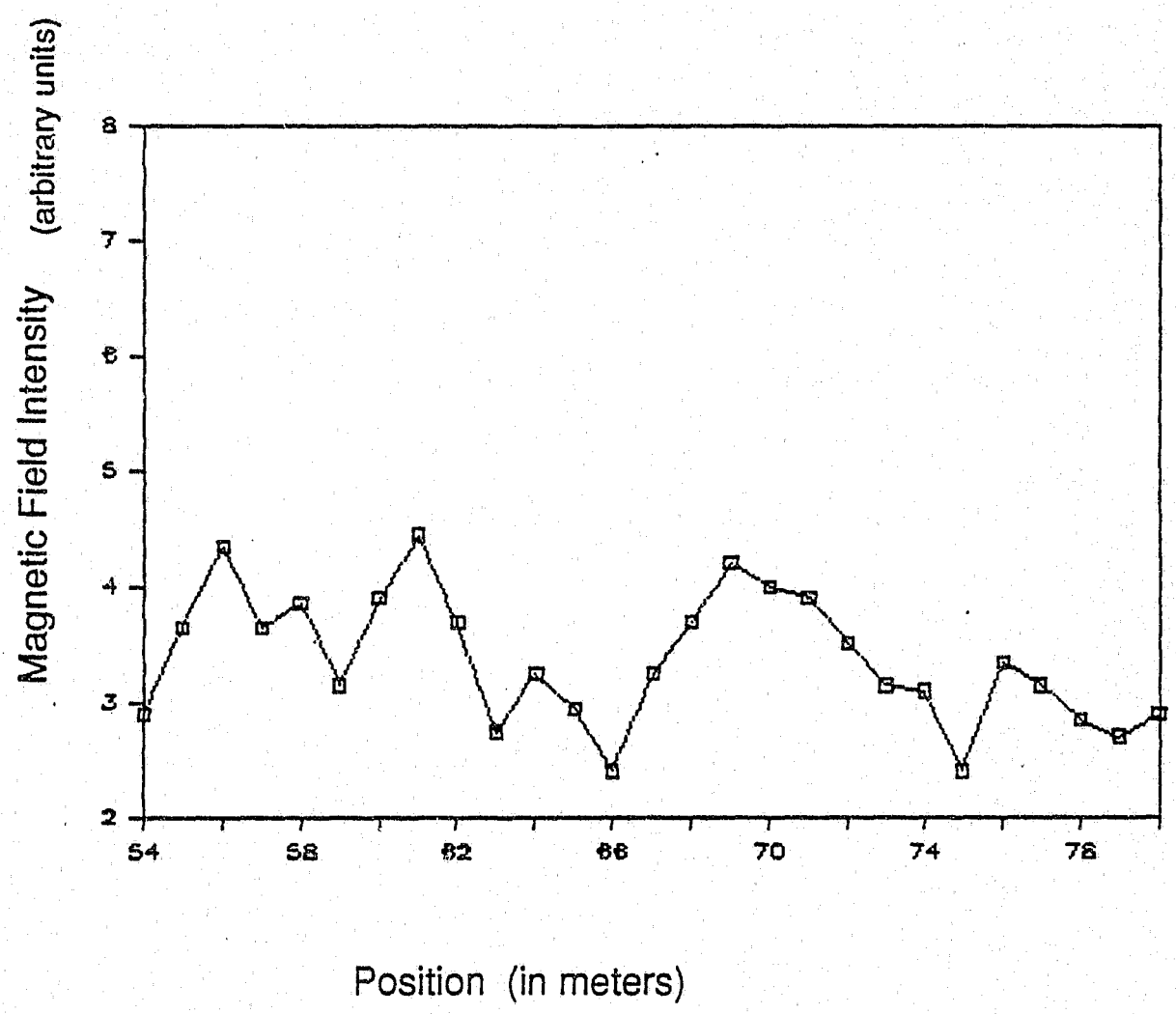

Figure 5.24 Magnetic field intensity at ground surface directly above transmitter cable, for positions 54 through 80. Topsoil region of cell 2 is between positions 50 and 66.

From Figures 5.23 and 5.24 several main features are seen. First, the magnetic field intensity in much higher in the sand (meters 33 to 49) than it is in the topsoil (meters 50 to 66) and native soil regions. The fact that the magnetic field intensity is lower in the topsoil shows that the electrical structure (i.e. conductivity and permittivity) of the topsoil is causing the electromagnetic fields to have a smaller energy density in the soil compared to the sand. This correlates with the the conductivity and permittivity of the topsoil being higher in the topsoil than in the sand.

Secondly, we observe the presence of definite oscillations of the magnetic field intensity as a function of position along the transmitter cable. These oscillations occur on either side of the interfaces between different soil types. The interface at meter mark 50, that is, the interface between the two different homogeneous soils (sand and topsoil) illustrates this most clearly. Since the sand region is the most homogeneous soil region in the test site we expect no additional modes to be created by inhomogeneities in the sand, and therefore, the interference pattern on the sand side of the interface should be very well defined. In Figure 5.23 we see that the oscillations on the sand side of the sand/topsoil interface show a constant periodicity continuing about 10 meters from the interface. After about 10 meters the oscillations appear to die out.

On the sand side of the interface, the distance between adjacent peaks of the interference pattern is about 3 meters ($\pm$ 1/2 meter). On the topsoil side the adjacent peaks of the interference pattern are not periodically spaced, which is probably due to the slight inhomogeneity of the topsoil. The presence of these oscillations and the

fact that they exist on either side of an interface between two different soil types suggests that these oscillations are in fact the interference patterns predicted to exist by the theory of coupled modes discussed in Section 3.5.

In Section 5.4, the relative permittivity was found to be about 5 for the sand region and about 7.5 for the topsoil region. Using Figures 3.3 and 3.4 we see that lower permittivity causes the cut-off frequency of the Surface Wave mode to be higher. Thus, the low soil permittivities measured at the test site suggest that the interference pattern observed at the sand/topsoil interface is due to the interaction of only 2 eigenmodes, the Transmission Line mode and the Goubau mode.

To determine the propagation constant, β_i, of the mode which is interacting with the Transmission Line mode we can use the identity

$$z = \frac{2\pi}{\Delta\beta} = \frac{2\pi}{\beta_i - \beta_3} \tag{5.1}$$

where z is the distance, in meters, between the adjacent peaks of the interference pattern, and β_3 is the propagation constant of the Transmission Line mode.

Solving (5.1) for β_i we obtain

$$\beta_i = \beta_3 + \frac{2\pi}{z} \tag{5.2}$$

Since β_3 is approximately

$$\frac{\omega}{c}\sqrt{\varepsilon_{r1}} = 1.59$$

at 60 MHz for a soil with a relative permittivity of 12, we will use this as an approximate value in (5.2). The distance between the adjacent peaks of the interference pattern on the sand side of the interface is 3 meters, therefore

$$\beta_i = 1.59 + \frac{2\pi}{3} = 3.68 \text{ meters}^{-1} \qquad (5.3)$$

where β_i is the propagation constant for what is assumed to be the Goubau mode. Referring to Figures 3.3 and 3.4, we see that for a fixed frequency the propagation constant of the Goubau mode decreases as the relative permittivity of the soil decreases. At 60 MHz, the propagation constant of the Goubau mode was found to be about 6.0 for a relative soil permittivity of 50, and about 4.7 for a relative soil permittivity of 25. This trend lends credence to the conjecture that β_i is the propagation constant of the Goubau mode, and is approximately 3.68 [meters]$^{-1}$ for a relative soil permittivity of about 5, and, of course, a planar interface between soil and air.

5.5.5 Conclusions

From this experiment we draw two conclusions. First, we conclude that it is the electrical characteristics of the soil that determine the range of electromagnetic energy density. This can be concluded since the measured magnetic field intensity drops off significantly when passing from a soil with low conductivity and permittivity to a soil with a higher conductivity and permittivity. This is also supported by the α/σ plot (shown in Figure 3.13) for the Transmission Line mode, which is probably the dominant eigenmode.

Second, the theory of coupled modes (from Chapter 3) has been tentatively validated by the observation of an interference pattern which is clearly noticeable at the interface between the homogeneous sand and the homogeneous topsoil located at meter mark 50.

5.6 Response Number vs. Varying Cable Separation Test

5.6.1 Test Objective

The objective of this experiment is to determine the effect that changing the cable separation distance has on the response number profile. This experiment consists of two tests which were each conducted in different cells with different soil types. Since it appears that the electromagnetic energy density decreases as a function of radial distance away from the transmitter cable, it is assumed that moving the cables closer together will result in raising the response profile. This assumption will be verified, but, more importantly, we will develop a rule of thumb approximation that will allow us to predict a particular increase (or decrease) in the response profile after moving the cables a particular distance closer together (or further apart).

Such a predictive approximation will be needed to separate out the effects on the response number profile from the two main influencing factors: cable separation distance and the conductivity/permittivity of the soil.

5.6.2 Implementation

Test #1 was conducted along a 4 meter section in the middle of cell 4 where the cable was buried in sand- filled trenches 18 inches wide and 12 inches deep. The soil between the trenches is native soil. Using the electronic cable locater the cable separation distance was measured and recorded for positions 115 through 119. The

cable locater was found to be accurate to within ± 1/2 inch.

As in the response number profile test, the standard person then made two crossings at each meter mark between 115 and 119. The PCCS operator recorded the response numbers along with the corresponding meter mark numbers.

The transmitter cable was then uncovered between meter marks 115 and 119 and the middle of the exposed cable (at mark 117) was pulled about an inch closer to the receiver cable. The cable was then reburied and the cable separation distance and response profile were measured and recorded for all 5 crossing points.

The cable was uncovered, moved, and reburied 2 more times, each time moving the cable about 2 inches towards the center line of the cable pair and recording the new cable separation and response profiles. By the end of test #1 the cable had been moved 4 times (i.e. 4 runs) and the cable separation distance had been decreased by a total of 6 inches.

A second test (test #2) was conducted, this time across a 6 meter section and varying the cable separation distance over a 26 inch range. In order to eliminate the effects of nonhomogeneous soil on the response number profile, this experiment was conducted in the homogeneous sand trench of cell 2. The transmitter cable was uncovered between meter marks 39 and 45 and the middle of the exposed cable (at mark 42) was pulled as far as possible away from the center line of the cable-pair. The cable was then reburied and the same procedure was repeated for the receiver cable. Using the electronic cable locater the cable separation distance was measured and recorded for positions 39 through 45.

As in the response number profile test the standard person then made two

crossings at each meter mark between 39 and 45. The PCCS operator recorded the response numbers along with the corresponding meter mark numbers.

The transmitter cable was then uncovered, moved about 3 inches towards the center line, and reburied. The cable separation distances were measured again and the response profile test for the 7 crossing points was repeated. The entire procedure was repeated 7 more times, each time moving the cables about 3 inches towards the center line. After the 9th run the cables were as close to each other as possible.

5.6.3 Test Results and Discussion of Data

Figures 5.25 and 5.26 show the cable separation distance profiles and the response profiles for each run of test #1 plotted as a function of position. The 5 crossing points selected are located in the middle of cell 4, the test cell with the 2-foot wide, sand-filled trenches. Figures 5.27 and 5.28 show the cable separation distance profiles and the response profiles for each run of test #2. The 7 crossing points selected are located in the middle of the homogeneous sand region of cell 2. The complete data for this experiment is available in tabular form and can be found in Appendix B.

Figures 5.25 through 5.28 graphically illustrate the relationship between cable separation distance and response number. When the cables are at a maximum separation the corresponding response number is at a minimum. As the cable separation is slowly reduced the response profile starts to rise.

In the fifth run of test #2 the cables were nearly parallel over the 6 meter length of this test range. When the cables are parallel any variation in the response number is due to variations in the soil. In test #2 we chose homogeneous sand as .

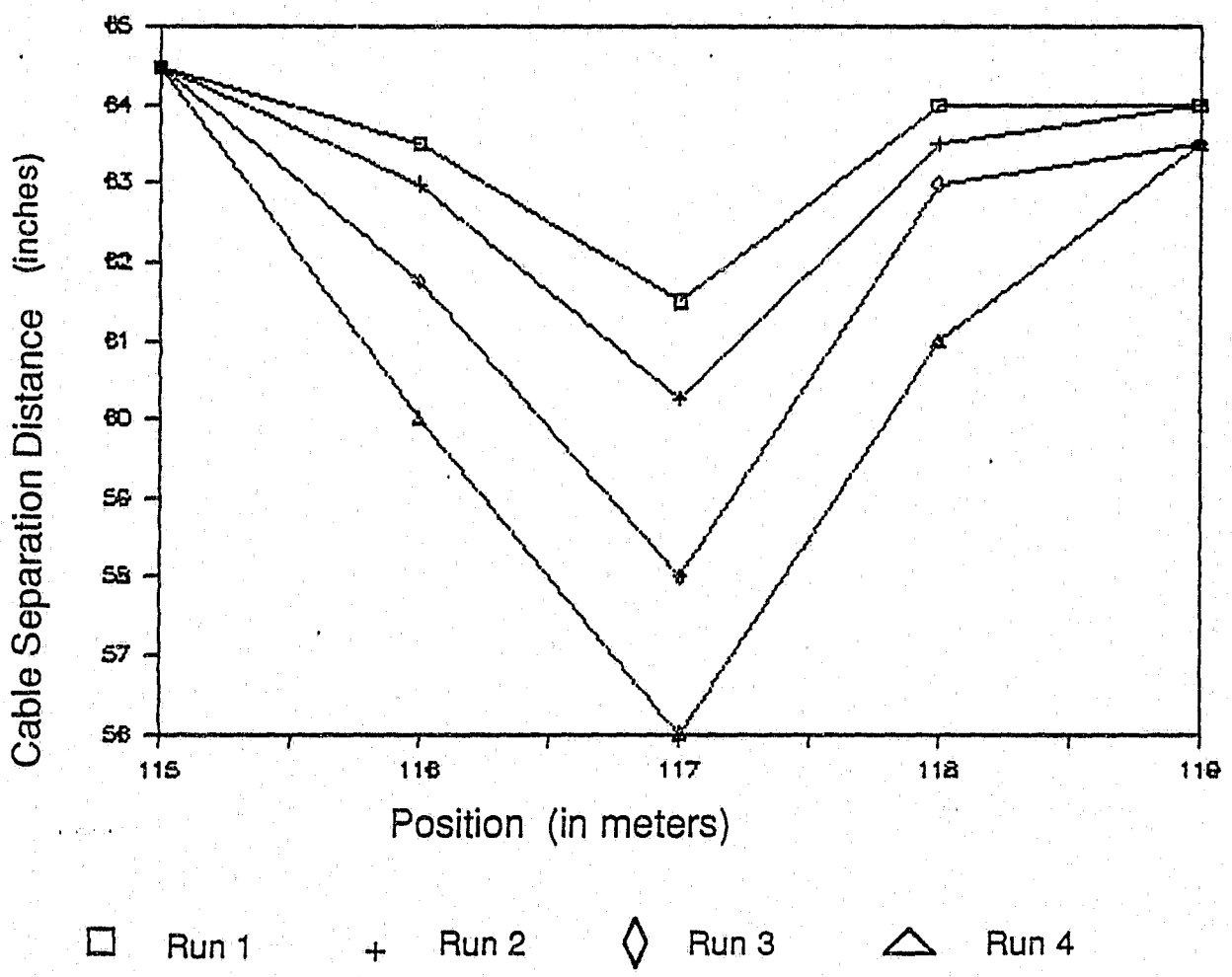

Figure 5.25 Cable separation distance at each position, after each run of "Response number vs. varying cable separation test #1." Fig. 5.26 shows resulting response number profiles.

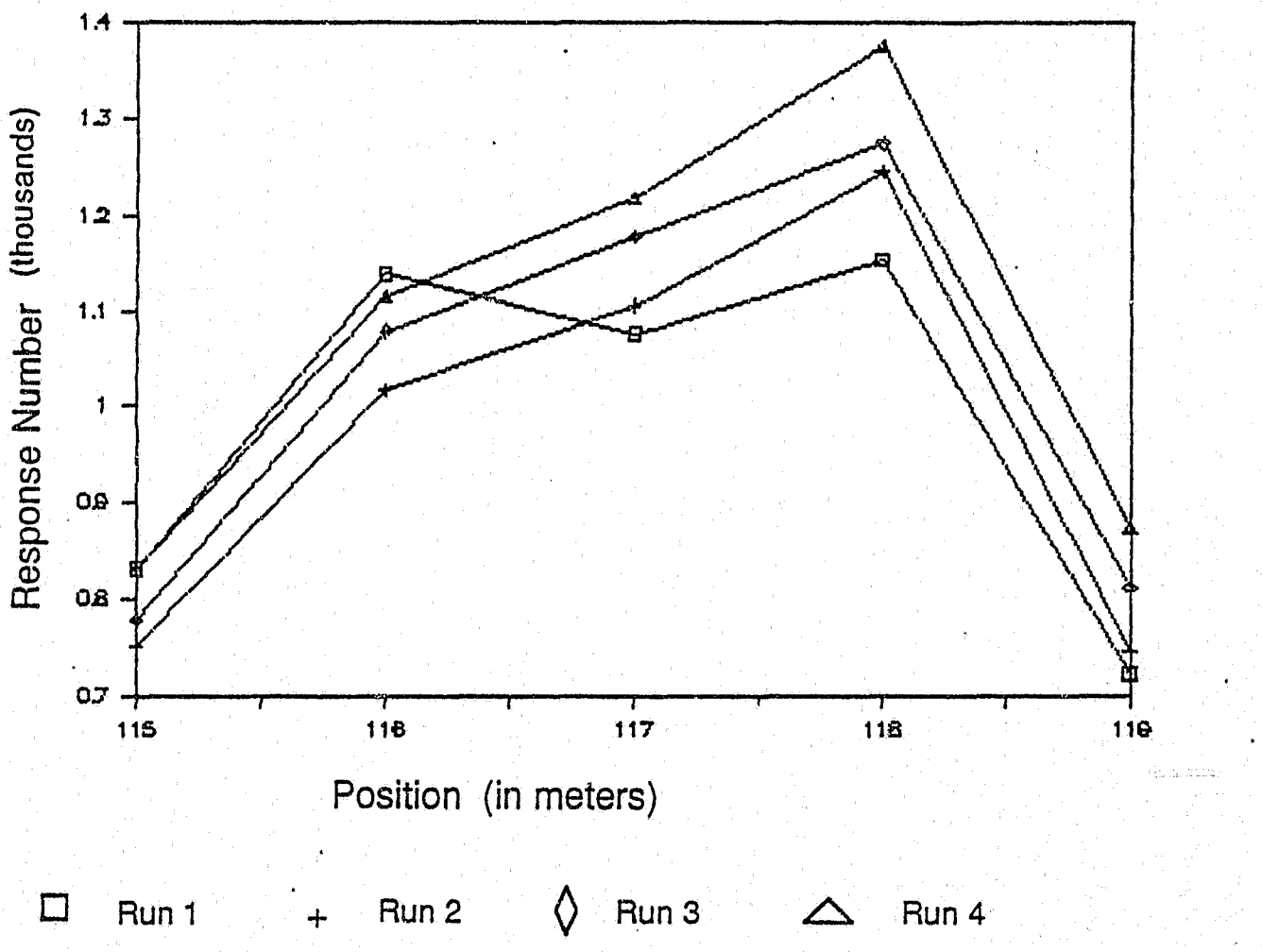

Figure 5.26 Response number profiles which resulted from four consecutive cable displacements in "response number vs. varying cable separation test #1." Corresponding cable separation profiles are shown in Fig. 5.25.

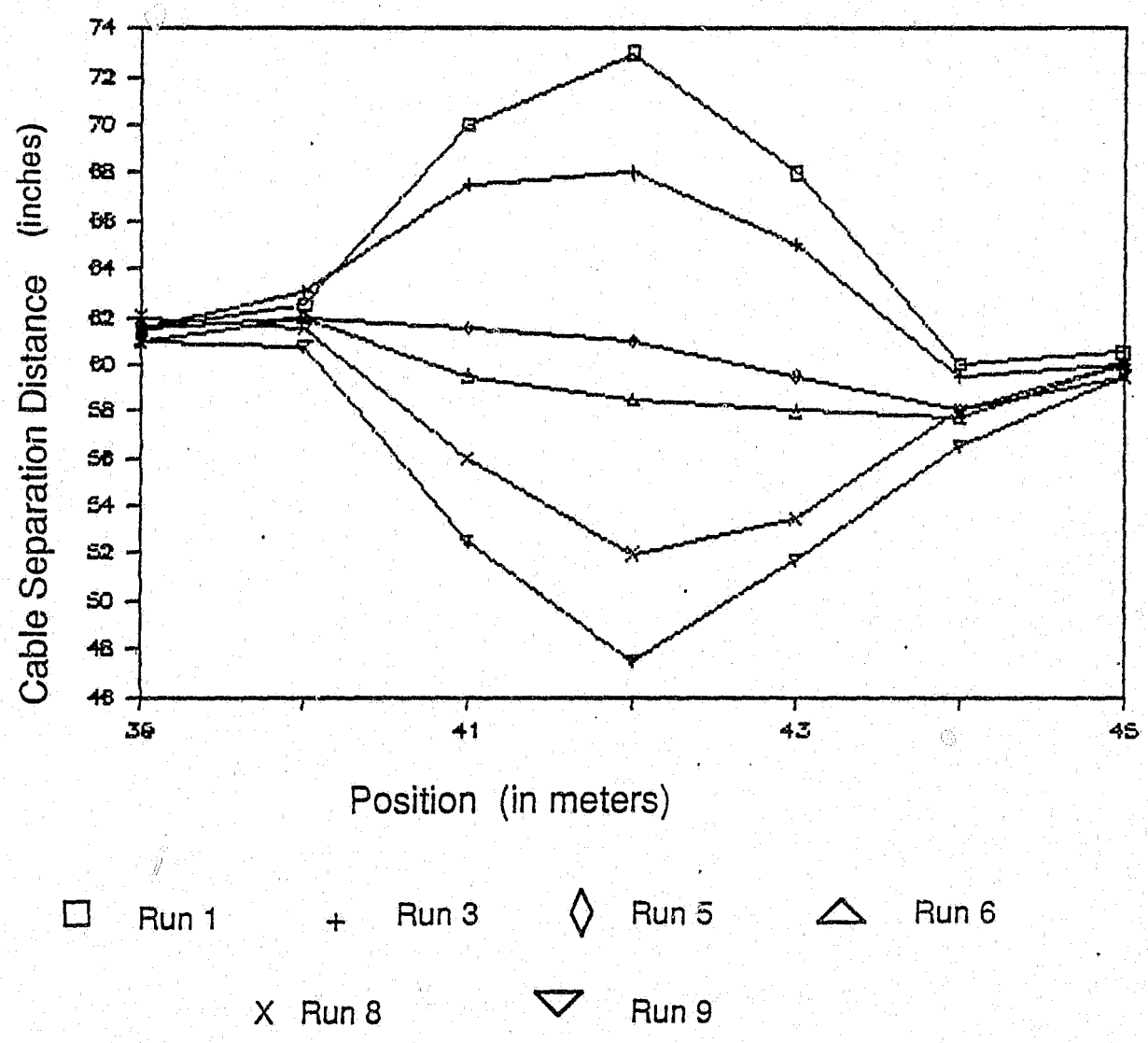

Figure 5.27 Cable separation distance at each position, after each run of "response number vs. varying cable separation test #2." Fig. 5.28 shows the resulting response number profiles.

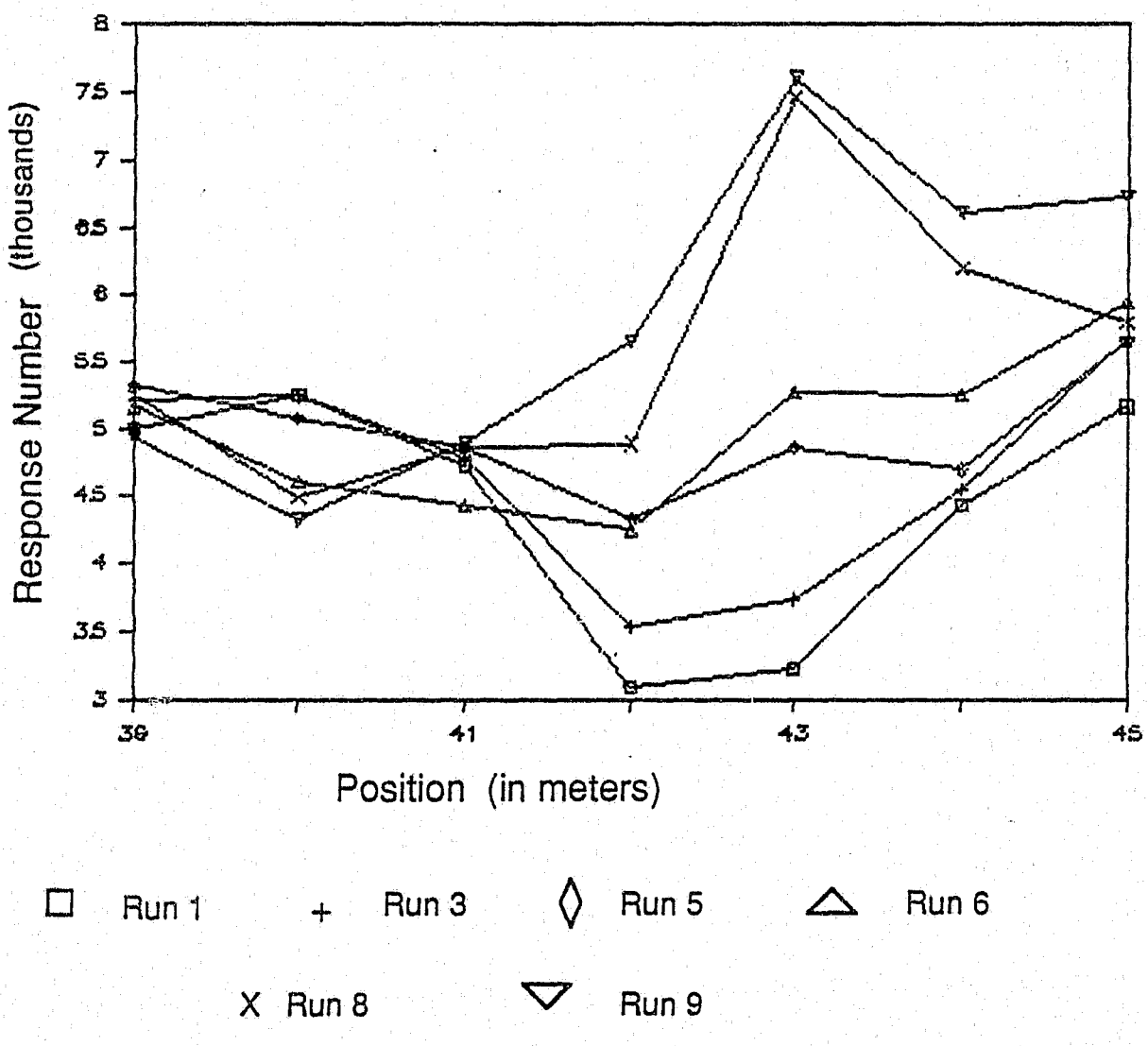

Figure 5.28 Response number profiles which resulted from six consecutive cable displacements in "response number vs. varying cable separation test #2." Corresponding cable separation profiles are shown in Fig. 5.27.

our soil; thus we expect the parallel cable configuration to yield a flat response profile. Referring to the response profile for the fifth run, shown on Figure 5.28, we see that the response profile is indeed nearly flat, with the response numbers staying within a few hundred of 4800.

As the cables are moved even closer together the response number continues to increase. In the ninth run of test #2 the cables are as close as possible and the response number profile has reached a maximum.

An observation that was unexpected is the apparent downline shift from the cause (cable separation variation) to the effect (change in response number). For example, in test #2 the maximum cable separation occurs at mark 42 but the largest increase in response number occurs at mark 43. At mark 44 the response number also shows an increase while the cable separation at this point has only changed by a few inches. This effect is also seen in the response profiles for test #1. The shift appears most pronounced for cable separation distances less than 52 inches. As of yet, this phenomenon remains unexplained.

In order to determine the effect that incremental changes in cable separation distance have on the response number, the response numbers at position 117 have been plotted as a function of the cable separation distance at position 117 after each run. In trying to predict the effect that cable separation distance has on response number the downline effect discussed above must be taken into account, therefore, the response numbers at position 118 have also been plotted as a function of the change in cable separation distance at position 117. This plot is shown in Figure 5.29.

Similarly, Figure 5.30 shows the response numbers at position markers 42

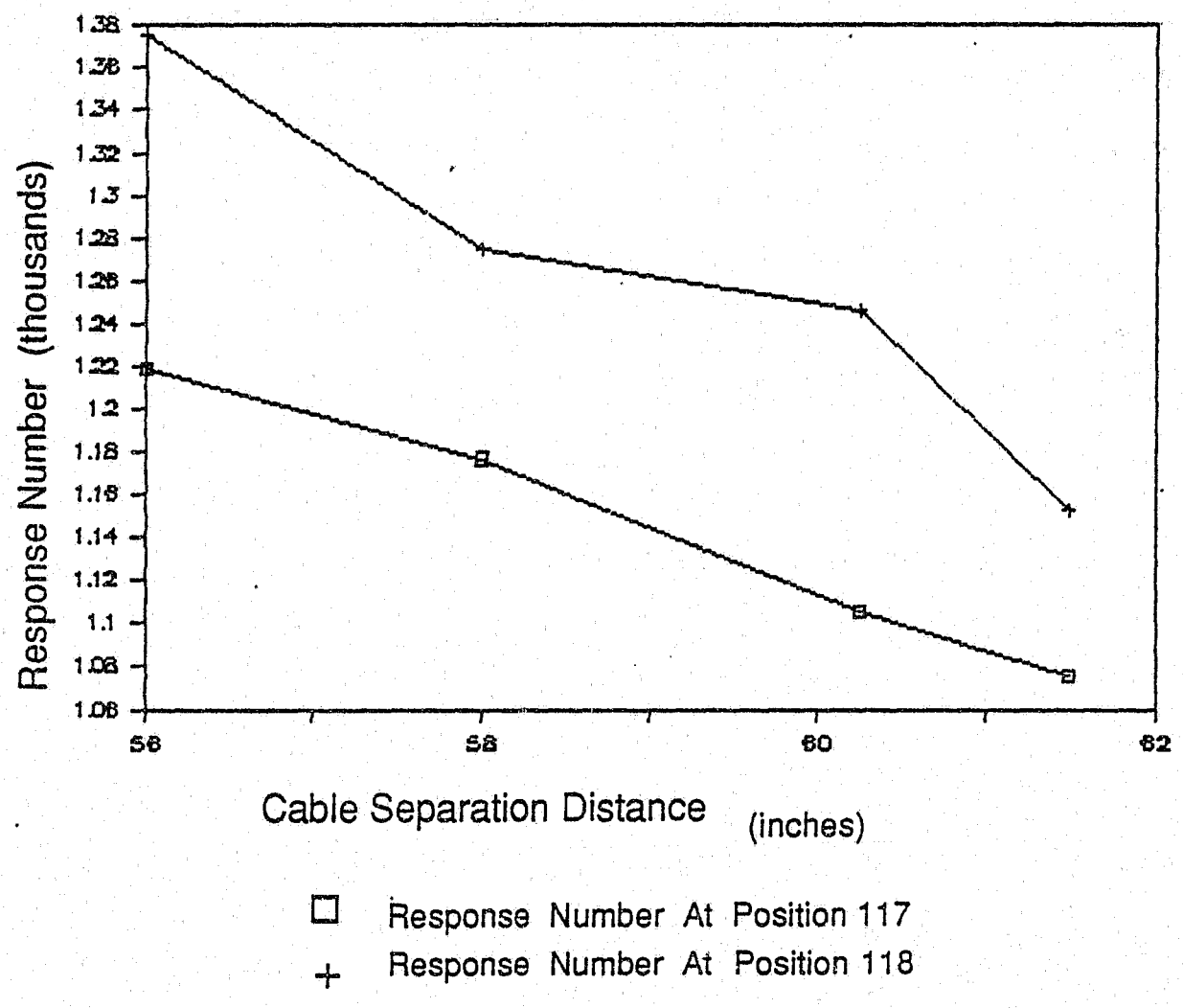

Figure 5.29 Response number at positions 117 and 118 as a function of changing cable separation distance at position 117. Results taken from "response number vs.varying cable separation test #1."

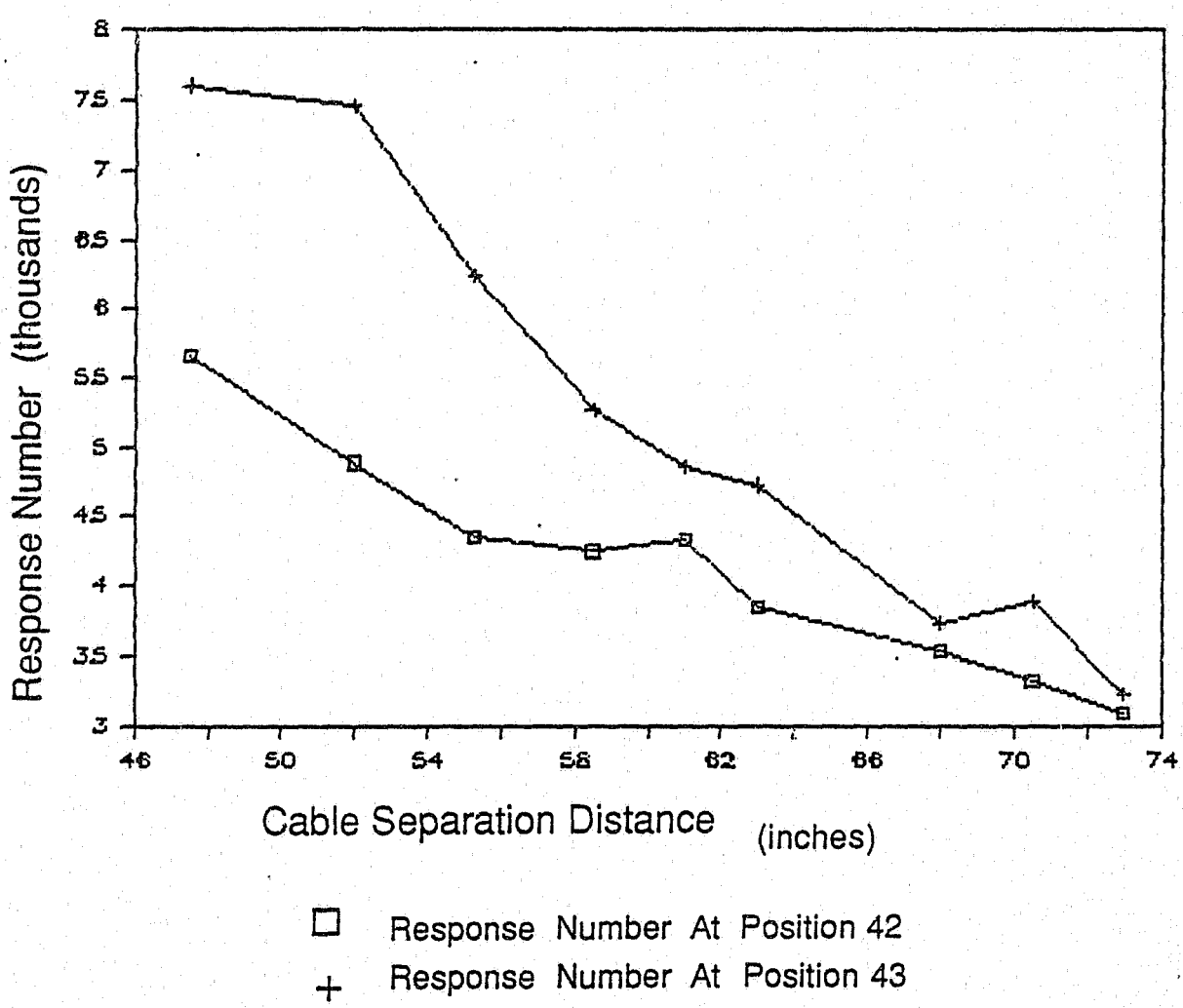

Figure 5.30 Response number at positions 42 and 43 as a function of changing cable separation distance at position 42. Results taken from "response number vs.varying cable separation test #2."

and 43 plotted as a function of the cable separation distance at mark 42 for each run.

Both plots show that the relationship between cable separation and response number is fairly linear within the range of cable separation used in these tests. The response numbers at the center position (117 or 42) and at the adjacent downline point (118 or 43) were averaged together and linear regression techniques were used to find a line that will best fit the averaged response values. For test #1, the equation for this "best fit" line is:

$$y = -31.54x + 3062 \qquad (5.4)$$

For test #2 the equation is:

$$y = -135.88x + 12{,}968 \qquad (5.5)$$

where y is the response number and x is the cable separation distance in inches.

Note that the slopes of the two equations are very different; that is, a unit increase in cable separation distance results in a larger decrease in response number in the homogeneous sand (as shown by equation 5.5) than for the case where the cables are buried in a sand and native soil mixture (represented by equation 5.4). Note also that due to the y-intercept term in (5.5) the magnitude of the response number in the homogeneous sand will be greater than in the native soil region.

Equations 5.4 and 5.5 describe the relationship between cable separation and response number, but only for a specific soil type. The soil at the locations of tests #1 and #2 was measured and it was found that the sand at position 42 (test #2) had a relative permittivity of about 5.2, a conductivity of about 2.5 mmhos per meter, and a loss tangent of 0.143. The native soil between the cable trenches at position 117 (test #1) was found to have a relative permittivity of 5.84, and a

conductivity of 11.04 mmhos per meter, leading to a loss tangent of 0.564. Thus, although the permittivities of the two soil types are similar, the conductivities and loss tangents are quite different.

For equations 5.4 and 5.5 the percentage change in response number with respect to the response number at a cable separation of 60 inches is plotted as a function of cable separation distance in Figures 5.31 and 5.32. The arbitrary reference point is chosen to be 60 inches since this is the nominal cable separation distance for the PCCS system.

Figures 5.31 and 5.32 show the percentage change in response number vs. cable separation to be the same: about 2.75% per inch separation for both soil types tested; thus, we see from these 2 tests that this rate is independent of the soil type. If this result occurs for all soil types a predictive model relating response number to cable separation can be obtained which will be valid for any type of soil, i.e. a universal model. We have only investigated two soil types, and further testing in other soil types should be done. Nevertheless, we shall proceed on the assumption that the universal model is valid.

Returning to equations 5.4 and 5.5 which describe the relationship between the response number and cable separation distance for a specific soil type, we see that the ratio between the y-intercept term and the slope is almost the same: the average ratio for both equations is 96.3. This implies that one equation is simply a multiple of the other. For example, the right side of (5.5) equals 4.27 times the right side of (5.4).

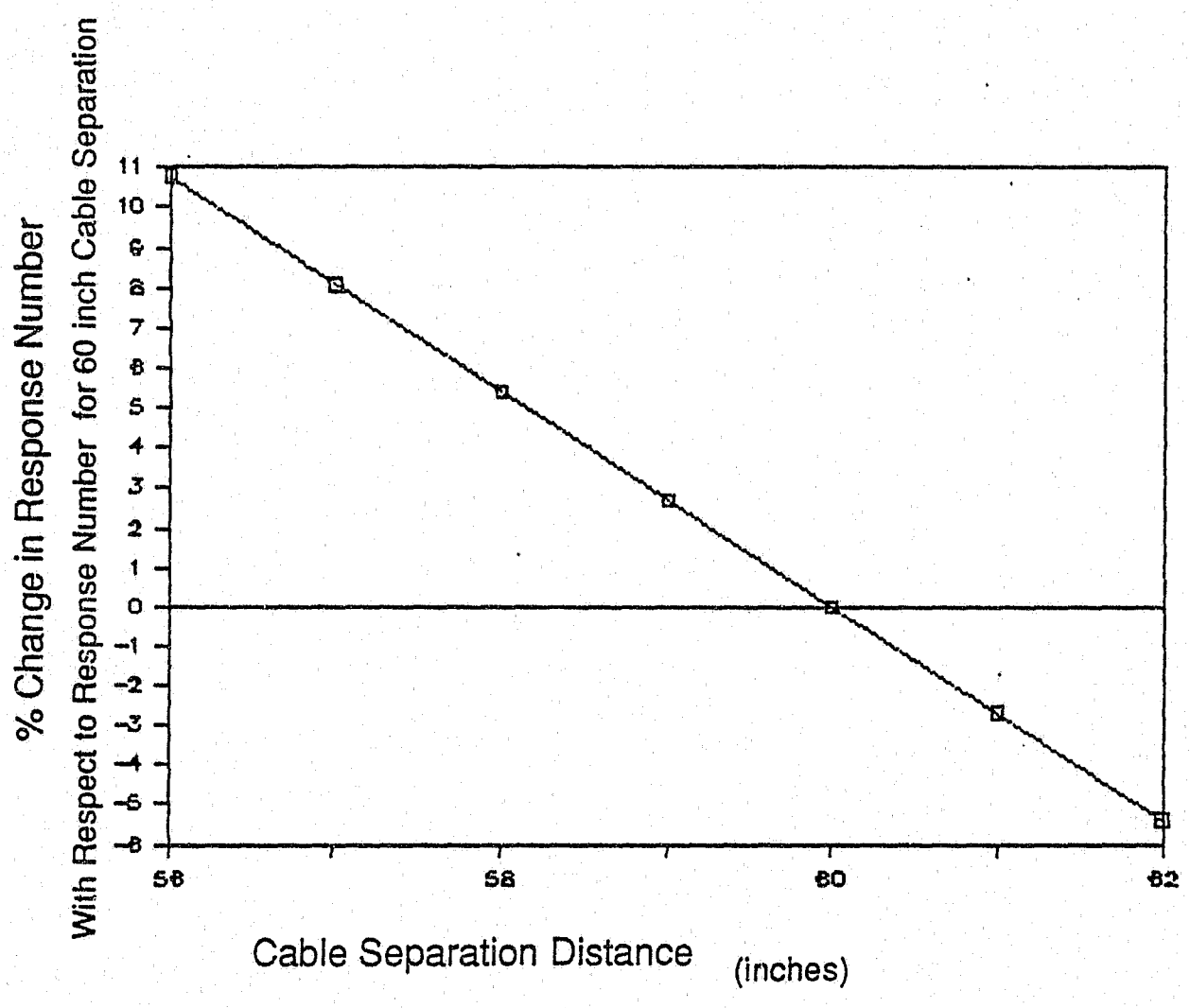

Figure 5.31 Percentage change in response number (with respect to response number at cable separation distance of 60 inches) as a function of changing cable separation distance. Results derived from "response number vs. varying cable separation test #1."

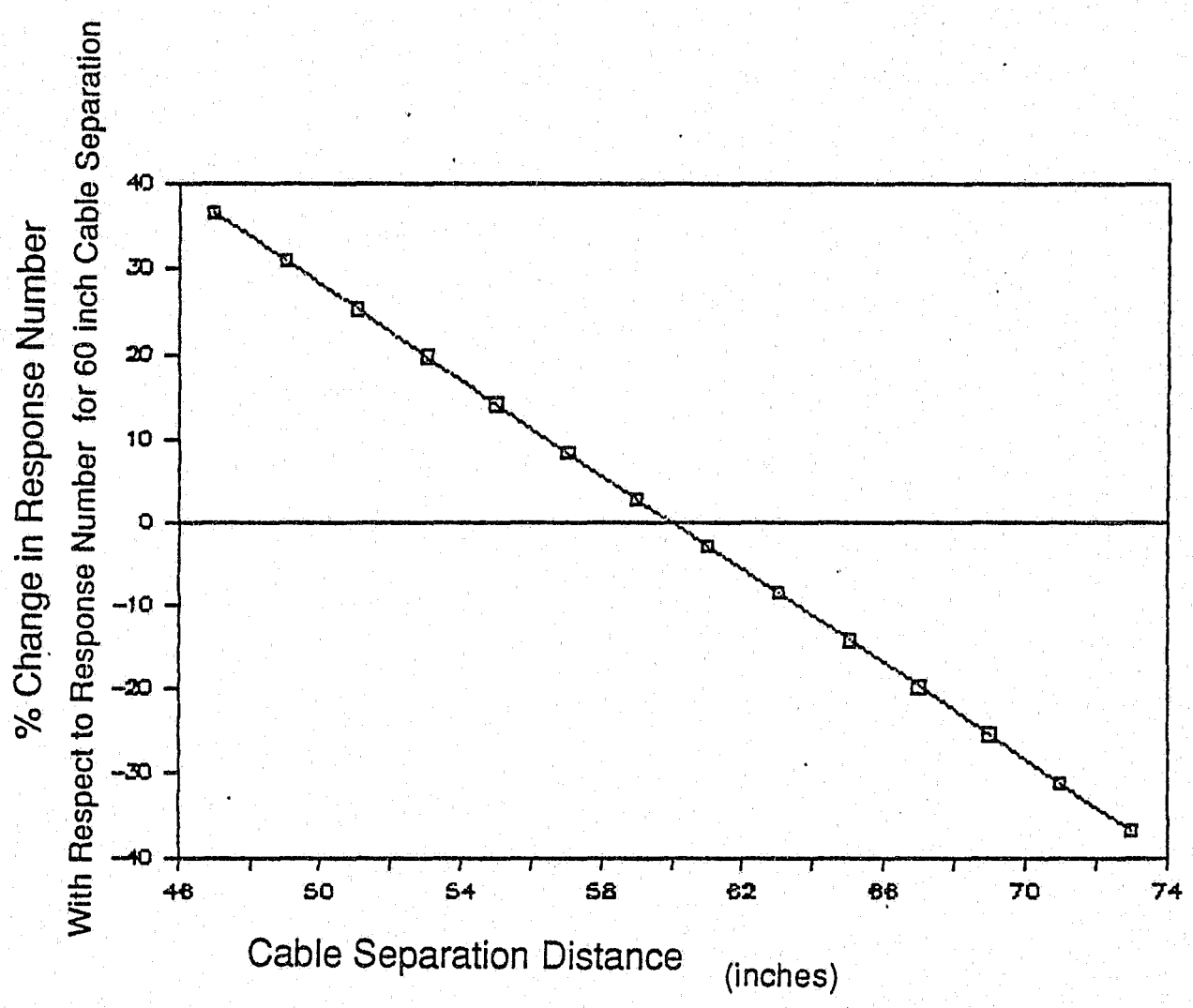

Figure 5.32 Percentage change in response number (with respect to response number at cable separation distance of 60 inches) as a function of changing cable separation distance. Results derived from "response number vs. varying cable separation test #2."

The equations, therefore, can be rewritten as a generic equation of the form:

$$y = B(-x + 96.3) \tag{5.6}$$

where y is the response number, x is the cable separation distance in inches, and B is the constant multiplier which is a function of the soil type. At a specific point where we know the measured response number, y*, and the measured cable separation distance, x*, B can be derived from:

$$B = (y^*)/(96.3 - x^*) \tag{5.7}$$

By substituting (5.7) into (5.6) we obtain:

$$y = (y^*)(96.3 - x)/(96.3 - x^*) \tag{5.8}$$

which can be rewritten in terms of the percentage change of the response number:

$$(y - y^*)/y^* = (x - x^*)/(x^* - 96.3) \tag{5.9}$$

Equation 5.9 implies that the percentage change between a measured response number and a desired response number is simply a function of the percentage change in cable separation regardless of the soil type. This agrees with the previous findings shown in Figures 5.31 and 5.32. Equation 5.8 can be rewritten to obtain the following design equations:

$$y = y^*(x - 96.3)/(x^* - 96.3) \tag{5.10}$$

and

$$x = 96.3 + (y/y^*)(x^* - 96.3) \tag{5.11}$$

where: y is the predicted or desired response number.

x is the predicted or desired cable separation distance.

y* is the measured response number.

x* is the measured cable separation distance.

With these design equations the PCCS operator can use the measured response number and cable separation distance at a certain crossing point and either obtain an approximate response number for a proposed change in cable separation distance or obtain the approximate cable separation distance required to obtain the desired response number. The outstanding feature of these equations is that they are applicable regardless of the soil type.

5.6.4 Conclusions

Now that we know the effect that cable separation distance has on response number, we need to know if it is feasible to achieve a maximum response number ratio of no larger than 3:1 simply by changing the cable separation distance. Currently, the method used to raise the response profile is the soil exchange method whereby soil is excavated from around the cable pairs and the soil is replaced with sand. To lower the response profile the excavated cell is backfilled with soil from an area where the response profile was very low.

This method works (Frankel, Van Horn and Carlile, 1984) but it is extremely expensive and time consuming due to the fact that much excavation is required. Also, the need to transport large amounts of fill soil and the environmental problems associated with the excavation process indicate that the soil exchange

method leaves much to be desired.

Adjusting the cable separation distance of a buried cable-pair involves digging a narrow 9 inch deep trench adjacent to the cable to be moved. The width of the trench equals the distance that the cable needs to be displaced while the length needs to extend about 6 or 7 times this distance on either side of the first and last adjacent points where the cable is moved. This in necessary so that the cable can be gradually bent. When the cable has been moved the trench is refilled with its original soil. Thus, for a cable displacement of 1 foot the adjacent trench needs to be 1 foot wide and at least 13 feet (about 4 meters) long. This suggests that the cable separation can be changed easily as long as the variation does not exceed a certain limit. This limit is defined by the maximum length of the trench that one wishes to dig. For example, if it is decided that for reasons of economy the maximum length of the adjacent trench is not to exceed 13 feet, then the cable can only be displaced by 1 foot from its original position.

While performing these cable separation tests it was arbitrarily decided that in order to minimize the trench digging time, the maximum variation in cable separation was not to exceed 1 foot. Thus, varying the cable separation distance was defined as being a "feasible" method for altering the response profile so long as a maximum response ratio no larger than 3:1 can be achieved without having to displace the cables by more than 1 foot at any one crossing point.

5.6.5 Design Example to Achieve a 3:1 Response Ratio

The following example will illustrate how the cable separation method can be used to obtain a response ratio no greater than 3:1.

In Figure 5.33 we see the response profile for the region between meter marks 26 and 80. Cell 2 lies between meters 33 and 66. Note that in the sand region (between meters 33 and 49) the profile is very high with the average response number being about 5000, and a high extreme of around 6000 at meter 49. In the topsoil region (between meters 50 and 66) the response profile is very low with the average response number around 1000, and a low extreme of around 600 at meter 56. Therefore, although the average response ratio in cell 2 is about 5:1, there are extremes where the response ratio (within cell 2) is closer to 10:1.

As described in earlier chapters, a high response ratio is undesireable because it results in the cell threshold being set either too high or too low. If the threshold is set too high then intruders crossing over the less sensitive regions of the cell will go undetected. If the threshold is set too low then small animals crossing over the highly sensitive regions of the cell will trigger unnecessary alarms. Therefore, the lower the response ratio, the better the ability of the PCCS system to correctly detect and resolve the size of intruders.

In order to differentiate between a person and a small animal the response ratio needs to be no greater than 3:1. In order to bring the response ratio for cell 2 down to a maximum of 3:1 we will need to lower the high responses by about a third and raise the low responses also by a third.

The first step is to see whether this is feasible as defined above. Referring to the response profile shown in Figure 5.33 and the corresponding cable separation profile shown in Figure 5.34 we see that for the high response region the cable separation is around 60 inches. Figure 5.35 shows the percentage change in response number which occurs when the cable separation distance is varied. Each

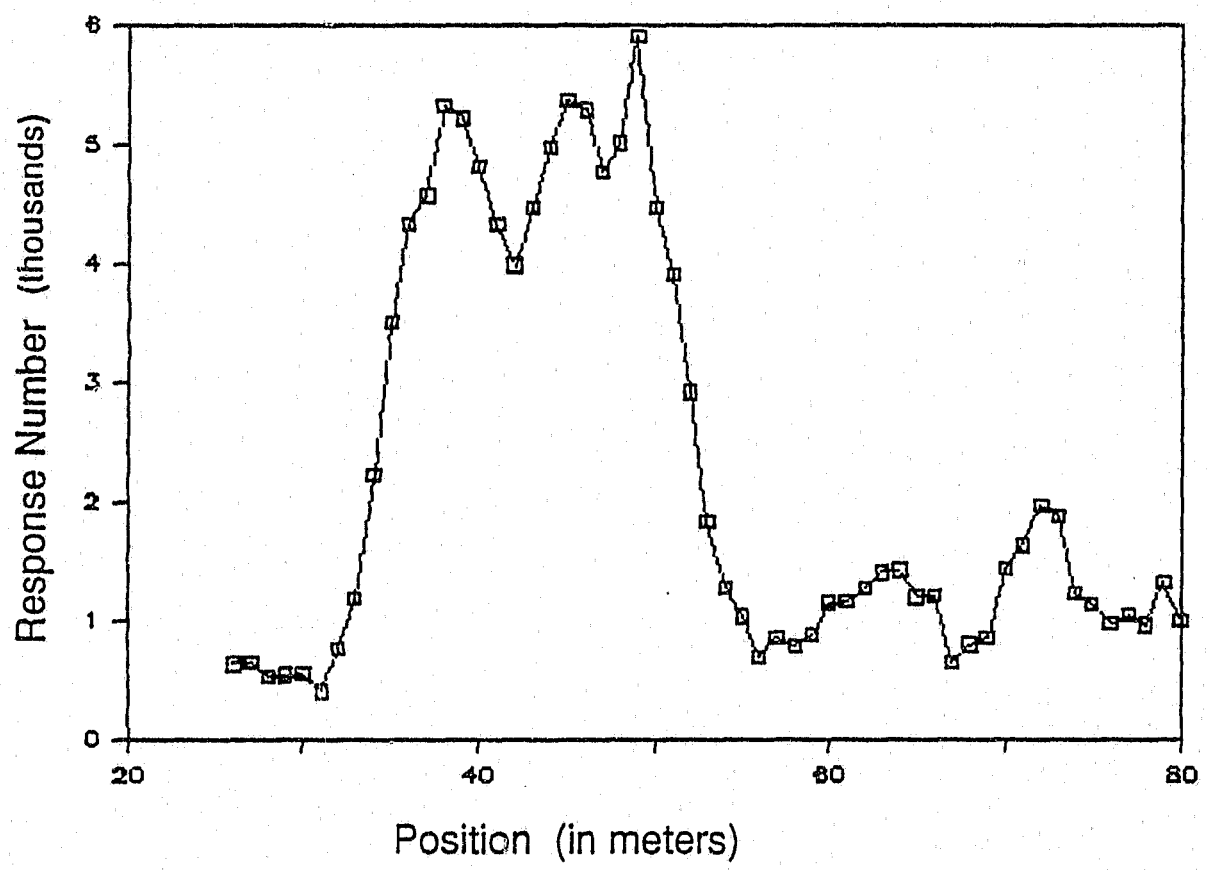

Figure 5.33 Response number profile for positions 26 through 80. Sand region of cell 2 is between positions 33 and 49. Topsoil region is between positions 50 and 66.

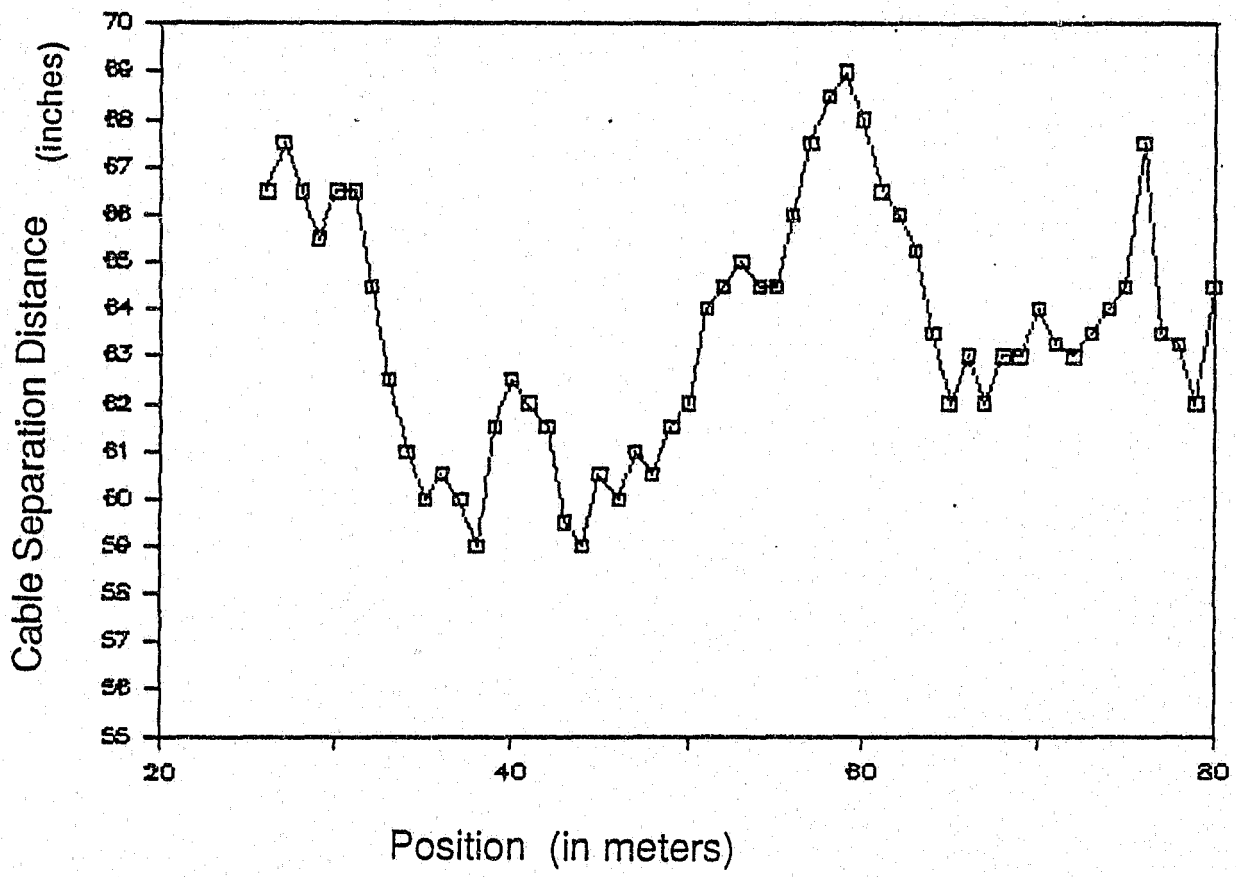

Figure 5.34 Cable separation profile for positions 26 through 80.

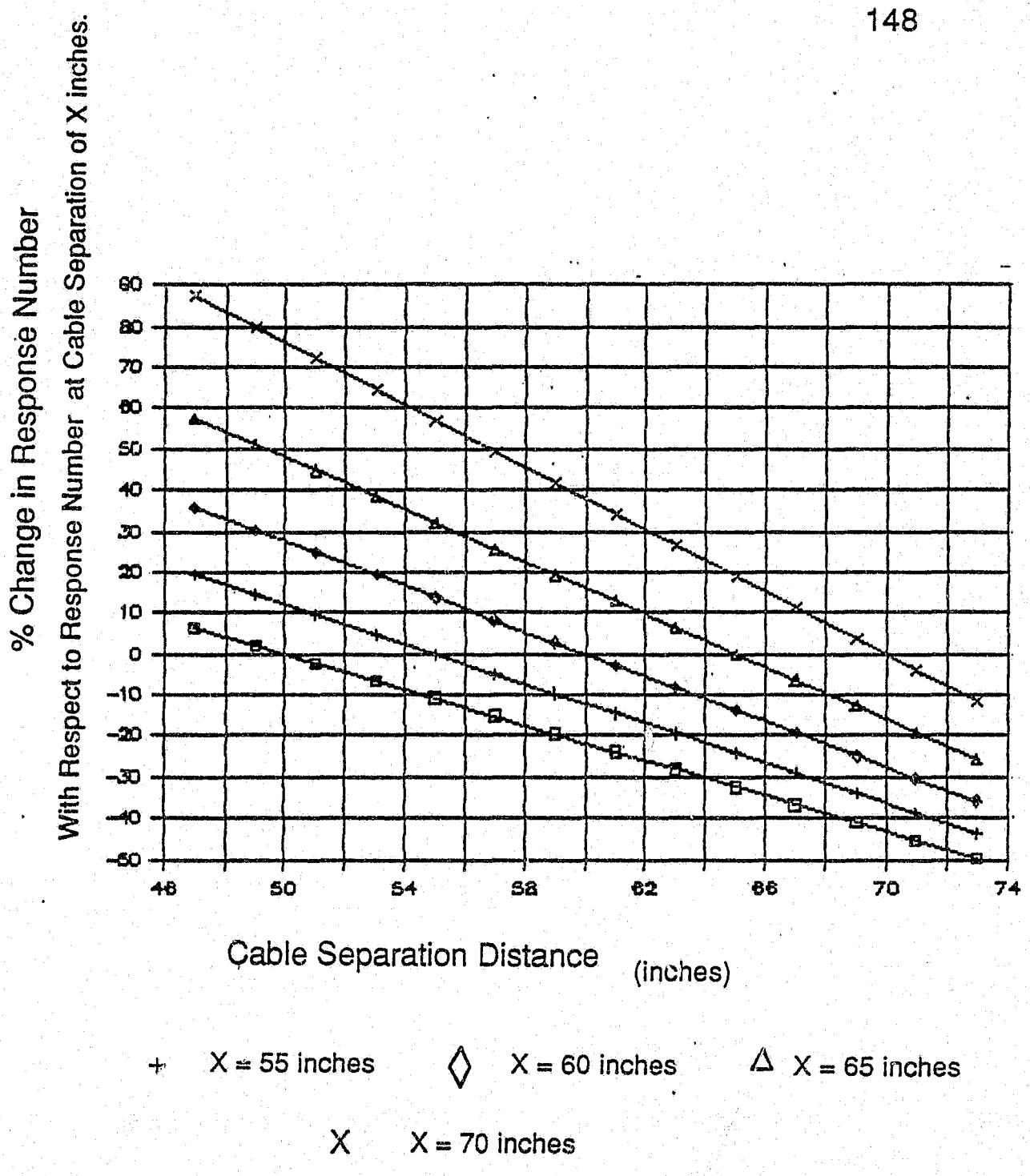

Figure 5.35 Percentage change in response number (with respect to response number at cable separation distance of X inches) as a function of changing cable separation distance. Results derived from Equation 5.9.

line in Figure 5.35 is derived from equation 5.9 and shows the percentage change in response number with respect to the response number at a different, specified cable separation distance. Referring to the line corresponding to a cable separation of 60 inches we see that in order to reduce the response number by 30% the cables need to be 71 inches apart; that is, the cables need to be moved apart by 11 inches. Since this is less than 1 foot, the process of moving the cables apart will be relatively easy, and therefore, it is feasible to lower the response profile using this method.

Figures 5.33 and 5.34 show that the lowest response number in the topsoil region of cell 2 occurs at meter mark 56 where the cable separation is about 65 inches. In Figure 5.35 we refer to the line corresponding to a cable separation of 65 inches and find that to raise the response by 30% the cables need to be 55 inches apart; that is, the cables need to be moved 10 inches closer together which we have defined as feasible.

Now that we know it is feasible to adjust the response profile by varying the cable separation distance we can use the design equations to more precisely determine the cable separation necessary to produce a desired response number. The design equations can also be used to simulate the response profile that would result for a given cable separation profile.

Given the response profile and the cable separation profile from Figures 5.33 and 5.34 and using the design equations we can simulate what the profile would look like if the cable separation was 60 inches at all crossing points. This simulation is seen in Figure 5.36. The response profile that is observed is due to soil variations only since the cable-pairs are parallel in this simulation.

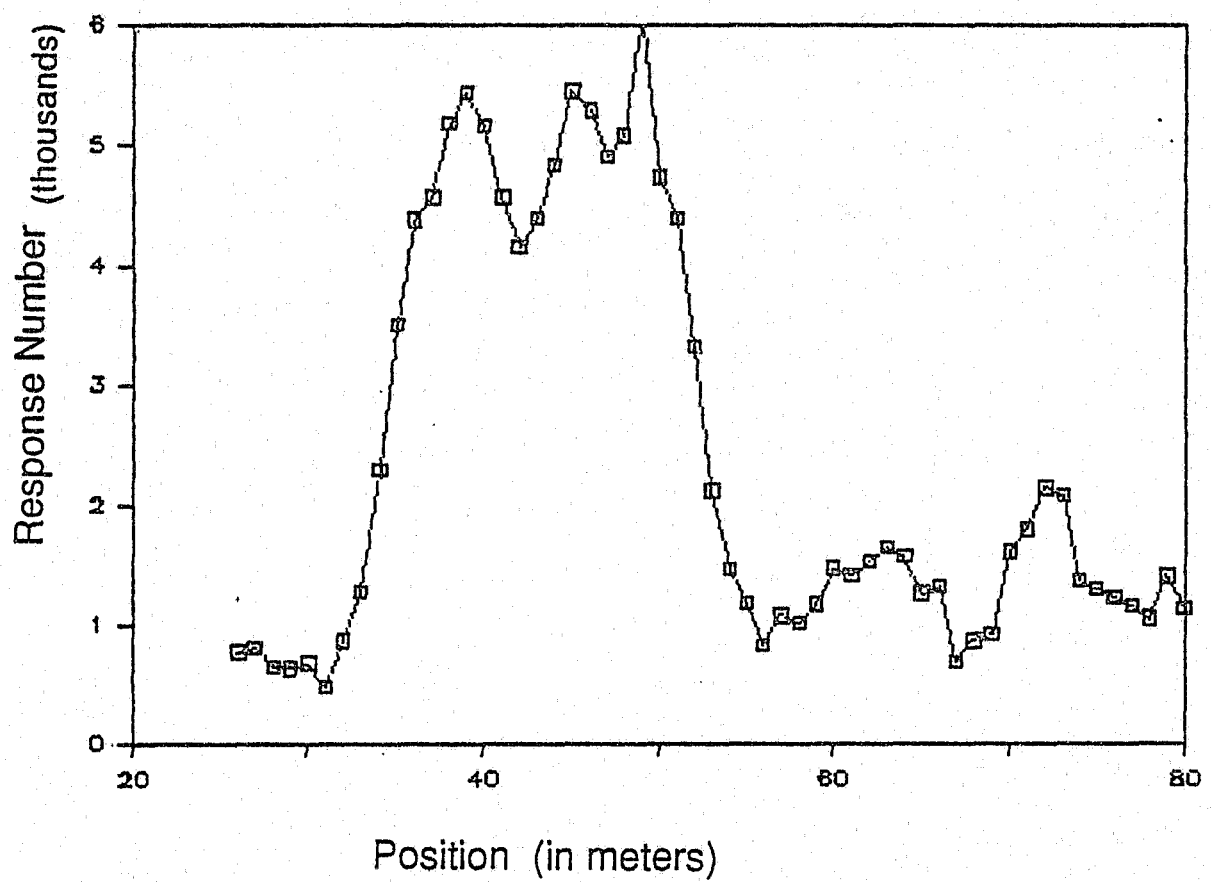

Figure 5.36 Simulated response profile. Response profile between positions 26 and 80 (from Fig. 5.33) is modified to simulate the effect of constant 60 inch cable separation (parallel cables). Variations are due to soil variations only. Simulation based on Equation 5.10.

Next, we simulated the response profile that would result if the cable separation in the sand region (meters 33 to 50) was increased to 70 inches while the separation in the non-sand region was reduced to 50 inches. To actually deploy the cable-pair in this configuration would require that there be a transition of about 3 meters so as to keep the bend in the cable to a minimum. Figure 5.37 shows the result of this simulation. Note that this results in a lower response profile in the sand region and a higher response profile in the non-sand region.

In this simulation, the typical response number in the sand region has been reduced to around 3500 while the typical response number in the topsoil region has increased to around 1500. Thus, the average response ratio for cell 2 has been lowered (in simulation) to less than 3:1, not including the high and low extremes at positions 49 and 56, respectively, where the ratio between the response numbers at these 2 points is 4.5:1. Thus, the simulated cable deployment results in the PCCS being able to distinguish between human intruders and small animals everywhere in the cell except 2 crossing points, which is quite an improvement over the original situation where the response ratio was higher than 5:1 everywhere in the cell. With additional cable displacement the response profile for the entire cell could be adjusted to be less than 3:1.

This simulation shows that varying the cable separation distance between the cable-pairs is an effective way of obtaining a 3:1 response ratio even in situations where the cell contains very different soil types.

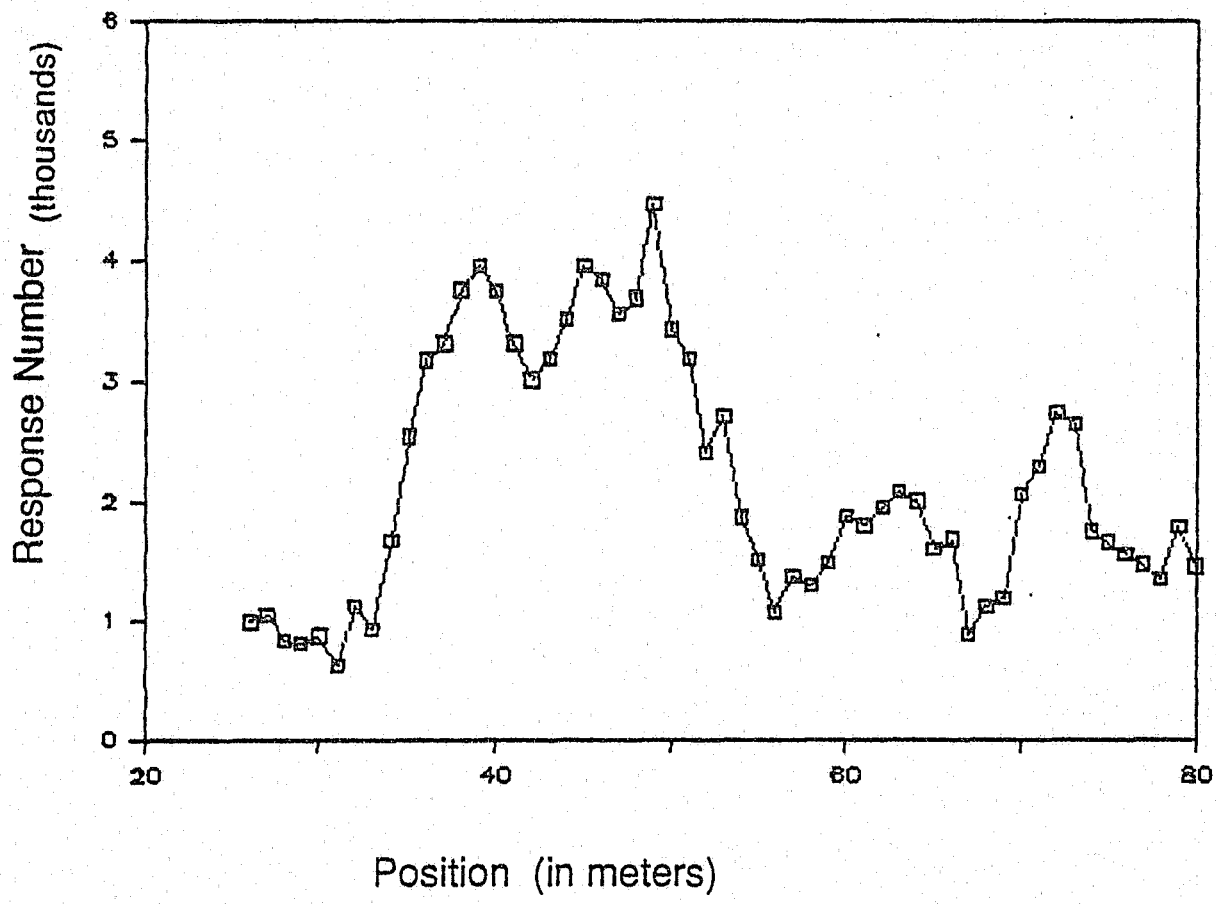

Figure 5.37 Simulated response profile. Response profile between positions 26 and 80 (from Fig. 5.33) is modified to simulate the effect of a cable separation distance of 70 inches in the sand (positions 33 to 49) and a cable separation distance of 50 inches in the topsoil region (positions 50 to 66). Except for a single high response number at position 49, and a single low response number at position 56, the response ratio for cell 2 (positions 33 to 66) is well within 3:1. The simulation is based on Equation 5.10.

CHAPTER 6

SUMMARY AND RECOMMENDATIONS

The five experiments which were described in the previous chapter were conducted in order to determine the factors which affect the sensitivity of the PCCS system. Although the observations and results for each individual experiment have already been reported, we will now review and compare those results in order to draw final conclusions from these experiments. These final conclusions will serve as the basis for a suggested deployment scheme for the PCCS which will enable the system to succesfully differentiate between human intruders and small animals.

6.1 Summary and Conclusions of Test Results

6.1.1 Response Number Profile Test

This test shows that the sensitivity of the system varies with position along the cable-pair. As an example, Figure 5.33 shows a portion of the system between positions 26 and 80; the homogeneous sand/topsoil region (cell 2) is located between positions 33 and 66. From this figure we see that the response profile is quite high in the sand region (positions 33 to 49) and much lower in the topsoil region (positions 50 to 66). This indicates that the soil plays a role in affecting the sensitivity of the system.

6.1.2 Soil Conductivity and Permittivity Test

This test shows how the electrical properties of the soil (i.e., the conductivity and permittivity) vary as a function of position along the cable-pair, thus revealing the different soil types that constitute the burial path of the PCCS cable-pair. Figures 6.1, 6.2 and 5.22 show the conductivity, relative permittivity and loss tangent (at 60 MHz) for the sand and topsoil sections of cell 2. The conductivity and permittivity are noticeably lower in the sand (positions 33 to 49) than in the topsoil (positions 50 to 66). These figures also show that while the sand region was indeed homogeneous, the topsoil region was not completely homogeneous.

Comparing Figures 6.1 and 6.2 to the response profile of Figure 5.33, we can conclude that regions with a high response profile, and thus a high sensitivity, correspond to regions where the conductivity and permittivity of the soil is low. As the conductivity and permittivity of the soil rises, the result is lower sensitivity.

6.1.3 Magnetic Field Intensity Test

This test shows how the magnetic field intensity on the ground surface above the transmitter cable varies as a function of position along the cable. Figure 6.3 shows the variation in magnetic field strength between positions 26 and 80. A noticeable feature of this magnetic field profile is the rapid variation in field intensity that occurs over short distances. These oscillations, and the fact that they occur at

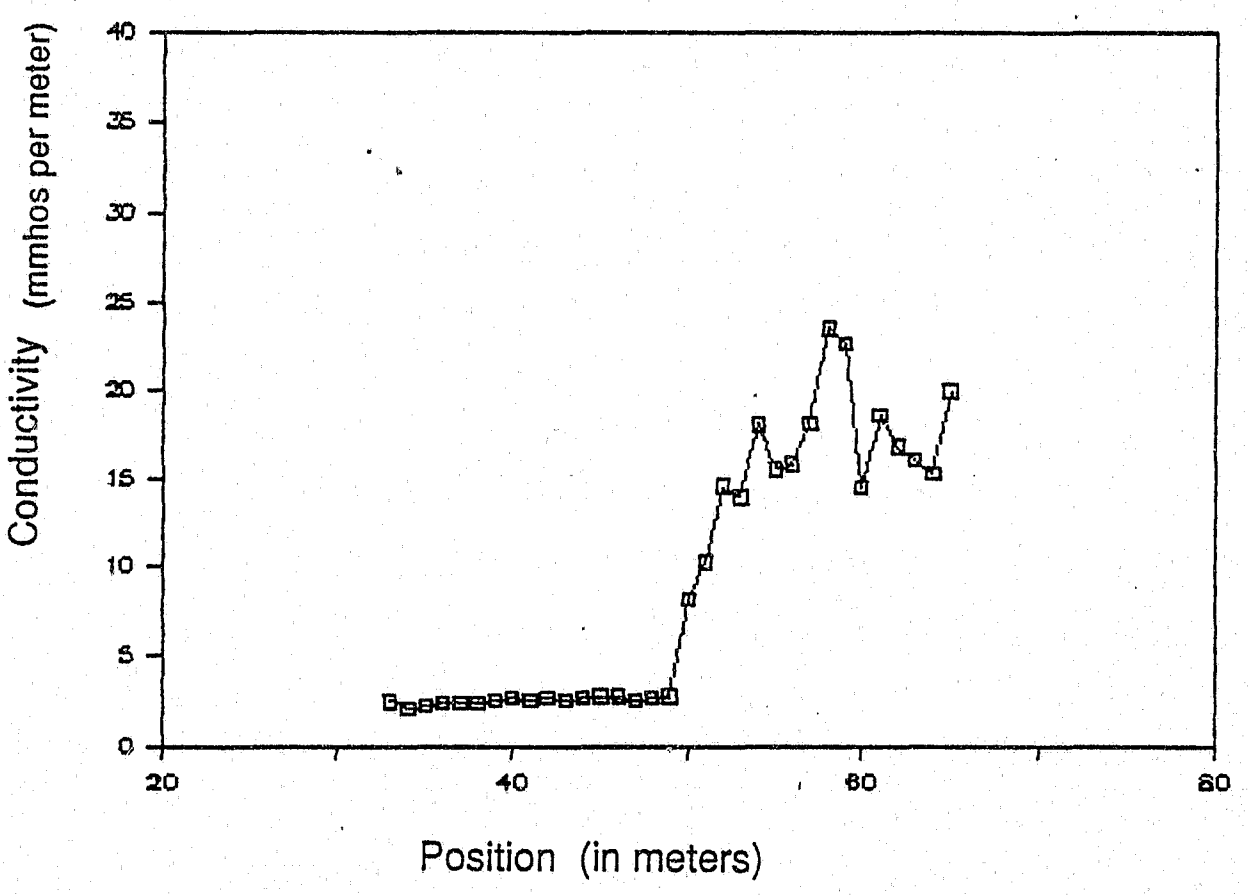

Figure 6.1 Conductivity of the soil at each position in cell 2. Sand region is between positions 33 and 49. Topsoil region is between positions 50 and 66.

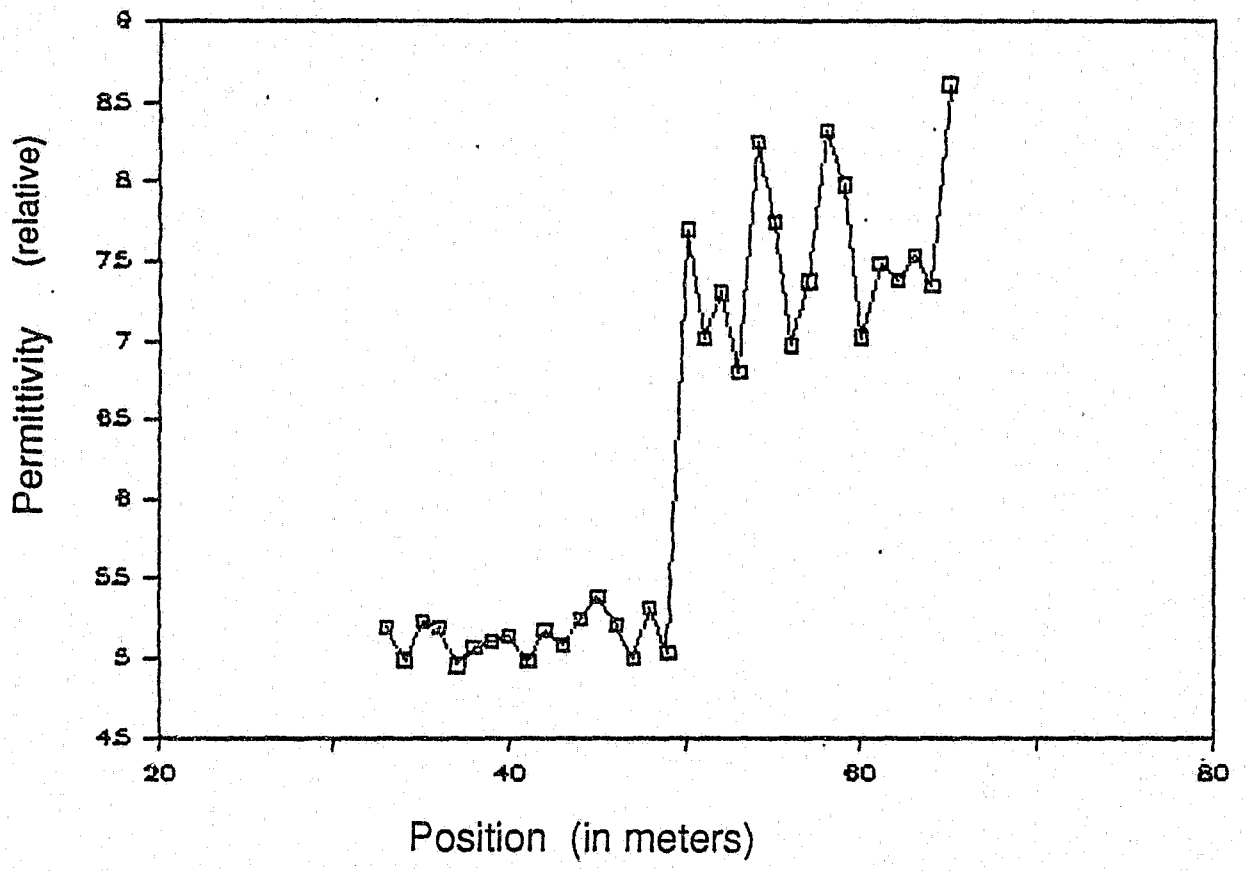

Figure 6.2 Relative permittivity of the soil at each position in cell 2. Sand region is between positions 33 and 49. Topsoil region is between positions 50 and 66.

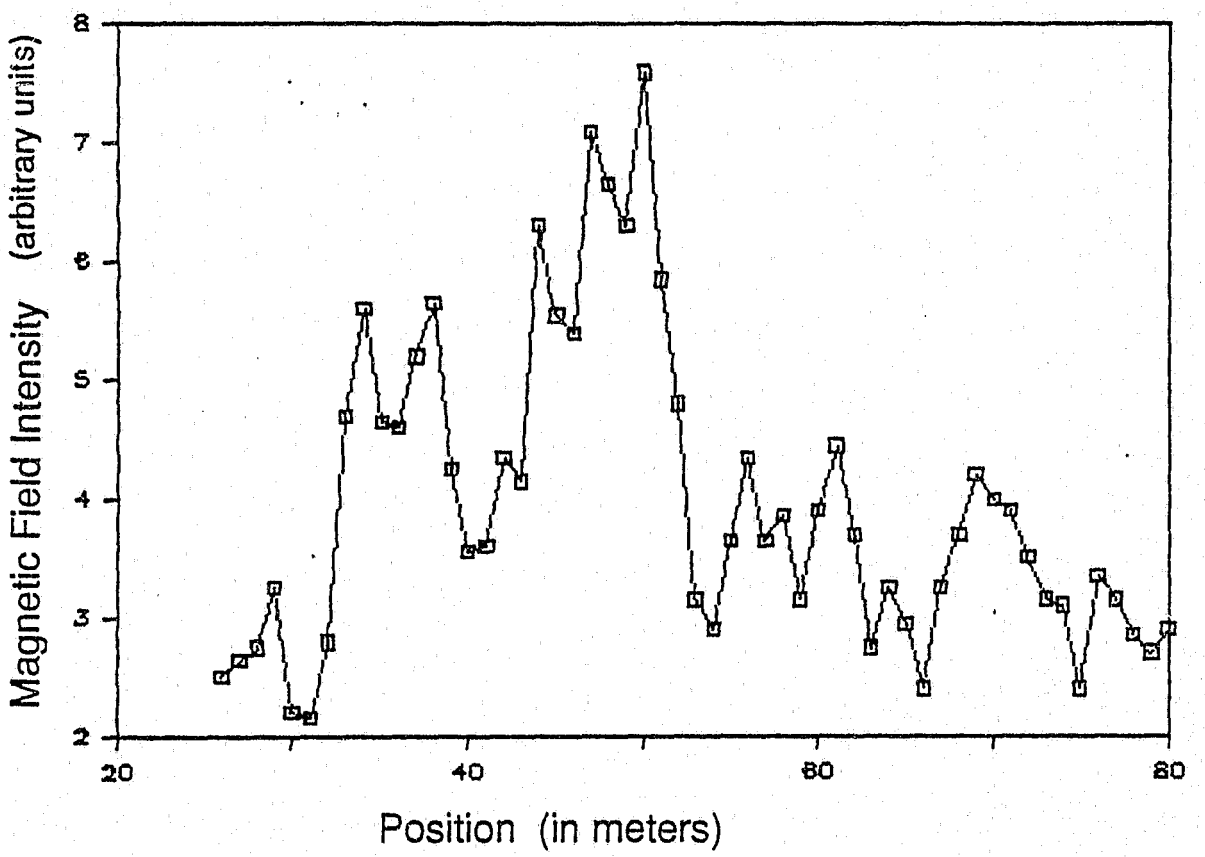

Figure 6.3 Magnetic field intensity on ground surface directly above transmitter cable, at positions 26 through 80. Sand region of cell 2 is between positions 33 and 49. Topsoil region is between positions 50 and 66.

interfaces between soils of differing conductivities and permittivities, are assumed to be caused by interference patterns. As discussed in Section 3.6, these interference patterns are caused by the interaction of modes which are excited at the interface between different soil types. From our calculation of the propagation constant of the interfering mode (see Section 5.5) we conclude that the interfering mode is probably the Goubau mode.

Comparing the magnetic field intensity profile of Figure 6.3 to the response profile of Figure 5.33, we can see that variations in the response profile correspond to variations in the "envelope" of the magnetic field profile. That is, a response number at a certain crossing point is proportional to the average strength of the electromagnetic field within several meters of that crossing point.

Comparing the magnetic field intensity profile of Figure 6.3 to the soil conductivity and permittivity profiles of Figures 6.1 and 6.2, clearly shows that the electromagnetic field strength (i.e. energy density) that extends from the transmitter cable is directly affected by the conductivity and permittivity of the soil in which the cable is buried. As the permittivity and conductivity of the soil increases, the electromagnetic field strength a fixed distance away from the transmitter cable becomes weaker.

6.1.4 Cable Separation Distance Test

The Cable Separation Distance Test reveals that although the transmitter and receiver cables were carefully deployed so that they would be 5 feet apart and parallel to each other, the distance between them varies with position along the cable

pair. This variation as a function of position is shown in Figure 5.34, which shows the portion of the test site between positions 26 and 80.

For the entire 6-cell test site, the cable separation distance ranged from 55 inches to 71 inches. Since this variation was more than expected, it was necessary to run additional tests (see Section 6.1.5) to determine the extent to which cable separation affected the sensitivity of the PCCS system. These additional tests showed that although cable separation does affect sensitivity, the random variation that was found (from 55 to 71 inches) did not significantly alter the response profiles (such as Figure 6.1) which were recorded.

6.1.5 Response Number vs. Varying Cable Separation Test

This test was undertaken in order to determine the effect that the cable separation distance has on the sensitivity of the PCCS system. It was previously shown that the sensitivity of the system was a function of the electrical characteristics of the soil, so it was necessary to determine if the effects of the soil could be compensated for (i.e. overridden) by varying the cable separation distance.

In this test, the cable separation distance was repeatedly changed, and the resulting response profiles were recorded. Figures 5.25 through 5.28 show the different cable separation distance profiles and the corresponding response number profiles. These graphs illustrate that the cable separation distance is an important factor in determining the magnitude of the response number, and therefore, can be a useful tool in adjusting the sensitivity of the PCCS system.

Repeated tests in a different soil type reveal that changing the cable separation distance by a fixed number of inches will result in any number of possible changes in the response number, depending on the conductivity and permittivity of the soil in which the moved cable is buried. The electrical properties of the soil are revealed, however, by the relationship between the response number at a particular crossing point and the cable separation distance at the same crossing point. Thus, knowing the response profile and the cable separation distance profile for a system, a predictive model can be obtained which will yield the cable separation distance necessary to obtain the desired response number.

The equations describing this predictive model were found (in Section 5.6) to be:

$$y = y^*(x - 96.3)/(x^* - 96.3) \qquad (6.1)$$

or rewriting in terms of x

$$x = 96.3 + (y/y^*)(x^* - 96.3) \qquad (6.2)$$

where: y is the predicted or desired response number.

x is the predicted or desired cable separation distance.

y* is the measured response number.

x* is the measured cable separation distance.

Initial tests indicate that this predictive model is universal, i.e., valid for all soil types, although additional testing in other soil types should be done to prove this.

Thus, if a PCCS system is deployed and the response profile and cable separation profile is obtained, equation 6.1 can be used to predict the response

profile that would result from changes in the cable separation profile. Conversely, equation 6.2 could be used to determine the cable separation distance required to obtain a desired response number.

These equations, then, provide a useful design tool which will enable the sensitivity of a deployed PCCS system to be adjusted so that high or low points in the response profile can be evened out. As was discussed in Chapter 2, a relatively even response profile (i.e., a response ratio no greater than 3:1) is necessary in order for the PCCS to successfully distinguish between a human intruder and a small animal. Without such a differentiation ablility, the PCCS system would, depending on the threshold setting, either fail to detect human intruders, or else would issue an inordinate number of nuisance alarms caused by animals.

In order for the cable separation method to be feasible, the response profile needs to be able to be significantly changed by a relatively small cable displacement, so that the amount of cable that needs to be uncovered and moved is minimized. In Section 5.6, it was shown that cells with response ratios of about 8:1 could be converted to around 3:1, by varying the cable separation distance no more than one foot at any particular crossing point. This indicates that the cable separation method is a feasible method for altering the response profile.

6.2 Deployment Suggestions

As discussed in the previous section, the PCCS needs to be deployed such that the response ratio within each cell is no greater than 3:1. A strategy that has been used in a previous experimental study (Frankel et al, 1984) has been to deploy

the cable-pair, measure the response profile, and use the soil exchange method (described in Section 2.4) to raise the response profile in an insensitive region.

As was mentioned, the soil exchange method is undesireable due the large amount of time and labor (and therefore money) required to excavate large amounts of soil; and the logistics problem becomes more severe if the PCCS is deployed in a remote area. The environmental impact of large scale soil excavation and transport also poses a problem. Finally, although the soil exchange method does work in changing the response profile, it is very difficult to accurately predict the extent to which the response profile will be changed.

It is the conclusion of this thesis that varying the cable separation distance is the most feasible method to obtain a response ratio less than 3:1. In following this method, the PCCS is deployed, the response profile and cable separation profiles are measured, and the response ratio is kept below the 3:1 ratio by adjusting the cable separation distance to those separation distances called for by equation 6.1.

Altering the position of a buried cable is accomplished by digging a 9-inch deep trench alongside the cable to be moved, displacing the cable into this trench, and refilling the trench with the original soil. The width of this adjacent trench is the distance that the cable needs to be moved; in this study, we found that a 6:1 ratio between trench length and cable displacement distance is required on either side of the point where the cable is displaced, in order to give the cable enough "play" to facilitate the displacement. For example, if the cable separation at a single crossing point is to be displaced by 1 foot, then the adjacent trench would need to be 1 foot wide and 12 feet long, centered on the crossing point.

The advantage of this method is that the required trenching is minimal, especially when compared with the soil exchange method. Also, the narrow adjacent trench is refilled with its original soil, eliminating the need for the transport of different soil types.

The main advantage of this method, however, lies in the ability to adjust the response profile to the desired profile shape and response ratio. This means that a response ratio of no greater than 3:1 is possible, which in turn allows the PCCS system to more accurately resolve the size of intruders. Such resolution enables the PCCS to detect human intruders while ignoring small animals. For a system which is deployed in a relatively remote, wildlife- inhabited area, the ability to ignore the intrusion of small animals greatly enhances the detector's effectiveness.

6.3 Additional Recommendations

The main purpose of this thesis was to find a method for lowering the response ratio to at least 3:1, the minimum necessary for the PCCS system to distinguish between a human and a small animal. This 3:1 response ratio requirement is due to the fact that only one threshold setting can be set for each cell, thus, very high and/or low sensitivity regions within the same cell will result in detection zones where the PCCS will either fail to detect intruders or will signal intrusion alarms when small animals traverse the cable-pair.

Since the typical response profile for a cell contains high and low variations, the ability of the PCCS to resolve the size of an intruder would be enhanced if the length of each cell were reduced from the present 33 meters. The smaller the cell

size, the greater the probability that areas of high or low sensitivity would be wholly contained within separate cells; and each cell's threshold setting would correctly compensate for the sensitivity level.

The length of a cell, as pointed out in Chapter 2, is a function of the rate at which the PDR samples the return signal from the receiver cable, and thus any decrease in cell size will have to rely on faster signal processing circuits being incorporated into the next generation of PCCS detectors.

Finally, it is suggested that the PCCS should incorporate an adaptive threshold system, where the signal processing algorithms are continually adapted to the changing soil conditions and nuisance alarm rates (Harrison, 1986). A PCCS system with an adaptive threshold would be more effective in screening out nuisance alarms, and additionally, would be able to automatically adjust cell thresholds to compensate for rain and other transitory environmental effects which affect sensitivity.

APPENDIX A*

Coupled Mode Theory

Consider a system that is uniform about the z coordinate axis. The cross-section in any plane normal to the z-axis has circular cylidrical symmetry, e.g., the cross-section in Figure A.1; the cross-sectional plane is described by the usual cylindrical coordinates (r, ϕ). We shall be interested in the eigenmodes of this system where we assume:

1. Azimuthal symmetry $\partial/\partial\phi = 0$.
2. TM modes only. (E_z, E_r, H_ϕ only).
3. No loss ($\sigma = 0$).

I. Orthogonality relation

Let A(r) be a general vector.

Gauss' Theorem (2-Dimensional case) is:

$$\int_s \nabla_t \cdot A \, ds = \int_c A \cdot n \, d\ell \tag{A.1}$$

where:

1. A and $\nabla_t \cdot A$ are continuous on surface, S, (including bounding curve, c), in a cross-sectional plane.

2. n is unit vector pointing out from s.

3. $\nabla_t = \hat{r} \frac{\partial}{\partial r} \qquad \nabla_t^2 = \frac{1}{r} \frac{\partial}{\partial r} \left[r \frac{\partial}{\partial r} \right] = \frac{\partial^2}{\partial r^2} + \frac{1}{r} \frac{\partial}{\partial r}$.

*The material in this Appendix is due to Dr. R.N. Carlile.

Consider a multi-region system with cylindrical symmetry as shown in Figure A.1.

$A = Ai(r)$ and $\nabla_t \cdot A_i$ are continuous in region i, but discontinuous across a boundary.

For region i: (where i = 1, 2, 3, 4)

$$\int_{S_i} \nabla_t \cdot A_i ds = A_i(a_i) \cdot 2\pi a_1 (-a_r) + A_i(a_{i+1}) \cdot 2\pi\, a_{i+1}\, a_r$$

$$= 2\pi \left[A_{r_i}(a_{i+1})\, a_{i+1} - A_{r_i}(a_i) a_i\right] \qquad (A.2)$$

where $A_{r_i} = A_i a_r$ and where a_r = radially directed unit vector.

Path of integration is clockwise around inner boundary and CCW around outer boundary. Assume $\lim_{r \to \infty} A_{r_4}(r) \to 0$. This implies that

$$\int_{S_4} \nabla_t \cdot A_4 = -2\pi A_r(a_4) a_4$$

Thus,

$$\frac{1}{2\pi} \int_S \nabla_t \cdot A \, ds = \frac{1}{2\pi} \sum_{i=1}^{4} \int_{S_i} \nabla_t \cdot A_i \, ds$$

$$= [A_{r_1}(a_2)a_2 - A_{r_1}(a_1)a_1] + [A_{r_2}(a_3)a_3 - A_{r_2}(a_2)a_2]$$

$$+ [A_{r_3}(a_4)a_4 - A_{r_3}(a_3)a_3] + [0 - A_{r_4}(a_4)a_4]$$

$$= -A_{r_1}(a_1)a_1 - [A_{r_2}(a_2) - A_{r_1}(a_2)]a_2$$

$$- [A_{r_3}(a_3) - A_{r_2}(a_3)]a_3 - [A_{r_4}(a_4) - A_{r_3}(a_4)]a_4 \qquad (A.3)$$

Note that s is the entire cross-section except for r<a.

Let,

$$A_i(r) = F(\epsilon_i)\psi_i(r)\nabla_t \phi_i(r) \qquad (A.4)$$

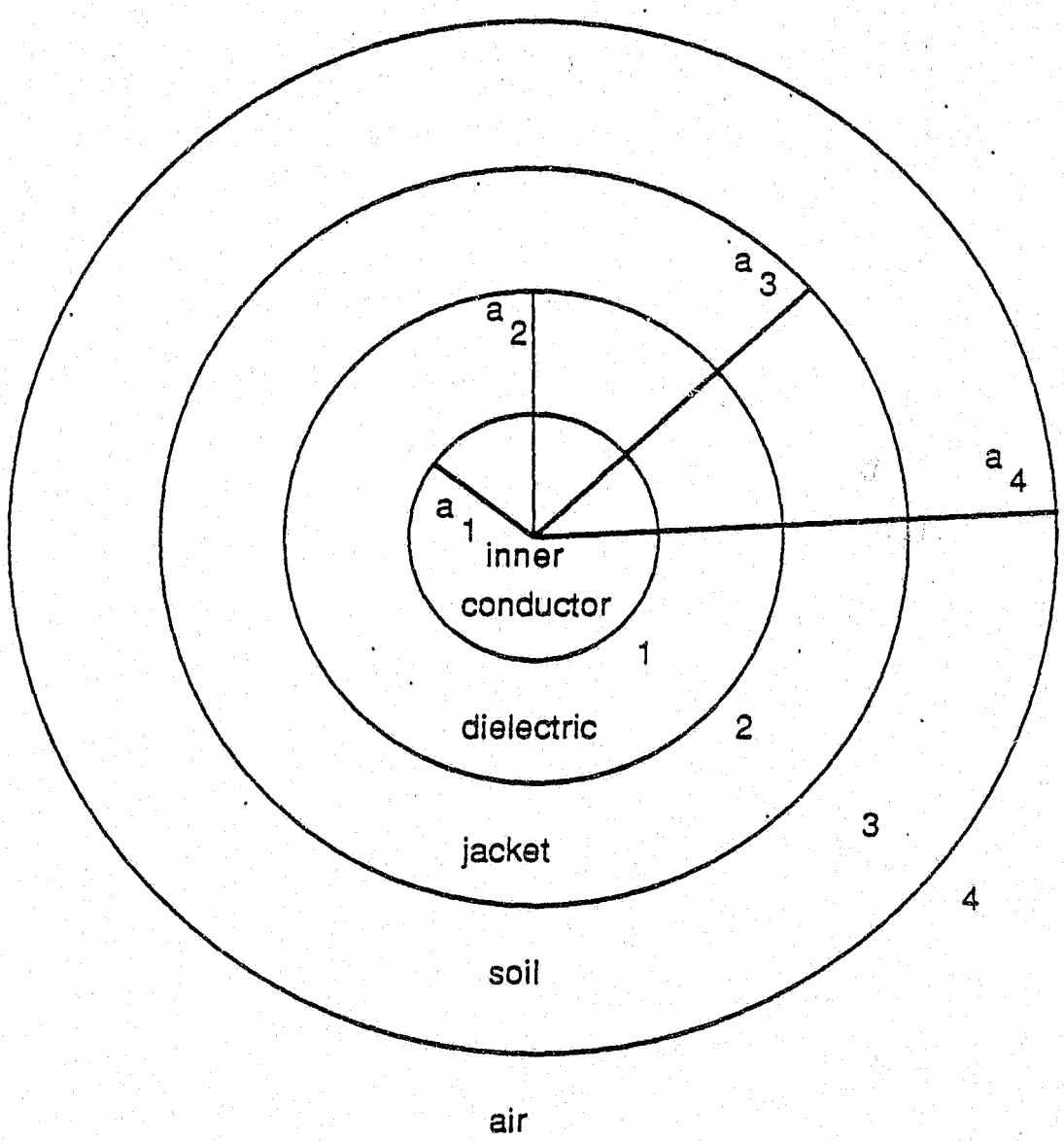

Figure A.1 Multi-region system with azimuthal symmetry.

where ϵ_i is the permittivity of region i and F, ψ and ϕ are unspecified functions. Using vector identities we know that

$$\nabla_t \cdot [\psi \nabla_t \phi] = \nabla_t \psi \cdot \nabla_t \phi + \psi \nabla^2_t \phi \tag{A.5}$$

Therefore,

$$\frac{1}{2\pi} \int_S \nabla_t \cdot A_i ds = \frac{1}{2\pi} \int_S \nabla_t \cdot [F(\epsilon_i)\psi_i(r)\nabla_t \phi_i(r)] ds$$

$$= \frac{1}{2\pi} \int_S F(\epsilon_i)\,(\nabla_t \psi_i(r) \cdot \nabla_t \phi_i(r) + \psi_i(r)\nabla^2_t \phi_i(r)) ds \tag{A.6}$$

Using (A.4) in (A.3) and using $A_t = \hat{r}\ \frac{\partial}{\partial r}$ we obtain:

$$\frac{1}{2\pi} \int_{S_i} F(\epsilon_i)\,[\nabla_t\ \psi_i(r) \cdot \nabla_t \phi_i(r) + \psi_i(r)\nabla_t{}^2 \phi_i(r)]\ ds$$

$$= -a_1\ F(\epsilon_1)\psi_1(a_1)\ \frac{\partial \phi_1(a_1)}{\partial r} - a_2 \left[F(\epsilon_2)\psi_2(a_2)\ \frac{\partial \phi_2(a_2)}{\partial r} - F(\epsilon_1)\psi_1(a_2)\ \frac{\partial \phi_1(a_2)}{\partial r} \right]$$

$$- a_3 \left[F(\epsilon_3)\psi_3(a_3)\ \frac{\partial \phi_3(a_3)}{\partial r} - F(\epsilon_2)\psi_2(a_3)\ \frac{\partial \phi_2(a_3)}{\partial r} \right]$$

$$- a_4 \left[F(\epsilon_4)\psi_4(a_4)\ \frac{\partial \phi_4(a_4)}{\partial r} - F(\epsilon_3)\psi_3(a_4)\ \frac{\partial \phi_3(a_4)}{\partial r} \right] \tag{A.7}$$

Now, if we let

$$B_i(r) = F(\epsilon_i)\phi_i(r)\nabla_t \psi_i(r) \tag{A.8}$$

and evaluate

$$\frac{1}{2\pi}\int_{s_i}\nabla_t\cdot B_i\ ds \tag{A.9}$$

we will obtain the same expression as in (A.7) but with ψ replaced by ϕ and vice-versa.

Subtracting (A.9) from either side of (A.7) yields

$$\frac{1}{2\pi}\int_i F(\epsilon_i)\ [\nabla_t\psi_i(r)\cdot\nabla_t\phi_i(r)+\psi_i(r)\nabla^2{}_t\phi_i(r)]$$

$$-\frac{1}{2\pi}\int_{s_i}F(\epsilon_i)\left[\nabla_t\phi_i(r)\cdot\nabla_t\psi_i(r)+\phi_i(r)\nabla^2{}_t\psi_i(r)\right]ds$$

$$=\frac{1}{2\pi}\int_{s_i}F(\epsilon_i)\ [\psi_i(r)\nabla^2{}_t\ \phi_i(r)-\phi_i(r)\nabla^2{}_t\psi_i(r)]ds \tag{A.10a}$$

$$=\sum_{i=1}^{4}(RS)_i \tag{A.10b}$$

where the term (RS) is used to signify the components of the right side of (A.7) and the implied right side of (A.9).

Using the form used in the right side of (A.7) we can rewrite the components of $\sum_{i=1}^{4}(RS)_i$ as:

$$-\frac{(RS)_1}{a_1}=F(\epsilon_1)\left[\psi_1(r)\cdot\frac{\partial\phi_1(r)}{\partial r}-\phi_1(r)\ \frac{\partial\psi_1(r)}{\partial r}\right]\Big|_{r=a_1} \tag{A.11}$$

$$-\frac{(RS)_2}{a_2} = \left\{F(\epsilon_2)\left[\psi_2(r)\,\frac{\partial\phi_2(r)}{\partial r} - \phi_2(r)\,\frac{\partial\psi_2(r)}{\partial r}\right]\right.$$

$$\left. - F(\epsilon_1)\left[\psi_1(r)\,\frac{\partial\phi_1(r)}{\partial r} - \phi_1(r)\,\frac{\partial\psi_1(r)}{\partial r}\right]\right\}\Big|_{r=a_2} \qquad \text{(A.12)}$$

$$-\frac{(RS)_3}{a_3} = \left\{F(\epsilon_3)\left[\psi_3(r)\,\frac{\partial\phi_3(r)}{\partial r} - \phi_3(r)\,\frac{\partial\psi_3(r)}{\partial r}\right]\right.$$

$$\left. - F(\epsilon_2)\left[\psi_2(r)\,\frac{\partial\phi_2(r)}{\partial r} - \phi_2(r)\,\frac{\partial\psi_2(r)}{\partial r}\right]\right\}\Big|_{r=a_3} \qquad \text{(A.13)}$$

$$-\frac{(RS)_4}{a_4} = \left\{F(\epsilon_4)\left[\psi_4(r)\,\frac{\partial\phi_4(r)}{\partial r} - \phi_4(r)\,\frac{\partial\psi_4(r)}{\partial r}\right]\right.$$

$$\left. - F(\epsilon_3)\left[\psi_3(r)\,\frac{\partial\phi_3(r)}{\partial r} - \phi_3(r)\,\frac{\partial\psi_3(r)}{\partial r}\right]\right\}\Big|_{r=a_4} \qquad \text{(A.14)}$$

II. Orthogonality of $H\phi$

A. Operator L

Maxwell's equation for TM case and $\frac{\partial}{\partial\phi} = 0$ yields:

$$\frac{1}{r}\,\frac{\partial}{\partial r}\,r\,H\phi = j\omega\epsilon E_Z \qquad \text{(A.15)}$$

$$\frac{\partial H\phi}{\partial z} = -j\omega\epsilon E_r \qquad \text{(A.16)}$$

$$\frac{\partial E_r}{\partial z} - \frac{\partial E_z}{\partial r} = -j\omega\mu_0\,H\phi \qquad \text{(A.17)}$$

From (A.16)

$$E_r = -\frac{1}{j\omega\epsilon}\,\frac{\partial H\phi}{\partial z} \qquad \text{(A.18)}$$

From (A.15)

$$E_z = \frac{1}{j\omega\epsilon}\,\frac{1}{r}\,\frac{\partial}{\partial r}(rH\phi) \tag{A.19}$$

Inserting (A.18) and (A.19) into (A.17) we get:

$$\frac{-1}{j\omega\epsilon}\,\frac{\partial^2 H\phi}{\partial z^2} - \frac{1}{j\omega\epsilon}\,\frac{\partial}{\partial r}\,\frac{1}{r}\,\frac{\partial}{\partial r}(rH\phi) = -j\omega\mu_0\, H\phi \tag{A.20}$$

Using separation of variables we let

$$H\phi \equiv \psi(r)Z(z) \tag{A.21}$$

and in the usual way we find

$$\frac{1}{z}\,\frac{\partial^2 Z}{\partial z^2} \equiv -\beta^2 = \text{const.} \tag{A.22}$$

If we substitute (A.21) and (A.22) in (A.20) we obtain:

$$\left(\frac{\partial^2}{\partial r^2} + \frac{1}{r}\,\frac{\partial}{\partial r} - \frac{1}{r^2} + k^2 - \beta^2\right)\psi(r) = 0 \tag{A.23}$$

which can be rewritten as:

$$\left(\frac{\partial}{\partial r}\,\frac{1}{r}\,\frac{\partial}{\partial r}\,r + k^2 - \beta^2\right)\psi(r) = 0 \tag{A.24}$$

where $k = \omega\sqrt{\mu_0\epsilon_0\epsilon_r}$, $\quad k_0 = \omega\sqrt{\mu_0\epsilon_0}$.

Equation (A.24) can be rewritten as:

$$\Big[\underbrace{\frac{\partial}{\partial r}\,\frac{1}{r}\,\frac{\partial}{\partial r}r + (k^2 - k_0^2)}_{L} + \underbrace{(k_0^2 - \beta^2)}_{\nu}\Big]\psi(r) = 0 \tag{A.25}$$

which in operator form is:

$$L\psi = -\nu\psi \tag{A.26}$$

Since, $L = \frac{\partial^2}{\partial r^2} + \frac{1}{r}\frac{\partial}{\partial r} - \frac{1}{r^2} + (k^2-k_0^2)$ (A.27)

and since $\nabla^2_t = \frac{\partial^2}{\partial r} + \frac{1}{r}\frac{\partial}{\partial r}$ (A.28)

we can rewrite ∇^2_t as: $\nabla^2_t = L + \frac{1}{r^2} - (k^2-k_0^2)$ (A.29)

B. Self-Adjointness of L (conditions for self-adjointness)

Consider 2 functions of r; $\psi(r)$ and $\phi(r)$

$$\psi\nabla^2_t\phi - \phi\nabla^2_t\psi = \psi\left[L\phi+\frac{1}{r^2}\phi-(k^2-k_0^2)\phi\right] - \phi\left[L\psi+\frac{1}{r^2}\psi-(k^2-k_0^2)\psi\right]$$

$$=\psi L\phi-\phi L\psi \quad \text{(A.30)}$$

Therefore,

$$\int_S F(\epsilon)[\psi\nabla^2_t\phi - \phi\nabla^2_t\psi]ds$$

$$=\int_S F(\epsilon)[\psi L\phi - \phi L\psi]ds \quad \text{(A.31)}$$

If (A.31) equals 0 then L is said to be self-adjoint. If we solve $L\psi = -\nu\psi$ subject to the following boundary conditions:

at $r = a_1$ $E_Z = 0$ (A.32)

at $r = a_2$ $E_{Z_1} = E_{Z_2}$ and $H\phi_2(a_2) - H\phi_1(a_2) = Y_t E_{Z_2}$ (A.33)

(Y_t = transfer admittance)

at $r = a_3, a_4$ E_Z, $H\phi$ continuous (A.34)

we may find several solutions of ψ i.e. ψ_a, ψ_b, ψ_c, ... which are eigenfunctions of L, subject to the previously stated boundary conditions. For each ψ_a ψ_b, ... there's a ν_a, ν_b, ... which are the eigenvalues of L.

From (A.25) we see that $\nu = k_0^2 - \beta^2$, therefore, if ν_a, ν_b, ... and k_0^2 are known then we can determine β_a, β_b, ...

Let ψ = any eigenfunction, e.g. ψ_a (A.35a)

Let ϕ = any other eigenfunction, e.g. ψ_b (A.35b)

Using (A.31):

$$\int_s (\psi_a \nabla^2_t \psi_b - \psi_b \nabla^2_t \psi_a) F(\epsilon)\, ds$$

$$= \int_s (\psi_a L \psi_b - \psi_b L \psi_a) F(\epsilon)\, ds \tag{A.36}$$

Inserting (A.26) into the right side of (A.36) yields:

$$\int_s F(\epsilon) (-\psi_a \nu_b \psi_b + \psi_b \nu_a \psi_a) ds \tag{A.37}$$

Simplifying (A.37) we get

$$\int_s F(\epsilon) (\nu_a - \nu_b) \psi_a \psi_b \, ds \equiv 2\pi (RS) \tag{A.38}$$

We now try to adjust $F(\epsilon)$ so that (RS) = 0. Thus, if

$$(\nu_a - \nu_b) \int_s F(\epsilon) \psi_a \psi_b \, ds \equiv 0 \equiv RS \tag{A.39}$$

then this implies

$$\int_s F(\epsilon) \psi_a \psi_b \, ds = 0 \text{ for } \nu_a \neq \nu_b \tag{A.40}$$

i.e. ψ_a and ψ_b are orthogonal, which will be true if we can show that RS = 0.

If $\nu_a = \nu_b$ (i.e., same mode) then,

$$\int_S F(\epsilon)\, \psi_a\, \psi_b\, ds \neq 0 = \text{const.} \tag{A.41}$$

Choose amplitude of ψ_a, ψ_b to make the integral in (A.41) equal unity, therefore,

$$\int_S F(\epsilon)\, \psi_a \psi_b\, ds = \delta_{ab} \tag{A.42}$$

where

$$\delta_{ab} = \begin{cases} 1 & a=b \\ 0 & (a \neq b) \end{cases}$$

III. Evaluation of (RS)

Inserting (A.35a) and (A.35b) into (A.11) we obtain,

$$-\frac{(RS)}{a_1} = F(\epsilon_1) \left[\psi_{a_1} \frac{\partial \psi_{b_1}}{\partial r} - \psi_{b_1} \frac{\partial \psi_{a_1}}{\partial r} \right] \Big|_{r=a_1} \tag{A.43}$$

Using $H_\phi = \psi(r)Z(z)$ in (A.19) we obtain,

$$E_z = \frac{1}{j\omega\epsilon} \frac{1}{r} \frac{\partial}{\partial r} (r\psi Z) = \frac{Z(z)}{j\omega\epsilon} \left[\frac{\partial \psi}{\partial r} + \frac{\psi}{r} \right] \tag{A.44}$$

Equation (A.43) can be rewritten in the following form,

$$-\frac{(RS)_1}{a_1} = F(\epsilon_1) \left[\left(\psi_{a_1} \frac{\partial \psi_{b_1}}{\partial r} + \psi_{a_1} \frac{\psi_{b_1}}{r} \right) - \left(\psi_{b_1} \frac{\partial \psi_{a_1}}{\partial r} + \psi_{b_1} \frac{\psi_{a_1}}{r} \right) \right] \Big|_{(r=a_1)} \tag{A.45}$$

Let

$$\psi_{a_1} = \frac{H\phi_a}{Z_a(z)} \tag{A.46}$$

$$\psi_{b_1} = \frac{H\phi_b}{Z_b(z)} \tag{A.47}$$

Substituting (A.44) into (A.45) we get.

$$-\frac{(RS)_1}{a_1} = F(\epsilon_1)\left[\psi_{a_1}\left(\frac{j\omega\epsilon_1}{Z_b(z)}E_{z_{b_1}}\right) - \psi_{b_1}\left(\frac{j\omega\epsilon_1}{Z_a(z)}E_{z_{a_1}}\right)\right]\Big|_{r=a_1} \tag{A.48}$$

Substituting (A.46) and (A.47) into (A.48) we get,

$$-\frac{(RS)_1}{a_1} = F(\epsilon_1)\left[H\phi_{a_1}E_{z_{b_1}} - H\phi_{b_1}E_{z_{a_1}}\right]\Big|_{(r=a_1)} \frac{j\omega\epsilon_1}{Z_a(z)\,Z_b(z)} \tag{A.49}$$

$$=0$$

due to boundary conditions (A.32) at $r = a_1$.

In the same manner as above we can rewrite (A.13) as

$$-\frac{(RS)_3}{a_3} = F(\epsilon_3)\left[H\phi_{a_3}E_{z_{b_3}} - H\phi_{b_3}E_{z_{a_3}}\right]\Big|_{(r=a_3)} \frac{j\omega\epsilon_3}{Z_a(z)Z_b(z)}$$

$$- F(\epsilon_2)\left[H\phi_{a_2}E_{z_{b_2}} - H\phi_{b_2}E_{z_{a_2}}\right]\Big|_{(r=a_3)} \frac{j\omega\epsilon_2}{Z_a(z)Z_b(z)}. \tag{A.50}$$

If we let $F(\epsilon_i) = \frac{1}{\epsilon_i}$ then (A.50) becomes,

$$-\frac{(RS)_3}{a_3} = \frac{j\omega}{Z_a(z)Z_b(z)}\left[\left(H\phi_{a_3}E_{z_{b_3}} - H\phi_{a_2}E_{z_{b_2}}\right) - \left(H\phi_{b_3}E_{z_{a_3}} - H\phi_{b_2}E_{z_{a_2}}\right)\right]\Big|_{(r=a_3)} \tag{A.51}$$

$= 0 - 0 = 0$ from boundary conditions (A.34).

Similarly, (A.14) can be found to be

$$-\frac{(RS)_4}{a_4} = 0 \tag{A.52}$$

Also, (A.12) can be rewritten as,

$$-\frac{(RS)_2}{a_2} = \frac{j\omega}{Z_a(z)Z_b(z)} \left\{ \left[H\phi_{a_2} E_{z_{b_2}} - H\phi_{b_2} E_{z_{a_2}} \right] - \left[H\phi_{a_1} E_{z_{b_1}} - H\phi_{b_1} E_{z_{a_1}} \right] \right\} \Big|_{(r=a_2)} \tag{A.53}$$

or since $E_{z_{b_2}} = E_{z_{b_1}}$ and $E_{z_{a_2}} = E_{z_{a_1}}$ at $r = a_2$

$$-\frac{(RS)_2}{a_2} = \left(E_{z_{b_2}} \left[H\phi_{a_2} - H\phi_{a_1} \right] - E_{z_{a_2}} \left[H\phi_{b_2} - H\phi_{b_1} \right] \right) \Big|_{(r=a_1)} \frac{j\omega}{Z_a(z)Z_b(z)} \tag{A.54}$$

Using boundary condition (A.33) in (A.53) we get

$$-\frac{(RS)_2}{a_2} = \frac{j\omega}{Z_a(z)Z_b(z)} \left(E_{z_{b_2}} Y_t E_{z_{a_2}} - E_{z_{a_2}} Y_t E_{z_{b_2}} \right) \tag{A.55}$$

$$= 0 \ .$$

From (A.49), (A.51), (A.52) and (A.55) we see that for $F(\epsilon_i) = 1/\epsilon_i$,

$$RS = \sum_{i=1}^{4} (RS)_i = 0 \tag{A.56}$$

Equations (A.56) with (A.39), (A.40), (A.46) and (A.47) tell us that $H\phi_a$ is orthogonal to $H\phi_b$. Thus (A.42) can be rewritten as

$$\int_S \frac{\psi_a \psi_b}{\epsilon} ds = \delta_{ab} = \begin{cases} 1 & a=b \\ 0 & (a \neq b) \end{cases} \tag{A.57}$$

$$\int_S \frac{H\phi_a H\phi_b}{Z_a(z)Z_b(z)\epsilon} ds = \delta_{ab} = \begin{cases} 1 & a=b \\ 0 & (a \neq b) \end{cases} \tag{A.58}$$

If we redefine $A \equiv F(E)\psi\nabla_t\phi^*$ then,

$$\int_s \frac{H\phi_a H\phi_b^*}{Z_a(z)Z_b(z)\epsilon}\, ds = \delta_{ab} \tag{A.59}$$

If we let $Z = e^{-j\beta z}$ and remember $H\phi = \psi Z$, and insert these into (A.18) we get,

$$E_r = \frac{-\psi}{j\omega\epsilon}\frac{\partial e^{-j\beta z}}{\partial z} = \frac{-j\beta\psi}{-j\omega\epsilon}e^{-j\beta z} = \frac{\beta}{\omega\epsilon}\psi Z = \frac{\beta}{\omega\epsilon}H\phi = E_r \tag{A.60}$$

or

$$H\phi = \frac{\omega\epsilon}{\beta}E_r \tag{A.61}$$

If we insert (A.61) into (A.59) we get,

$$\int_s \frac{\omega\epsilon}{Z_a(z)\beta_a}\frac{\omega\epsilon}{Z_b(z)\beta_b}\frac{1}{\epsilon}E_{r_a}E_{r_b}^*\, ds = \delta_{ab} \tag{A.62}$$

Equation (A.62) can be written as,

$$\int_s \epsilon E_{r_a}E_{r_b}^*\, ds = \frac{Z_a(z)Z_b(z)\beta_a\beta_b}{\omega^2}\delta_{ab} \tag{A.63}$$

If we insert (A.61) into (A.58) we get,

$$\int_s \frac{\omega\epsilon}{\beta_a}\frac{\omega\epsilon}{\beta_b}\frac{1}{Z_a(z)Z_b(z)\epsilon}E_{r_a}E_{r_b}\, ds = \delta_{ab} \tag{A.64}$$

Equation (A.64) can be written as,

$$\int_S \epsilon \, E_{r_a} \, E_{r_b} \, ds = \frac{Z_a(z) Z_b(z) \beta_a \beta_b}{\omega^2} \, \delta_{ab} \qquad (A.65)$$

which tells us that the "a" modes and the "b" modes are orthogonal to each other.

In summary, (A.58) and (A.65) are orthogonality relations for the electric and magnetic fields, respectively, of the eigenmodes a, b, ..., of the cylindrical system whose cross-section is shown in Figure A.1. These relations are equivalent to those found by Delogne (1982).

APPENDIX B

TABULATED EXPERIMENTAL RESULTS

The following tables contain data obtained from the experiments described in this thesis.

Response Number Profile and Cable Separation Distance Tests

Position - location along cable, in meters from ported cable beginning.
Cable Sep - cable separation distance at the specified position.
Resp # E-W - Response numbers obtained from first crossing (east to west direction).
Resp # W-E - Response numbers obtained from second crossing (west to east direction).
Resp # Ave - Average of Resp # E-W and Resp # W-E.

Position	Cable Sep	Resp # E-W	Resp # W-E	Resp # Ave
0	63.00	400	400	400.0
1	61.00	400	400	400.0
2	63.00	836	716	776.0
3	66.00	784	777	780.5
4	68.00	804	678	741.0
5	65.50	834	781	807.5
6	66.00	773	737	755.0
7	64.00	820	701	760.5
8	63.00	800	674	737.0
9	64.00	787	743	765.0
10	63.00	615	588	601.5
11	62.00	614	580	597.0
12	63.50	525	590	557.5
13	63.00	573	513	543.0
14	65.00	572	491	531.5
15	66.00	447	400	423.5
16	67.00	431	400	415.5
17	68.50	400	400	400.0
18	68.00	400	400	400.0
19	65.00	400	400	400.0

Response Number Profile and Cable Separation Distance Test continued

Position	Cable Sep	Resp # E-W	Resp # W-E	Resp # Ave
20	64.00	400	400	400.0
21	63.50	562	514	538.0
22	64.00	478	427	452.5
23	64.50	556	486	521.0
24	65.50	723	623	673.0
25	67.00	781	733	757.0
26	66.50	655	611	633.0
27	67.50	648	637	642.5
28	66.50	529	532	530.5
29	65.50	566	507	536.5
30	66.50	599	513	556.0
31	66.50	400	400	400.0
32	64.50	773	749	761.0
33	62.50	1211	1157	1184.0
34	61.00	2381	2094	2237.5
35	60.00	3650	3368	3509.0
36	60.50	4414	4237	4325.5
37	60.00	4740	4410	4575.0
38	59.00	5735	4938	5336.5
39	61.50	5469	4987	5228.0
40	62.50	4819	4817	4818.0
41	62.00	4474	4176	4325.0
42	61.50	3914	4066	3990.0
43	59.50	4605	4327	4466.0
44	59.00	5099	4865	4982.0
45	60.50	5466	5306	5386.0
46	60.00	5408	5187	5297.5
47	61.00	4722	4824	4773.0
48	60.50	5126	4905	5015.5
49	61.50	5910	5907	5908.5
50	62.00	4849	4103	4476.0
51	64.00	3883	3948	3915.5
52	64.50	2921	2915	2918.0
53	65.00	1841	1828	1834.5
54	64.50	1332	1231	1281.5
55	64.50	1064	1000	1032.0
56	66.00	666	727	696.5
57	67.50	878	831	854.5
58	68.50	765	794	779.5
59	69.00	916	839	877.5
60	68.00	1117	1171	1144.0
61	66.50	1253	1061	1157.0
62	66.00	1240	1305	1272.5
63	65.25	1467	1341	1404.0
64	63.50	1476	1369	1422.5

Response Number Profile and Cable Separation Distance Test continued

Position	Cable Sep	Resp # E-W	Resp # W-E	Resp # Ave
65	62.00	1209	1175	1192.0
66	63.00	1245	1169	1207.0
67	62.00	639	652	645.5
68	63.00	735	856	795.5
69	63.00	873	826	849.5
70	64.00	1498	1377	1437.5
71	63.25	1725	1550	1637.5
72	63.00	2013	1929	1971.0
73	63.50	1890	1871	1880.5
74	64.00	1258	1188	1223.0
75	64.50	1184	1091	1137.5
76	67.50	973	960	966.5
77	63.50	1048	1035	1041.5
78	63.25	1009	908	958.5
79	62.00	1349	1309	1329.0
80	64.50	985	999	992.0
81	65.00	980	961	970.5
82	63.50	880	847	863.5
83	64.50	1232	1031	1131.5
84	65.50	918	934	926.0
85	66.00	912	887	899.5
86	64.50	767	787	777.0
87	65.00	911	900	905.5
88	64.00	720	786	753.0
89	64.50	957	901	929.0
90	66.25	811	834	822.5
91	67.00	734	760	747.0
92	67.50	774	752	763.0
93	66.00	747	621	684.0
94	64.00	784	770	777.0
95	63.50	537	486	511.5
96	63.25	521	634	577.5
97	64.00	490	506	498.0
98	60.50	565	527	546.0
99	61.00	647	671	659.0
100	64.00	1060	991	1025.5
101	64.00	952	842	897.0
102	65.00	1371	1386	1378.5
103	66.00	1119	989	1054.0
104	65.00	956	956	956.0
105	64.50	767	707	737.0
106	64.50	520	564	542.0
107	64.00	573	538	555.5
108	63.00	701	576	638.5
109	62.00	410	400	405.0

Response Number Profile and Cable Separation Distance Test continued

Position	Cable Sep	Resp # E-W	Resp # W-E	Resp # Ave
110	62.00	452	411	431.5
111	62.00	473	528	500.5
112	60.50	515	509	512.0
113	62.50	692	760	726.0
114	64.00	931	807	869.0
115	63.00	897	843	870.0
116	62.50	1250	1142	1196.0
117	63.00	1087	1044	1065.5
118	64.00	1223	1163	1193.0
119	64.50	832	861	846.5
120	63.50	1010	975	992.5
121	63.50	818	793	805.5
122	64.00	1073	898	985.5
123	65.00	1067	1048	1057.5
124	64.00	1099	1062	1080.5
125	61.00	820	776	798.0
126	61.50	710	699	704.5
127	61.00	964	890	927.0
128	59.00	873	796	834.5
129	58.50	743	780	761.5
130	60.50	507	455	481.0
131	58.50	522	559	540.5
132	58.50	743	638	690.5
133	56.00	744	564	654.0
134	56.50	650	626	638.0
135	55.00	612	611	611.5
136	56.50	782	690	736.0
137	59.00	807	759	783.0
138	62.00	985	868	926.5
139	63.00	901	839	870.0
140	63.00	1030	977	1003.5
141	63.00	876	866	871.0
142	62.00	1094	1080	1087.0
143	65.00	913	804	858.5
144	67.00	1078	1050	1064.0
145	69.50	953	815	884.0
146	69.50	1139	1066	1102.5
147	68.50	959	825	892.0
148	69.00	1044	1004	1024.0
149	69.00	688	684	686.0
150	69.00	915	874	894.5
151	70.00	736	710	723.0
152	70.00	869	766	817.5
153	70.00	797	657	727.0
154	67.50	766	733	749.5

Response Number Profile and Cable Separation Distance Test continued

Position	Cable Sep	Resp # E-W	Resp # W-E	Resp # Ave
155	67.00	700	621	660.5
156	65.50	768	820	794.0
157	64.50	893	811	852.0
158	62.00	818	659	738.5
159	63.50	863	812	837.5
160	63.50	665	656	660.5
161	64.00	557	522	539.5
162	65.00	415	400	407.5
163	63.50	400	400	400.0
164	63.50	400	400	400.0
165	62.50	436	400	418.0
166	64.50	400	400	400.0
167	65.00	400	400	400.0
168	65.00	400	400	400.0
169	66.50	400	400	400.0
170	66.00	400	400	400.0
171	67.00	400	400	400.0
172	68.00	552	458	505.0
173	67.00	400	400	400.0
174	66.25	434	400	417.0
175	65.00	400	400	400.0
176	66.50	475	481	478.0
177	65.00	429	400	414.5
178	65.00	740	667	703.5
179	66.50	791	680	735.5
180	67.00	817	654	735.5
181	66.50	603	496	549.5
182	67.00	752	606	679.0
183	68.00	702	588	645.0
184	70.00	641	562	601.5
185	70.50	647	526	586.5
186	69.00	624	457	540.5
187	68.50	451	471	461.0
188	66.00	545	550	547.5
189	67.50	636	553	594.5
190	67.00	713	646	679.5
191	63.00	567	558	562.5
192	63.00	1306	1074	1190.0
193	63.00	788	642	715.0
194	63.00	1488	1490	1489.0
195	63.00	798	800	799.0
196	65.00	1243	1152	1197.5
197		611	645	628.0
198		1157	1167	1162.0
199		607	598	602.5
200		482	505	493.5

Magnetic Field Intensity Test

Position - location along cable, in meters from ported cable beginning.
Mag1 - first run of measurement. Arbirary units.
Mag2 - repeat of measurements. Arbitrary units.
Mag Ave - average of Mag1 and Mag2. Arbitrary units.

Position	Mag1	Mag2	Mag Ave
26	2.4	2.6	2.50
27	2.5	2.8	2.65
28	2.6	2.9	2.75
29	3.0	3.5	3.25
30	2.0	2.4	2.20
31	2.1	2.2	2.15
32	2.7	2.9	2.80
33	4.6	4.8	4.70
34	5.4	5.8	5.60
35	4.4	4.9	4.65
36	4.6	4.6	4.60
37	5.1	5.3	5.20
38	5.0	6.3	5.65
39	3.7	4.8	4.25
40	3.3	3.8	3.55
41	2.8	4.4	3.60
42	3.9	4.8	4.35
43	4.1	4.2	4.15
44	5.8	6.8	6.30
45	5.0	6.1	5.55
46	4.9	5.9	5.40
47	6.4	7.8	7.10
48	5.9	7.4	6.65
49	5.9	6.7	6.30
50	7.3	7.9	7.60
51	5.6	6.1	5.85
52	4.8	4.8	4.80
53	3.1	3.2	3.15
54	1.8	4.0	2.90
55	3.5	3.8	3.65
56	4.0	4.7	4.35
57	3.5	3.8	3.65
58	3.8	3.9	3.85
59	3.1	3.2	3.15
60	3.8	4.0	3.90

Magnetic Field Intensity Test continued

Position	Mag1	Mag2	Mag Ave
61	4.2	4.7	4.45
62	3.5	3.9	3.70
63	2.8	2.7	2.75
64	3.1	3.4	3.25
65	3.0	2.9	2.95
66	2.3	2.5	2.40
67	3.1	3.4	3.25
68	3.5	3.9	3.70
69	4.2	4.2	4.20
70	3.8	4.2	4.00
71	3.8	4.0	3.90
72	3.4	3.6	3.50
73	3.1	3.2	3.15
74	3.0	3.2	3.10
75	2.3	2.5	2.40
76	3.2	3.5	3.35
77	3.1	3.2	3.15
78	2.8	2.9	2.85
79	2.8	2.6	2.70
80	3.0	2.8	2.90

Soil Conductivity and Permittivity Test

Position - location along cable, in meters from ported cable beginning.
Conductivity - conductivity of the soil in millimhos per meter.
Rel Perm - relative permittivity of the soil.
Loss Tan - loss tangent of the soil at a frequency of 63 MHz.

Position	Conductivity	Rel Perm	Loss Tan
33	2.51	5.19	0.1380
34	2.12	4.99	0.1212
35	2.27	5.23	0.1238
36	2.40	5.19	0.1319
37	2.45	4.96	0.1409
38	2.45	5.07	0.1379
39	2.56	5.11	0.1429
40	2.69	5.14	0.1493
41	2.63	4.98	0.1507
42	2.69	5.18	0.1482
43	2.63	5.09	0.1474
44	2.69	5.25	0.1462
45	2.82	5.39	0.1493
46	2.82	5.21	0.1544
47	2.57	5.00	0.1467
48	2.70	5.32	0.1448
49	2.80	5.03	0.1588
50	8.21	7.70	0.3042
51	10.29	7.01	0.4188
52	14.63	7.30	0.5718
53	14.03	6.80	0.5887
54	18.06	8.25	0.6246
55	15.60	7.75	0.5743
56	15.86	6.97	0.6492
57	18.11	7.37	0.7011
58	23.51	8.33	0.8053
59	22.61	7.98	0.8084
60	14.61	7.02	0.5938
61	18.61	7.48	0.7099
62	16.82	7.38	0.6503
63	16.13	7.54	0.6104
64	15.36	7.34	0.5971
65	19.91	8.61	0.6598

Response Number vs. Varying Cable Separation Test

Position - location along the cable, in meters from the ported cable beginning.
Cab Sep n - cable separation, in inches, for run n of test #1.
Response n - response number for run n of test #1.

Position	Cab Sep 1	Cab Sep 2	Cab Sep 3	Cab Sep 4
115	64.50	64.50	64.50	64.50
116	63.50	63.00	61.75	60.00
117	61.50	60.25	58.00	56.00
118	64.00	63.50	63.00	61.00
119	64.00	64.00	63.50	63.50

Position	Response 1	Response 2	Response 3	Response 4
115	831.00	751.00	777.00	831.00
116	1139.00	1016.50	1078.50	1114.50
117	1075.50	1105.50	1177.00	1218.50
118	1153.00	1246.00	1274.50	1376.00
119	722.00	746.00	810.50	873.50

Response Number vs. Varying Cable Separation Test continued

Position - location along the cable, in meters from the ported cable beginning.
Cab Sep n - cable separation, in inches, for run n of test #2.
Response n - response number for run n of test #2.

Position	Cab Sep 1	Cab Sep 2	Cab Sep 3	Cab Sep 4	Cab Sep 5
39	61.50	61.50	61.50	61.50	61.50
40	62.50	63.50	63.00	62.00	62.00
41	70.00	68.50	67.50	65.50	61.50
42	73.00	70.50	68.00	63.00	61.00
43	68.00	67.50	65.00	61.50	59.50
44	60.00	60.00	59.50	59.50	58.00
45	60.50	60.50	60.00	60.00	60.00

Position	Cab Sep 6	Cab Sep 7	Cab Sep 8	Cab Sep 9
39	61.00	61.00	62.00	61.00
40	62.00	61.50	61.50	60.75
41	59.50	57.50	56.00	52.50
42	58.50	55.25	52.00	47.50
43	58.00	55.00	53.50	51.75
44	57.75	58.00	58.00	56.50
45	60.00	59.50	59.50	59.50

Position	Response 1	Response 2	Response 3	Response 4	Response 5
39	4988	5312	5199	5067.5	5331.5
40	5244.5	4965.5	5238.5	5059.5	5073.5
41	4719	4676.5	4781.5	4573.5	4864
42	3090	3323.5	3540	3848	4328
43	3228.5	3881.5	3727	4730	4865.5
44	4435	4237	4549	4704.5	4697.5
45	5162.5	5264.5	5671	5594.5	5648

Position	Response 6	Response 7	Response 8	Response 9
39	5164	5125	5247	4939.5
40	4604.5	4737	4495.5	4327
41	4433	4677	4851.5	4897
42	4247	4358.5	4885.5	5654.5
43	5265	6234	7470	7608
44	5245.5	5264	6204.5	6603.5
45	5948	6468.5	5798.5	6721

LIST OF REFERENCES

Caldecott, R., M. Poirier and D. Svoboda, "An RF Probe to Measure Soil Electrical Parameters," Final Report 715616-4, U.S. Army Engineer Waterways Experiment Station, January 1985.

Delogne, P., Leaky Feeders and Subsurface Radio Communications, Peter Peregrinus Ltd. (Institution of Electrical Engineers), London and New York, 1982.

Delogne, P. and M. Safak, "Electromagnetic Theory of the Leaky Coaxial Cable," The Radio and Electronic Engineer, Vol. 45, No. 5, pp. 233-240, May 1975.

Fernandes, A.S., "Propagation Characteristics of a Loose Braid Coaxial Cable in Free Space," The Radio and Electronic Engineer, Vol. 49, No. 5, pp. 255-260, May 1979.

Frankel, Harry D., George A. Van Horn and Robert N. Carlile, "Evaluation of the Ported Coaxial Cable Sensor (PCCS)," Final Report INS-RD-1001, Immigration and Naturalization Service, December 1984.

Guided Intrusion Detection and Ranging System, GIDR1, Maintenance Manual, Vols. 1 and 2, 24 October 1981, Computing Devices Company, Ottawa, Ontario, Canada.

Goubau, Georg, "Surface Waves and Their Application to Transmission Lines," Journal of Applied Physics, Vol. 21, pp. 1119-1128, November 1950.

Harman, R.K., "Burial Medium Effects on Leaky Coaxial Cable Sensors," Proceedings: 1983 Carnahan Conference on Security Technology, Zurich, Switzerland, pp. 185- 189, October 4-8, 1983.

Harman, R.K. and N.A.M. Mackay, "Guidar: An Intrusion Detection System For Perimeter Protection," Proceedings: 1976 Carnahan Conference on Crime Countermeasures, University of Kentucky Lexington, Kentucky, pp. 155-159, May 5-7, 1976.

Harman, R.K. and J.E. Siedlarz, "Advancements in Leaky Cable Technology For Intrusion Detection," Proceedings: 1982 Carnahan Conference on Security Technology, University of Kentucky, Lexington, Kentucky, pp. 115-121, May 12-14, 1982.

Harrington, R.F., Time-Harmonic Electromagnetic Fields, McGraw-Hill Book Co., New York, 1961, p. 113.

Harrison, James R., Design of a Long Line Intrusion Detection Sensor, Masters Thesis, University of Arizona, Tucson, Arizona, 1986.

Hill, David A. and James R. Wait, "Electromagnetic Characteristics of a Coaxial Cable With Periodic Slots," IEEE Transactions on Electromagnetic Compatibility, Vol. EMC-22, No. 4, pp. 303-307, November 1980.

Lundien, Jerry R., U.S. Army Engineer Waterways Experiment Station, private communication, January 1986.

Maki, M.C., "Coupling Mechanisms in Leaky Cable Sensors," Proceedings: 1984 Carnahan Conference on Security Technology, University of Kentucky, Lexington, Kentucky, pp. 195-201, May 16-18, 1984.

Miller, Charles A., Mark D. Flohr and Jerry R. Lundien, "Output Response Characteristics of a Ported Coaxial Cable Sensor (PCCS)," Final Report EL-84-2, U.S. Army Engineer Waterways Experiment Station, March 1984.

Parra, Jorge O., "Effects of Pipelines On Spectral Induced- Polarization Surveys," Geophysics, Vol. 49, No. 11, pp. 1979-1992, November 1984.

Patterson, R.E. and Neilson A.M. Mackay, "A Guided Radar System For Obstacle Detection," IEEE Transactions on Instrumentation and Measurement, Vol. IM-26, No. 2, pp. 137-143, June 1977.

Richmond, Jack H., "Propagation On a Ported Coaxial Cable Buried in a Flat Earth," Ohio State University ElectroScience Laboratory, February 1981.

Schelkunoff, S.A., "The Electromagnetic Theory of Coaxial Transmission Lines and Cylindrical Shields," The Bell System Technical Journal, Vol. XIII, pp. 532-579, 1934.

Stix, T.H., The Theory of Plasma Waves, McGraw-Hill Book Co., New York, 1962, p. 91.

Wait, James R., "On the Theory of Wave Propagation Along a Thin Dielectric Coated Wire in a Stratified Medium," International Journal of Electronics, Vol. 34, No. 2, pp. 265-272, 1973.

Wait, James R. and D.A. Hill, "Influence of Spatial Dispersion of the Shield Transfer Impedance of a Braided Coaxial Cable," IEEE Transactions on Microwave Theory and Techniques, pp. 72-74, January 1977.

Wait, James R. and K.R. Umashankar, "Analysis of the Earth Resistivity Response of Buried Cables," Pageoph, Vol. 117, pp. 711-741, 1978/79.